ISTANBUL TECHNICAL UNIVERSITY ★ GRADUATE SCHOOL OF SCIENCE ENGINEERING AND TECHNOLOGY

DEVELOPMENT AND CHARACTERISATION OF FUNCTIONAL NANOFIBERS FOR FACE MASK APPLICATIONS

M.Sc. THESIS

Tugba BAYSAL

Department of Nanoscience and Nanoengineering

Nanoscience and Nanoengineering Programme

JUNE 2020

ISTANBUL TECHNICAL UNIVERSITY ★ GRADUATE SCHOOL OF SCIENCE ENGINEERING AND TECHNOLOGY

DEVELOPMENT AND CHARACTERISATION OF FUNCTIONAL NANOFIBERS FOR FACE MASK APPLICATIONS

M.Sc. THESIS

Tugba BAYSAL
(513171007)

Department of Nanoscience and Nanoengineering

Nanoscience and Nanoengineering Programme

Thesis Advisor: Prof. Dr. Ali DEMIR

JUNE 2020

ISTANBUL TEKNİK ÜNİVERSİTESİ ★ FEN BİLİMLERİ ENSTİTÜSÜ

YÜZ MASKESİ UYGULAMALARI İÇİN FONKSİYONEL NANOLİFLERİN GELİŞTİRİLMESİ VE KARAKTERİZASYONU

YÜKSEK LİSANS TEZİ

Tuğba BAYSAL
(513171007)

Nanobilim ve Nanomühendislik Anabilim Dalı

Nanobilim ve Nanomühendislik Programı

Tez Danışmanı: Prof. Dr. Ali DEMIR

HAZİRAN 2020

Tugba BAYSAL, a M.Sc. student of ITU Graduate School of Science Engineering and Technology student ID 513171007 successfully defended the thesis entitled "DEVELOPMENT AND CHARACTERISATION OF FUNCTIONAL NANOFIBERS FOR FACE MASK APPLICATIONS", which she prepared after fulfilling the requirements specified in the associated legislations, before the jury whose signatures are below.

Thesis Advisor :	**Prof. Dr. Ali DEMIR** İstanbul Technical University	.....
Jury Members :	**Prof. Dr. Ali DEMIR** İstanbul Technical University	.....
	Assoc. Prof. Dr. Sule SELCUK İstanbul Technical University	.....
	Assoc. Prof. Dr. Nuruzzaman NOOR The Hong Kong Polytechnic University	.....

Date of Submission : 20 May 2020
Date of Defense : 30 June 2020

To my family, my friends and all beloved ones,

FOREWORD

First of all, I would like to thank my thesis supervisor Prof. Dr. Ali DEMIR for his valuable support and encouragement during my post graduate education.

Secondly, I would like to thank the company INOVENSO Technology Ltd., which has encouraged me to focus on nanotechnology and provided the financial support to the project, and its valuable researchers who shared their valuable knowledge with me throughout my studies.

I am grateful to work with my friends at ITU TEMAG Lab, and our dear professor, Doc. Dr. Ali KILIC.

I would like to thank Doc. Dr. Derya Yuksel IMER and her valuable students for their help and support during the adsorption test process.

Finally, I would like to express my sincere thanks to my family, which every time show me their love and support.

May 2020

Tugba BAYSAL

(Chemical Engineer)

TABLE OF CONTENTS

Page

ABBREVIATIONS

µl **:** microliter
µm **:** micrometer
1D **:** One dimension
ACNFs **:** Activated Carbon Nanofibers
APS **:** Average particle size
Ave **:** Average
BET **:** Brunauer–Emmett–Teller
CE **:** European Conformity
cm **:** centimeter
DNA **:** DeoxyriboNucleic Scid
dtex **:** Decitex
E. coli ***:*** *Escherichia coli*
EDX **:** Energy Dispersive X-ray Spectroscopy
FFP1 **:** Filtering Face Piece 1
FFP2 **:** Filtering Face Piece 2
FFP3 **:** Filtering Face Piece 3
g **:** Gram
GAC **:** Granular Activated Carbon
GC-MS **:** Gas Chromatography-Mass Spectrometry
gsm **:** grams per square meter
h **:** hour
HEPA **:** High Efficiency Particulate Air
in **:** inch
kV **:** kilovolt
l **:** liter
LPS **:** Lipopolysaccharide
m **:** meter
MAC **:** Maximum Allowed Concentration
mbar **:** milibar
mg **:** miligram

min : minute
MJ : Megajoule
ml : mililiter
mm : milimeter
MPa : Megapascal
NF : Nanofiber
nm : Nanometer
NP : Nanoparticle
Pa : Pascal
PM : Particulate matter
PM10 : Particulates matter with a diameter of less than 10 μm
PM2.5 : Particulates matter with a diameter of less than 2.5 μm
ppm : Parts per million
QF : Quality Factor
Ref : Reference
ROS : Reactive Oxygen Species
s : second
S. aureus *: Staphylococcus aureus*
SB : Solution Blowing
SEM : Scanning Electron Microscope
SSA : Specific Surface Area
TEM : Transmission Electron Microscope
UV : Ultraviolet
VOCs : Volatile Organic Compounds
wt : weight

SYMBOLS

2-CEES	**:** 2-chloroethyl ethyl sulfide
Ag	**:** Silver
Al_2O_3	**:** Aluminum Oxide
Au	**:** Gold
℃	**:** The degree celcius
Cd	**:** Cadmium
CO	**:** Carbon monoxide
CO_2	**:** Carbon dioxide
CuO	**:** Copper Oxide
DCM	: Dichloromethane
DMAC	**:** Dimethylacetamide
DMF	**:** N, N-dimethylformamide
Fe_2O_3	**:** Iron(III) oxide
H_2	**:** Hydrogen
H_2O	: Water
K	**:** The degree kelvin
KCl	**:** Potassium chloride
MgO	**:** Magnesium oxide
MnO_2	**:** Manganese dioxide
N	**:** Nitrogen
NaCl	**:** Sodium chloride
O_2	**:** Oxygen
P	**:** Phosphorus
PA	: Polyamide
PA6	**:** Polyamide 6
PAA	**:** Poly(acrylic acid)
PAN	**:** Polyacrylonitrile
PEI	**:** Polyetherimide
PEO	**:** Poly(ethylene oxide)
pH	**:** Power of hydrogen

PLA **:** Polylactic acid

PP **:** Polypropylene

PS **:** Polystyrene

PSU **:** Polysulfone

PU **:** Polyurethane

PVA **:** Poly(vinyl alcohol)

PVC **:** Poly(vinyl chloride)

PVDF **:** Poly(vinylidene fluoride)

rpm **:** Revolutions per minute

S **:** Sulfur

SiO_2 **:** Silicon dioxide

SnO_2 **:** Tin (IV) oxide

THF **:** Tetrahydrofuran

TiO_2 **:** Titanium dioxide

ZnO **:** Zinc oxide

ZrO_2 **:** Zirconium dioxide

ΔP **:** Pressure Drop

LIST OF TABLES

Page

LIST OF FIGURES

Page

DEVELOPMENT AND CHARACTERISATION OF FUNCTIONAL NANOFIBERS FOR FACE MASK APPLICATIONS

SUMMARY

Nowadays, air pollution is a major problem all around the world and human life is seriously and negatively affected by air pollution. It causes serious health problems including cancer. Air pollutants can be classified into three groups as ultra-fine particulates, toxic gases and biological pollutants involving viruses and bacteria. Very recent COVID-19 pandemic has clearly showed all humanity how a minute virus-based air pollution could be a human disaster.

In this study, the filtration application of nanofibrous mats to be functionalized with MgO or ZnO nanoparticles have been investigated. Firstly, effect of MgO NP concentration and thickness of nanofiber layer on particulate filtration have been investigated. 25% MgO/PAN filter produced with 60-min electrospinning time have showed high filtration efficiency of 97,6% and low pressure drop of 215 Pa, which meet the face mask standard of EN149+A1. It has been shown that as the nanoparticle concentration in the polymer solution increases; the surface of the nanofiber filter becomes rough, the nanofiber diameters increase, and the particle filtration performance of the filter increases. The increase in filtration efficiency of the filter is related to the adsorption ability of MgO NPs and the decrease in pressure drop value is related to the increased pore size among nanofibers.

Secondly, adsorption studies with toluene gas, one of the toxic volatile organic compounds, have been carried out using MgO/PAN NF with various MgO NP concentrations, various nanofiber layer thicknesses and two different adsorption times. Physical adsorption takes places between toluene gase and MgO NP by the means of hydroxyl and oxide groups on the surface of the nanoparticle. We have achieved a high amount of toluene adsorption of 53.31%.

Antibacterial efficacy of ZnO/PAN filter have been evaluated by using two types of bacteria, gram positive S. aureus and gramnegative E. coli. The antibacterial activity of ZnO NPs was found to be higher against E. coli than S. aureus due to differences in the cell membrane of two different bacteria type.

YÜZ MASKESİ UYGULAMALARI İÇİN FONKSİYONEL NANOLİFLERİN GELİŞTİRİLMESİ VE KARAKTERİZASYONU

ÖZET

Günümüzde hava kirliliği dünya çapında büyük bir sorundur ve hava kirliliğinden dolayı insan yaşamı olumsuz etkilenmektedir. Kanser, astım, akciğer yetmezliği, KOAH dahil ciddi sağlık sorunlarına neden olmaktadır. Dünya Sağlık Örgütünün 2019 yılı raporuna göre dünya nüfusunun %95'inden fazlasının kabul edilebilir limitin altındaki kalitede hava soluduğu bildirilmektedir. 2019 yılı sonu ve 2020 yılının ilk altı ayında tüm dünyanın yaşadığı COVID-19 pandemisi de küçücük bir virüsün nasıl bir hava kirliliğine yol açtığı ve tüm insanlık için ne kadar büyük bir felakete neden olabileceğini göstermiştir.

Hava kirleticileri genel olarak ultra ince parçacıklar, gaz formunda kirleticiler (NOx, SOx, CO, uçucu organik bileşikler…) ve virüslerin ve bakterilerin dahil olduğu biyolojik kirleticiler olarak üç gruba ayrılabilir. Gaz kirleticiler arasında özellikle iç mekanda sıklıkla bulunan, oda sıcaklığında dahi buharlaşabilen, evde kullandığımız birçok ürün vasıtasıyla soluduğumuz havaya karışan uçucu organik bileşiklere yoğunlaşılmıştır.

Bu çalışma kapsamında havada bulunan tüm kirleticilere karşı koruyucu özellikte olabilecek bir yüz maskesi üretmek hedeflenmiştir. MgO veya ZnO nanoparçacıkları ile fonksiyonelleştirilmiş PAN nanolifler filtrasyon uygulamaları için araştırılmıştır. PAN molekülü polar yapısından dolayı kirletici parçacıkları yakalamada diğer polimerlere kıyasla daha etkilidir ve bu sebeple tercih edilmiştir. Geleneksel nanoliflerle partikül kirleticiler büyük oranda yakalanabilmesine karşın daha küçük boyutta olan gaz kirleticilerin yakalanabilmesi için nanolif yüzeyinin işlevselleştirilmesi gerekmektedir. Metal oksit nanoparçık içeren nanolifler bu kapsamda son dönemde kullanılmaya başlanmıştır. MgO nanoparçacık yüzeyindeki yüksek reaktiviteye sahip oksit ve hidroksit iyonları nedeniyle havadaki parçacıkları/gazları gerek kimyasal gerek fiziksel olarak adsorplayabilmektedir. ZnO nanoparçacık ise bakteriler üzerindeki yüksek öldürme etkisinden de dolayı çalışmamızda kullanılmıştır. ZnO nanoparçacıklar üç farklı mekanizma ile bakteri gelişmesini engeller ve bakterilerin ölmesine neden olur. ZnO NPs nanometre boyutunda olduklarından direkt olarak bakterinin hücre duvarından geçerler ve buradaki lipitler, proteinler ve DNA gibi biyolojik maddelerle etkileşerek bakterinin ölmesine neden olurlar. İkinci olarak ZnO NPs bakteri hücresinde asidik ortamda Zn^{+2} iyonuna dönüşürler. Zn^{+2} iyonları ZnO NPs'a göre daha reaktiftir ve daha hızlı bir şekilde bakteri ölümüne yol açar. Son olarak ZnO NPs'lar hidrojen peroksit, süperoksit gibi reaktif oksijen türlerinin oluşmasına yol açarak bakterileri oksidatif strese sokarlar ve bakteri ölümüne neden olurlar.

Yapılan çalışmada ilk olarak, üretilen MgO/PAN ve ZnO/PAN filtrelerin morfolojik karakterizasyonu taramalı elektron mikroskopu (SEM) ile yapılmıştır. Enerji dağılım spektrometresi (EDX) ile MgO nanoparçacıkların lif yüzeyindeki

varlığı ispatlanmış ve lif yüzeyindeki homojen dağılımı gösterilmiştir. Ardından MgO NP konsantrasyonunun ve nanolif tabaka kalınlığının parçacık filtrasyonu üzerindeki etkisi araştırılmıştır. 60 dakikalık elektrospinning süresi ile üretilen 25% MgO/PAN filtresi, EN149+A1 standardını da karşılayan %97,6'lık yüksek filtreleme verimliliği ve 215 Pa'lık düşük basınç düşüşü göstermiştir. Ayrıca nanoliflere eklenen nanoparçacıklar, nanolifin var olan pürüzsüz yüzeyinin bozulmasına, girintili çıkıntılı bir morfoloji elde etmeye, nanolif çaplarındaki artışa ve filtrasyon performansında iyileşmeye neden olmuştur. Elektrospinning süresinin artırılması ile elde edilen lif morfolojiler genel olarak değişmemiş, daha fazla nanolifin üstüste gelmesinden dolayı nanolifler arası por çapının azalmasına neden olmuştur. Bu durum da yüksek filtrasyon verimliliğine karşın aynı zamanda yüksek basınç düşüşü ile sonuçlanmıştır. Çalışmamızda en yüksek filtrasyon performansına, elektrospinning ile kaplama süresi 20 dakika olduğunda ulaşılmıştır.

MgO NP'ların filtrasyon performansına etkisinin iyi anlaşılabilmesi için MgO NPs'lar lif yüzeyine homojen dağılmalı ve nanolif yüzeyinde herhangi bir topaklanma problemi gözlenmemelidir. Çalışmamızda 20% ve 25% MgO/PAN nanoliflerinde istenilen morfolojiye ulaşılmıştır ve bu örnekler filtrenin filtrasyon performansını iyileştirmişlerdir. Filtrasyon performansındaki iyileşme artan nanolif çapına bağlı olarak nanolifler arasında kalan por çaplarının artması ile ilişkilidir. Por çapları arttığı için daha düşük basınç düşüşü elde edilmiştir. Filtrasyon verimliliği artan por çapına bağlı olarak azalmıştır ancak MgO NP'ların yüksek adsorpsiyon yeteneğinden dolayı filtrasyon verimliliği fazla azalmamıştır ve yüksek filtrasyon performansı gösteren filtre üretilmesi başarılmıştır. 30% ve 35% MgO/PAN numunelerindeki topaklanma probleminden dolayı iyi bir filtrasyon performansı gösterememiştir.

Toksik uçucu organik bileşiklerden biri olan toluen gazı ile adsorpsiyon çalışmaları, çeşitli MgO NP konsantrasyonları, çeşitli nanolif tabaka kalınlıkları ve iki farklı adsorpsiyon süresiyle MgO/PAN NF kullanılarak gerçekleştirilmiştir. Bu çalışmada %53,31 oranında yüksek miktarda toluen adsorpsiyonu elde edilmiştir. Nanoparçacık konsantrasyonunun adsorpsiyon üzerindeki büyük etkisi gösterilmiştir. Nanoparçacık konsantrasyonu arttıkça ve nanoparçacıkların yüzeyindeki reaktif iyon sayısı da artmaktadır ve bu durum toluen adsorpsiyon miktarının artmasına yol açmıştır. 13% PAN numunesinde de bir miktar toluen adsorpsiyonu gözlenmiştir. Bu durum toluenin nanoparçacıklara adsorpsiyonu dışında porlar arasında da tutulduğunu ve üretilen filtrenin moleküler elek gibi davrandığını göstermiştir. Filtrasyondan sorumlu nanolif tabaka kalınlığının artması ile toluen adsorpsiyon miktarı artmıştır. Böylece toluen gazının MgO NP yüzeyine adsorpsiyonunun sadece filtre yüzeyinde değil filtrenin iç kısımlarında da gerçekleştiği bulunmuştur. Bunların ötesinde metal oksit nanoparçacıkların katalitik etkisi yaptığımız çalışmada görülmemiştir. Bu durum kullanılan nanoparçacıkların yüksek reaktivite gösteren atom sayısının az olmasından kaynaklandığı düşünülmektedir. Reaktivitenin parçacık boyutu ile yakından ilişkili olduğu bilinmektedir. Bu kapsamda daha küçük partikül çapına sahip nanoparçacıklar ile çalışmanın daha iyi sonuçlar vereceği öngörülmektedir.

Son olarak biyolojik kirleticilerden biri olan ve çeşitlerine bağlı olarak gerek insanlara gerek tüm canlılara hastalık getiren bakterilerin giderilmesine odaklanılmıştır. Bunun için çeşitli ZnO nanoparçacık konsantrasyonlarında ZnO/PAN nanolifleri üretilmiştir. ZnO/PAN filtresinin antibakteriyel etkinliği, gram pozitif S. aureus ve gram negatif E. coli olmak üzere iki tip bakteri kullanılarak değerlendirilmiştir.

ZnO NP'lerin E. coli'ye karşı antibakteriyel aktivitesinin S. aureus'tan daha yüksek olduğu bulunmuştur. Bu durum iki tip bakterinin sahip olduğu farklı hücre duvarı yapıları ile ilişkili olduğu düşünülmüştür.

Yaptığımız çalışma ile nanoliflerin nanoparçacıklar ile işlevselleştirilmesi sonucunda hem partikül, hem gaz, hem de bakterilere karşı koruyucu olacak bir yüz maskesi aktif tabakasının üretilebileceği gösterilmiştir.

1. INTRODUCTION

1.1 Air Pollution

Air is a natural resource and clean air is required for processes such as breathing, digestion and photosynthesis, which are vital for living things. In general, depending on urbanization, rapid population growth and industrialization, the deterioration of the natural composition of the air and ecological balance, which causes negative effects on humans and living things, is called air pollution [1].

There are various types of pollutants in the air. These pollutants can be found in the atmosphere as dust, smoke, gas, odor and impure water vapor. Unfortunately, industrial applications lead to pollution in the air because the released chemicals are not adequately filtered. Wars have also been increasing the number of particles and toxic gases in the air. Wood, coal, fuel oil and natural gas are usually burned for heating purposes or industrial applications and, as a result, volatile organic compounds (VOCs) and small particles are inevitably released into the atmosphere. Many VOCs are harmful air pollutants. Examples of volatile organic compounds are gasoline, benzene, formaldehyde, and solvents such as toluene and xylene, styrene. Types of pollutants have been classified in Figure 1.1 [2,3].

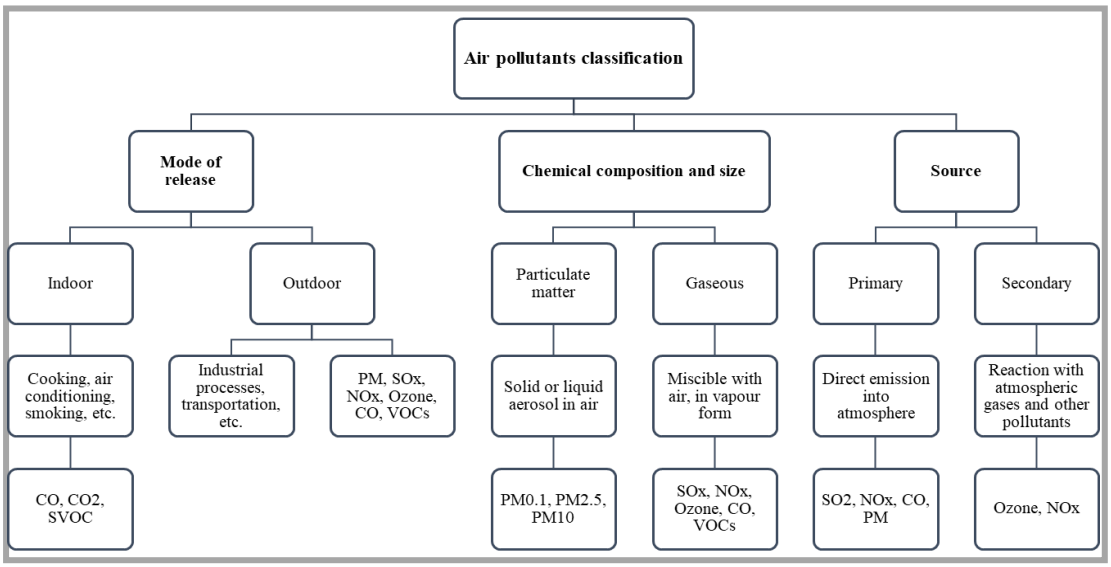

Figure 1.1 : Classification of air pollutants [3].

When the air pollution reaches a certain concentration, it starts to damage human health. Millions of people have serious health problems such as eye and respiratory tract irritation, respiratory distress, chest tightness, asthma, and heart disease, which stem from airborne particle pollution and toxic pollutants in the air.

In addition, prolonged exposure to air pollution can lead to an increased risk of developing cancer due to the weakening of the immune system and serious damage to the nervous, reproductive, and respiratory systems. In extreme exposures, this can even result in death [4].

In our study, we worked on the removal of particulate pollutants, volatile organic compounds (VOCs) and biological pollutants.

The size of the pollutant is one of the substantial parameters in filtration. The smaller the pollutant size, the more difficult it is for the filter to hold it. While particulates larger than 10 micrometers can be captured by conventional filters, more complex systems are required to capture smaller particles. The sizes of some important pollutants are shown in Figure 1.2.

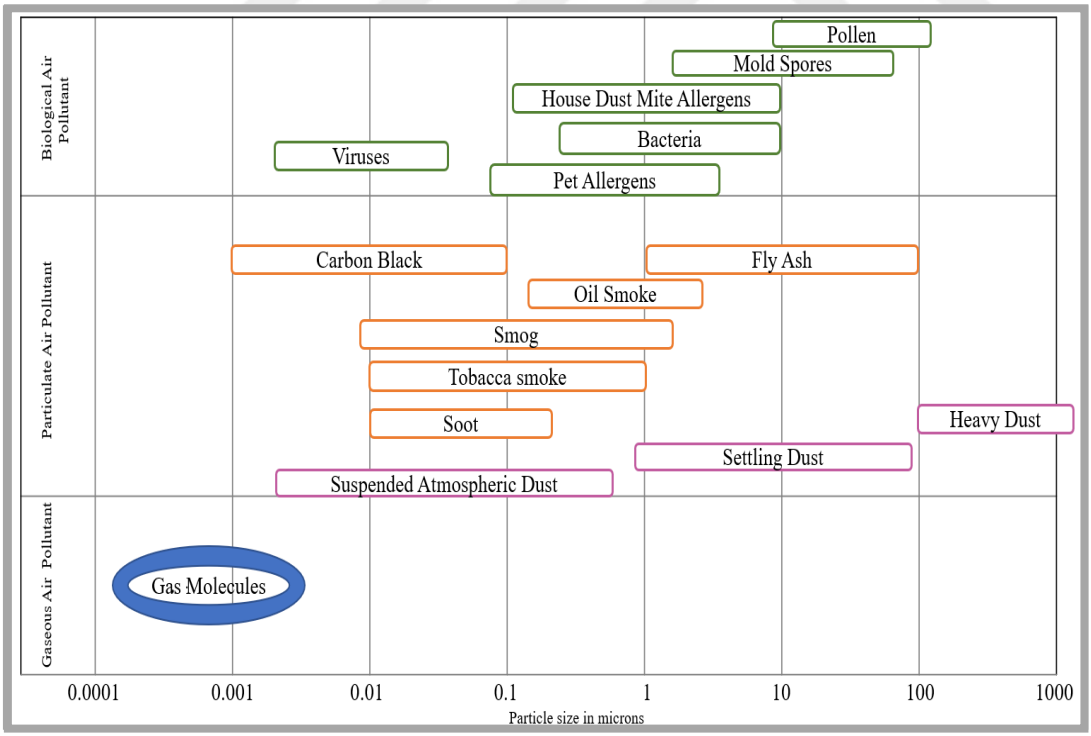

Figure 1.2 : Sizes of pollutants.

1.1.1 Particulate Matter

Particulate matter (PM), defined as solid or liquid aerosols in the air, is released into the air as a result of many factors such as emissions from the production industry,

fuel-based vehicles, heating, manufacturing facilities, fires of wild land, dust storms, volcanic eruptions etc. and unfortunately, it causes about 800,000 premature deaths each year [5,6].

The particle sizes suspended in the air are different and are roughly classified as PM2.5 and PM10 (particulates with an aerodynamic diameter of less than 2.5 and 10 micrometers, respectively). In addition, particles smaller than 0.1 μm in diameter are called ultra-fine particles, particles smaller than 1 μm are called fine particles and particles larger than 1 μm are called coarse particles [4].

The environmental and health effects of the particles may vary depending on their concentration, particle size, structure and chemical composition [7]. For example, the size of the particles effects the deposition area in which the particulates accumulate. The most dangerous particles are PM2.5. They can even reach the human blood circulation. They cause serious health problems such as lung cancer, asthma. In order for humans to live healthy, these materials must be filtered and removed [4,5].

1.1.2 Volatile Organic Compounds (VOCs)

Volatile organic compounds (VOCs) are known as odor molecules and they are complex molecules, usually compounds of elements such as carbon, oxygen, hydrogen, nitrogen, and sulfur. They are in the class of gaseous pollutants. They are one of the main sources of photochemical reactions that cause various environmental hazards in the atmosphere. Most solvent thinners, degreasers, cleaners, lubricants, and liquid fuels release VOCs [8].

Although most gaseous pollutants mainly affect the respiratory system, they can trigger hematological problems and cancer [4]. Even in the residential buildings, the concentration of VOCs has reached to notable value (Figure 1.3) [9]. For a livable world, it is necessary to limit and control vapor emissions that cause climate change, affect the growth and decay of plants, and health of humans and all animals [8].

The particles in the air are easily trapped by the nanofiber filters because they have small pore sizes, small fiber diameters and high surface area. By functioning the surface of the nanofiber filter, toxic gases and VOCs in the air can be adsorbed on the nanofiber surface either physically or chemically. VOCs can harm the human body when exposed to long-term exposure even at very low concentrations (ppm levels); For this reason, the usage of effective adsorbents such as activated carbon,

graphite, activated carbon nanofiber, and polymers are an important issue for the removal of VOCs [10].

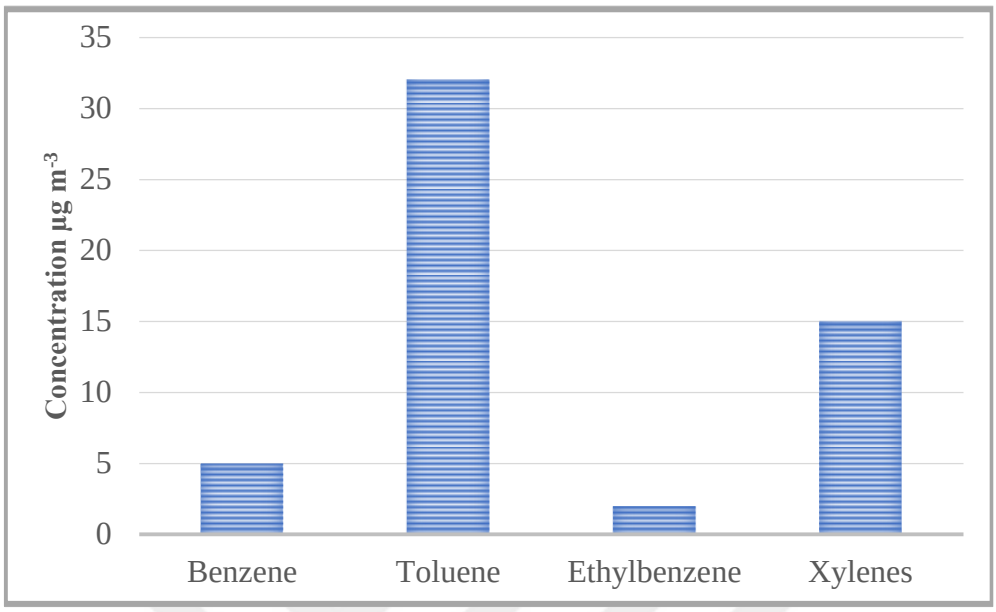

Figure 1.3 : The average concentration of some important VOCs in residential building/homes in Europe [9].

The maximum capacity for gas adsorption is closely related to the specific surface area of the material used, the pore size, pore size structure and the chemical affinity between the adsorbents and the VOC contaminants. Thus, the adsorbent materials must be chemically and thermally treated to form micro-and-meso sized pores. In addition, the adsorbate polarity, boiling point, density and molecular structure affect adsorption capacity (Figure 1.4) [11,12].

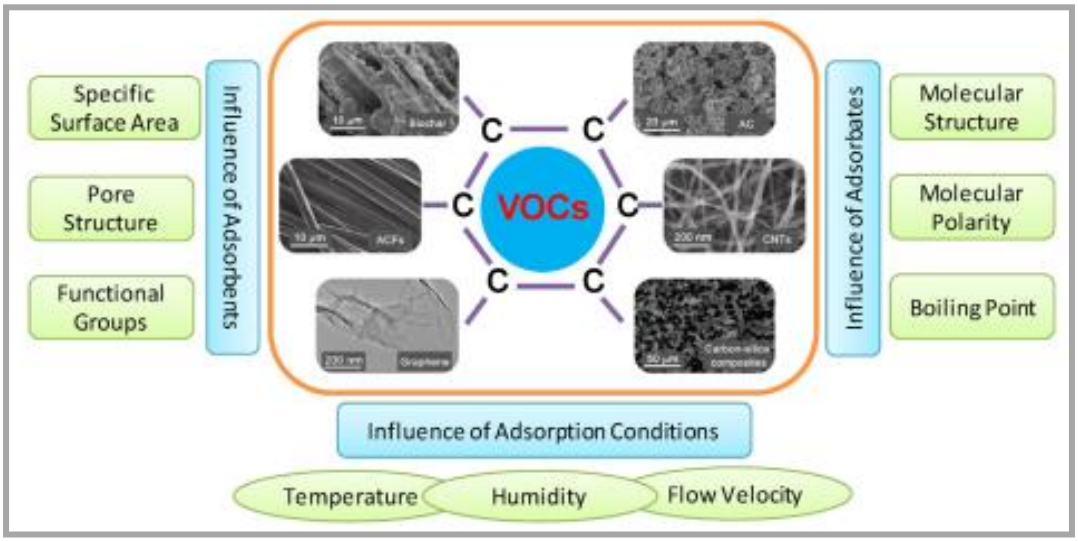

Figure 1.4 : Parameters that affect the adsorption process [12]

1.1.3 Biological Pollutants

Bacteria, viruses, mites, fungi, algae, and pollen are biological pollutants. These organisms reproduce quickly when basic conditions such as proper humidity, nutrients and temperature are available. To reduce biological pollutants in an environment, it is necessary to control the relative humidity level (30-50% is ideal for home) and temperature. Since many biological contaminants are very small, they are inhaled, causing serious health problem such as sneezing, watery eyes, coughing, shortness of breath, dizziness, and lethargy etc [13].

Bacteria are single-celled prokaryotic microorganisms that vary in size ranging from 0.1μm to 10μm. Although there are many different classifications, they are generally classified as gram-positive bacteria and gram-negative bacteria depending on whether they are stained with gram stain or not. Also, their cell wall composition is different.

Gram-positive bacteria have a thick layer of peptidoglycan on the cell walls. When exposed to gram staining procedure, they become purple. On the other hand, on the cell walls of gram-negative bacteria, there is a thin layer of peptidoglycan and an outer filter that is composed of lipopolysaccharide (LPS) molecules. When subjected to gram staining procedure, they become pink. The differences in cell wall composition of these two classes of bacteria can be seen in Figure 1.5 [14].

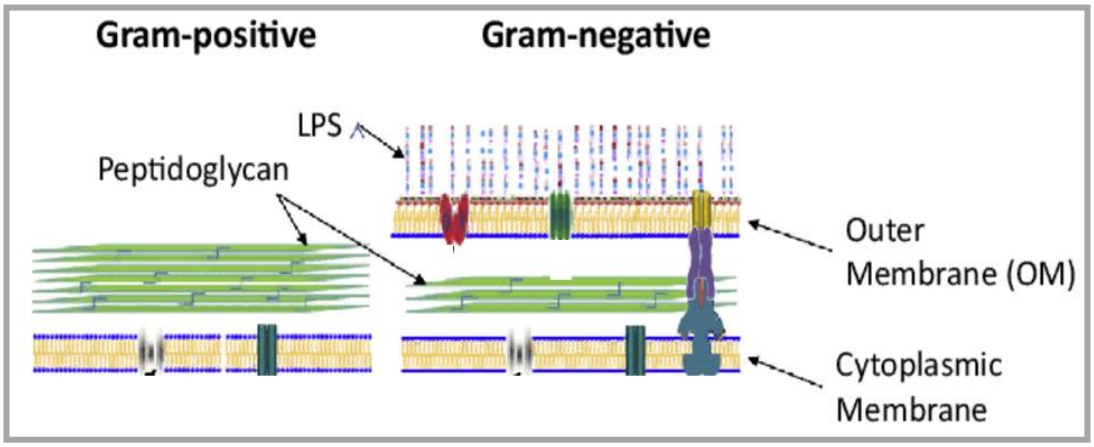

Figure 1.5 : The differences in the cell wall composition between gram-positive bacteria and gram-negative bacteria [14].

Some gram-positive and gram-negative bacteria are shown in Table 1.1 In our antibacterial studies, *Escherichia coli* was used as gram-negative bacteria and *Staphylococcus aureus* was used as gram-positive bacteria.

Despite the presence in the normal flora of the intestinal tract of human and warm-blooded animals, *E. coli* causes diarrheal diseases, especially urinary tract infections, meningitis, peritonitis, mastitis, septicemia when they infect us. Besides that, *S. aureus* is a highly virulent pathogen that causes meningitis, septicemia, pimples, abscesses, pus collection and significant food poisoning [15,16].

Table 1.1 : Some gram-positive and gram-negative bacteria.

GRAM-POSITIVE	GRAM-NEGATIVE
S. aureus	*Escherichia coli*
S. epidermidis	*Pseudomonas*
Bacillus cereus	*Enterobacteriaceae*
Clostridium perfringens	*Salmonella*

Some antibacterial compounds such as hypochlorites, peroxides, phenolic compounds (triclosan, trichlorophenol), dense alcohols (ethanol), metal oxides, and metal oxide nanoparticles can be used to be protected from these bacterial infections. In our study, we have added some metal oxide nanoparticles to the polymer solution to obtain an antibacterial filter.

This study had started much earlier than COVID-19 Pandemic, but it has reached to an end during the harsh days of nationwide lockdown and precautions. Facemask is an essential part of combat against COVID-19. It has been realized that there is a lack of knowledge about properties, production and use of face masks. Therefore, it is hoped that this work will add some scientific light onto the production of nanofiber-based facemasks.

1.2 Personal Protective Equipment Against Air Pollution

Respiratory protectors/face masks are used to protect against airborne pollutants. It is roughly divided into two group as dust masks and gas masks [17,18].

1.2.1 Dust Masks

Dust masks are the respiratory protecting equipment designed to provide protection against solid and liquid aerosols/particles consisting mainly of filter material covering the mouth, nose, and jaw. Face masks must be manufactured in accordance with the relevant standards (EN 149: 2001 + A1 2009). It was adopted by Turkey and has been in force (TS EN 149 + A1, July 2010) [17,18]. The face mask to be

produced must comply with the filtration performance criteria determined in the EN 149: 2001 + A1 2009 standard (Table 1.2).

Table 1.2 : Face mask types and the required performance criteria to be in compliance with EN 149: 2001 + A1 2009 standard.

Type of Face Mask	Flow Rate: 95 l/min	
	Filtration Efficiency	**Breathing Resistance (Inhalation)**
FFP1	≥ 80 %	0.21 kPa
FFP2	≥ 94 %	0.24 kPa
FFP3	≥ 99 %	0.3 kPa

It can be produced, marketed, and used by getting CE certificate after being tested by the organizations approved and authorized by European Union. Filters produced according to the standard provide protection in 3 categories. They are FFP1, FFP2 and FFP3 (Figure 1.6) [17,18].

FFP1 Dust Masks: It is used against dust with a MAC (Maximum Allowed Concentration) value greater than 5 mg/m^3. These dusts are nontoxic dusts generally produced by mechanical work such as sawing and grinding. Besides, it protects against solid and liquid aerosols [17,18].

Maximum Allowed Concentration (MAC): It is the maximum concentration of chemicals that is allowed to be present in a closed workplace for 8 hours per day and 45 hours per week. Lower concentrations than this value does not damage the health of the employees throughout the day. So, the MAC value indicates the limit that the chemical agent should never exceed in the environment. The term MAC is generally used for chemicals that have a toxic effect. [19].

FFP2 Dust Masks: It is used against dust with a MAC value greater than 0.1 mg/m^3 and toxic fine dusts, fumes, and fogs of MAC value of between 0.1 mg/m^3 to 5 mg/m^3. Besides, it protects against solid and liquid aerosols. It ensures higher protection than FFP1 [17,18].

FFP3 Dust Masks: It provides the highest protection when compared to other dust masks. It provides protection against toxic, radioactive, carcinogenic fine dusts with a MAC value of less than 0.1 mg/m^3. Besides, it protects against solid and liquid aerosols [17,18].

Figure 1.6 : FFP1, FFP2 and FFP3 face masks respectively.

1.2.2 Gas masks

In gas masks, contaminated air passes through the gas filter (cartridge) and, thus, the mask user breathes fresh/clean air. A cartridge filled with sorbent is used to absorb harmful gases. Once the sorbent has reached saturation, it cannot absorb any more toxic gas, and the wearer of the mask starts to breathe contaminated air and the mask loses its protective effect. Therefore, the life of gas masks is limited and the service life varies depending on concentration of toxic gas, sorbent used, and ambient conditions such as air flow rate, temperature, humidity [20].

2. NANOFIBERS AND THEIR PRODUCTION METHODS

2.1 Definition of Nanofibers

With the spread of nanoscience and nanotechnology, researchers have been demonstrating great interest in studying the superior properties of nano-sized materials, especially nanofibers. Nanofiber is a type of fiber having a diameter between 1 and 100 nm and high specific surface area that can reach up to 1000 m^2/g [21]. Nanofibers can also be defined as a nano-material having a diameter below 1μm (Figure 2.1) [22]. Nanofibers are 1D nanostructured materials whose one dimension is outside of the nanometric size, which compared to their diameters, their lengths are extremely long [23,24].

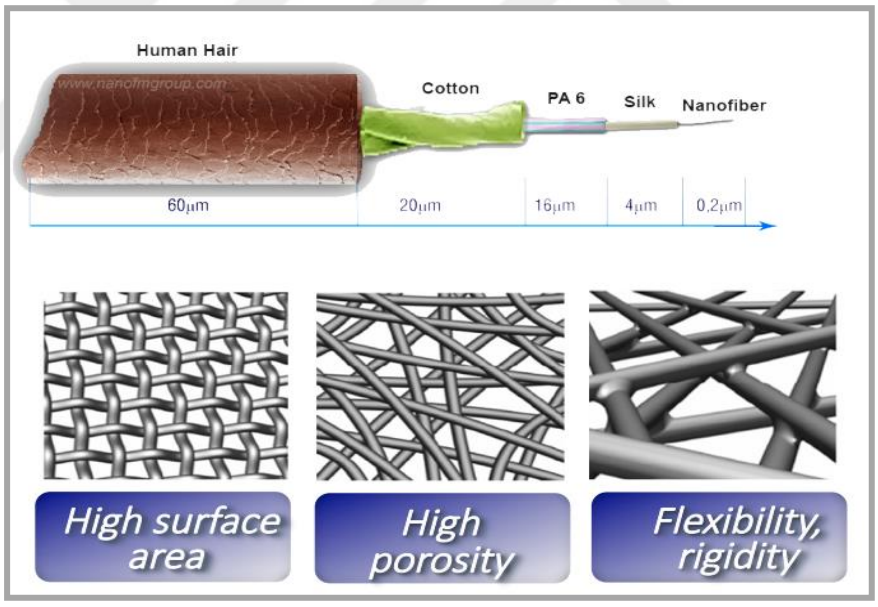

Figure 2.1 : Diameter and specific properties of nanofibers [25].

It is known that nanofibers were first produced by William Gilbert (1544-1603) who observed that when water drop on a dry surface was exposed to an electrical charged amber, it turned into a cone shape which is now called Taylor Cone. After that most scientists and inventors such as Lord Rayleigh, Charles Vernon Boys, John Francis and Anton Formhals worked on this subject and became leaders in the progression of electrospinning nanofibers. Subsequently, Doshi and Reneker made electrospinning popular in 1995 [26].

Nanofibers are produced from various organic and inorganic polymers such as polyacrylonitrile, polyamides, polyurethanes, polyimides, polyvinyl alcohol, polystyrene, pHEMA, chitosan, co-polymers, polymers containing various additives, silica, nanoparticles and others [27].

As mentioned previously, nanofibers have excellent features and that is why they are still most popular in many application areas. A huge number of studies about nanofibers are being published every day and many novel application fields are being explored.

2.2 Properties of Nanofibers

Nanofibers have some unique properties such as high specific surface area, high porosity (up to over 80%), low basis weight, small pore size, their ability to be embedded within other media, and possibility of production in different structures. Therefore, these fibers are recommended for a wide variety of applications [28] such as biomedical applications [29–31] (tissue engineering, controlled drug release, medical prostheses), filtration [32,33], composite [34–36], electrical and optic [37], [38], protective clothing [39,40], and environmental applications [41–43] (Figure 2.2).

In the Table 2.1 a comparison among conventional fibers, melt blown fibers and nanofibers is presented [27].

Table 2.1 : Comparison of conventional fibers, melt blown fibers and nanofibers [27].

Fibers	Fiber Diameter (µm)	Linear Density (dtex)	Specific Surface Area (m^2/g)
Conventional	10-40	1-30	ca. 0.2
Melt-Blown	1-5	ca. 0.01	ca. 2
Nanofibers	0.05-0.5	ca. 0.0001	ca. 20

The excellent specific surface area, together with small fiber diameters, allows the materials to interact quickly with the surrounding environment. For this reason, they are used in filters, membranes, wound dressings, chemical and biological protective clothing, energy storage and sensors [44].

Recently, so many new type nanofibers including some supporting materials such as Au, Ag, TiO_2, MgO, MnO_2 Al_2O_3, ZnO, and Fe_2O_3 have been produced to obtain multifunctional nanofibers. In this way nanofibers are given additional features as biodegradability, hydrophobicity, photocatalytic and electrical conductivity. Therefore, they can be used in more specific applications such as biological sensing, capacitors, gas filtration, photocatalysis and energy generation/storage [37,45].

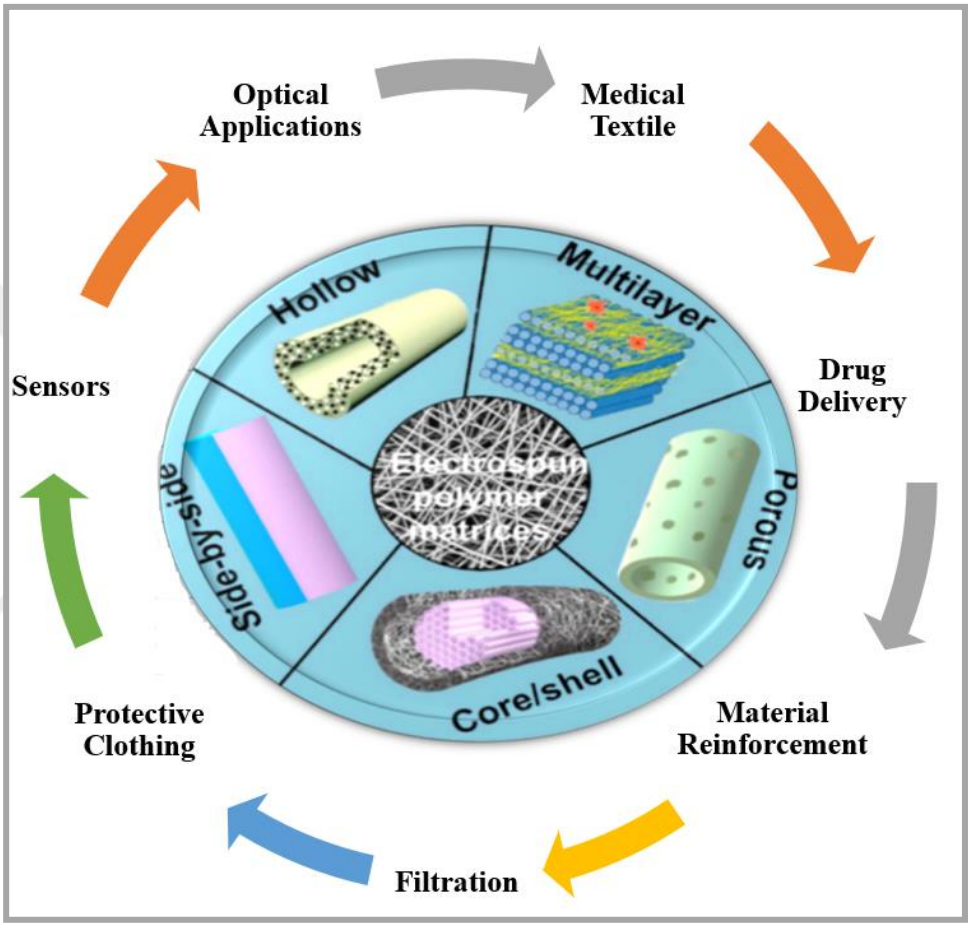

Figure 2.2 : Possible structures and application areas of nanofibers [46].

2.3 Production Techniques for Nanofibers

Nanofibers have become a popular research topic in recent years in academia and industry. According to the 'Nanofibers Market Size: Share and Trends Analysis Report' [47], the nanofiber market size is given as USD 477.7 million in 2016 and this number will increase exponentially depending on the growing industrial activities. When the fiber diameter is reduced to nanoscale, it has a high specific surface area and more functionality and excellent mechanical performance. To fabricate the polymer nanofibers, there are many methods such as drawing, template

synthesis, phase separation, self-assembly, electrospinning, solution blowing, centrifugal spinning, etc. Among them electrospinning, solution blowing, and centrifugal spinning have recently become frequently preferred methods. When choosing one of these methods; the desired nanofiber alignment, cost, quantity, and desired morphology of nanofiber materials are factors that need to be considered. For example, electrospinning or direct coaxial spinning to produce hollow nanofibers, or phase separation to produce porous nanofibers, should be preferred [48].

2.3.1 Conventional Methods

2.3.1.1 Template synthesis:

In the template synthesis, a nano-porous membrane is used as a template to get nanofibers from various materials such as conductive polymers, metals, semiconductors and carbon [49]. Briefly, the polymer solution passes through the nanopores in the template under the influence of water pressure and rapidly solidifies and nanofibers are formed (Figure 2.3) [48].

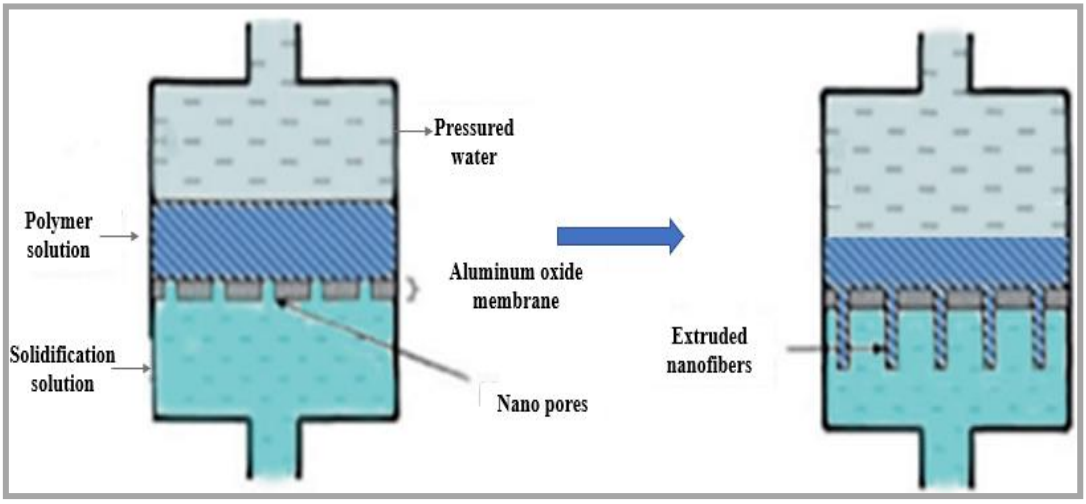

Figure 2.3 : Illustration of template synthesis method [48].

Final fiber size is strongly dependent on the pore size in the template used and the porosity of the obtained nanofibers is low [46].

2.3.1.2 Phase separation:

In the phase separation process, the polymer is dissolved in the proper solvent and phase separation step is started either thermal way or adding a non-solvent into prepared solution, to form gel. Under this condition the solution is thermodynamically unstable, so it can separate into two phases (polymer-rich phase

and polymer-poor phase). As a non-solvent, generally water is used, and it extracts the solvent from the gel. By decreasing temperature, polymer-rich phase solidifies and a porous nanofibers form with dimensions from 50 to 500 nm (Figure 2.4) [49,50].

This method is simple and requires only basic apparatuses, but it is only suitable for a few polymers and provides low yields [49,50].

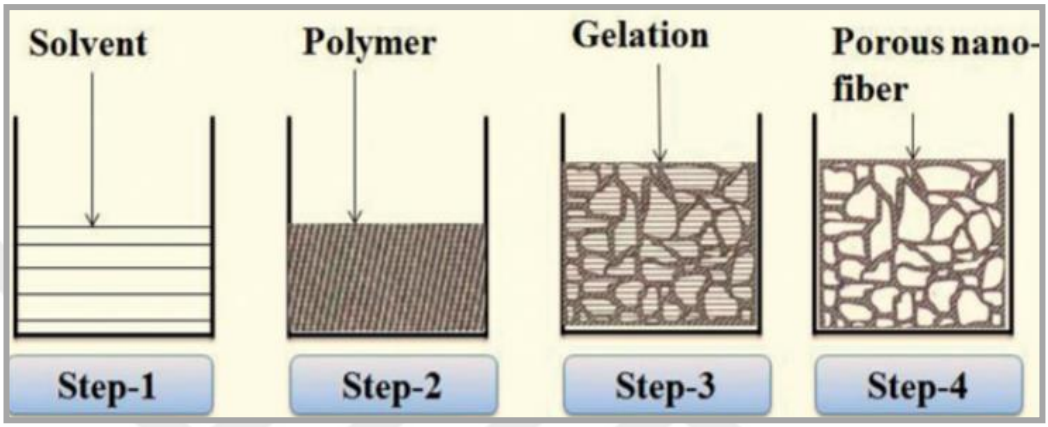

Figure 2.4 : Illustration of phase separation method [51].

2.3.1.3 Drawing:

There are three main steps in this technique. (1) a drop of polymer solution is dropped on the substrate material, (2) the micropipette is dipped into polymer droplet, (3) contact and by moving of micropipette backward, the fiber is drawn from the polymer drop to a certain rate (~10^{-4} m/s) (Figure 2.5) [48,51].

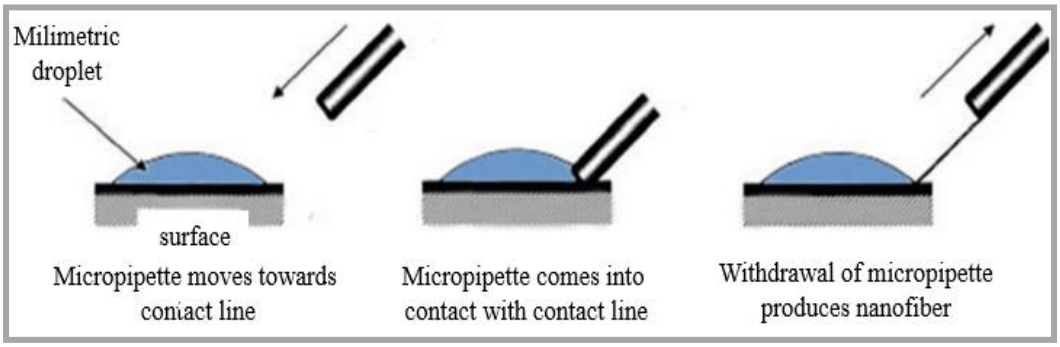

Figure 2.5 : Illustration of drawing method [48].

Uniform nanofibers with certain size can be obtained by adjusting the drawing speed and viscosity of the solution thoroughly. The resulting fiber diameter is in the range of 2-100 nm to several micrometers; and the length is from 10 mm to several centimeters [48,51].

The drawing method does not apply to all polymers (viscoelastic polymers only) and forms a very long single fiber. Whilst it requires more time, productivity is low. It enables to lab-scale production [48,51].

2.3.2 Modern methods

2.3.2.1 Electrospinning:

The electrospinning process is the most known and established method to fabricate nanofibers. In the electrospinning process, nanofiber (NF) is produced from polymer solutions or polymer melts with the help of electrostatic and coulombic forces. The main feature that distinguishes this method from others is that the diameters of the produced fibers can be easily adjusted by changing production parameters. It is easy to operate and relatively low costs [52].

The electrospinning method is as illustrated in Figure 2.6**.** It consists mainly of the feed unit, syringe, drum collector and high voltage power supply.

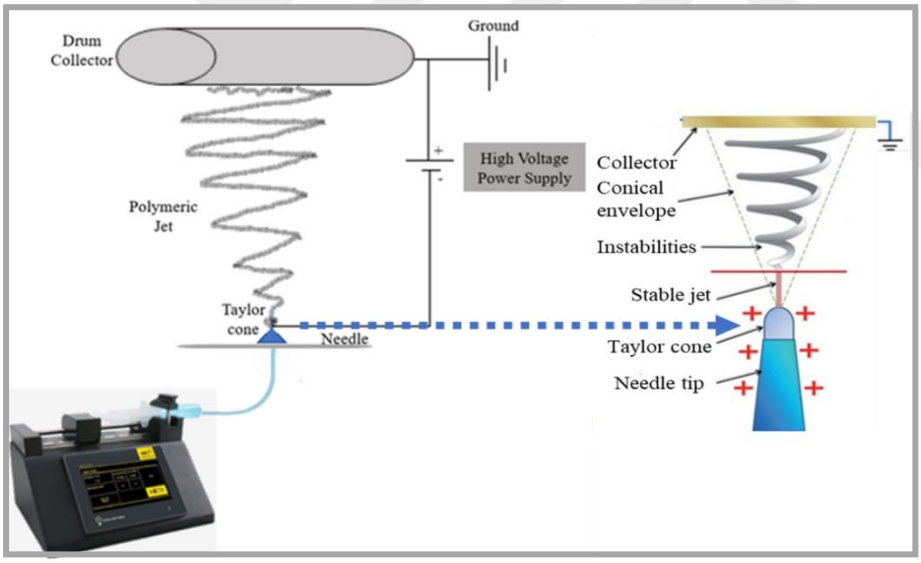

Figure 2.6 : Illustration of electrospinning set-up.

In this method, the polymer is either melted by heat or dissolved in any suitable solvent. Then it is pumped to tip of the needle by a suitable syringe pump. When high-voltage electrostatic forces applied overcome the surface tension of the droplet on the needle, hemispherical shape of droplet starts to transform, and it takes conic shaped, called Taylor Cone. In the case of exceeding the critical voltage, firstly stable straight jet is observed near the tip of the needle. If a polymer solution with a low viscosity is used, two or more jets occur from droplet due to the longitudinal

Rayleigh instability caused by surface tension. So, polymer solution with optimum viscosity must be prepared to get only one jet [53]. This jet is stretching and whipping under electrostatic forces and solvent used evaporates during the process. Secondly, depending on the further stretching of jet, it enters an unstable bending stage and the trajectory of the jet increases until it reaches the collector. Thus, the size of the fiber becomes tapered as the solvent evaporates and the path of the jet increases. Finally, solid-fibers are obtained in the size of varying from nanometer to micrometer on the grounded collector [46].

There are many parameters in the electrospinning which affect the final properties of nanofibers. All of these can be categorized into 3 main groups such as process parameters, solution parameters and ambient parameters. Their effects on nanofibers morphology is shown in Table 2.2.

Table 2.2 : Electrospinning parameters and their effects on the fiber morphology.

PARAMETERS		Fiber Morphology
Solution Parameters	**Solution Concentration & Viscosity**	**Low:** Decrease in fiber diameter, Bead generation [54]–[56] **High:** Increase in fiber diameter and uniform fiber morphology without beads [54]–[56]
	Conductivity	**Low:** Bead generation [57] **High:** Decrease in fiber diameter and uniform fiber morphology without beads [57]
	Surface Tension	**High:** Cause jet instability and generation of sprayed droplets [58]
Process Parameters	**Applied Voltage**	Effect of applied voltage on nanofiber diameter is not very clear [59]–[62]
	Flow Rate	**High:** Increase in fiber diameter, Bead generation [65,66] **Low:** Decrease in fiber diameter [65,66]
	Tip to Collector Distance	**High:** Decrease in fiber diameter [59]
	Time	**High:** Increase in packing density and solidity of fiber and decrease in pore size among fibers [33,39,67]
	Collector Type (Drum, Plate, Cocoon, Disc)	Strongly determine the final morphology of NF [58]
Ambient Parameters	**Temperature**	**High:** Decrease in fiber diameter [66]
	Humidity	**High:** Increase in the number, diameter, and distribution of the pores [67]

With this relatively simple technique, nanofibers of different diameters have been produced from more than 100 different natural and synthetic organic polymers [25], [46]. Electrospun nanofibers produced nowadays are based not only on polymers, but also on ceramics, metals, metal oxides, organic and inorganic composite systems. These electrospun membranes composed of copolymers, mixtures or organic fillers, always display improved mechanical behavior, barrier properties and thermal stability [54,55].

There are various fabrication techniques for producing nanofiber bio-composite nanofibers through electrospinning (Figure 2.7). In this way, nanofibers with various morphology can be produced [70].

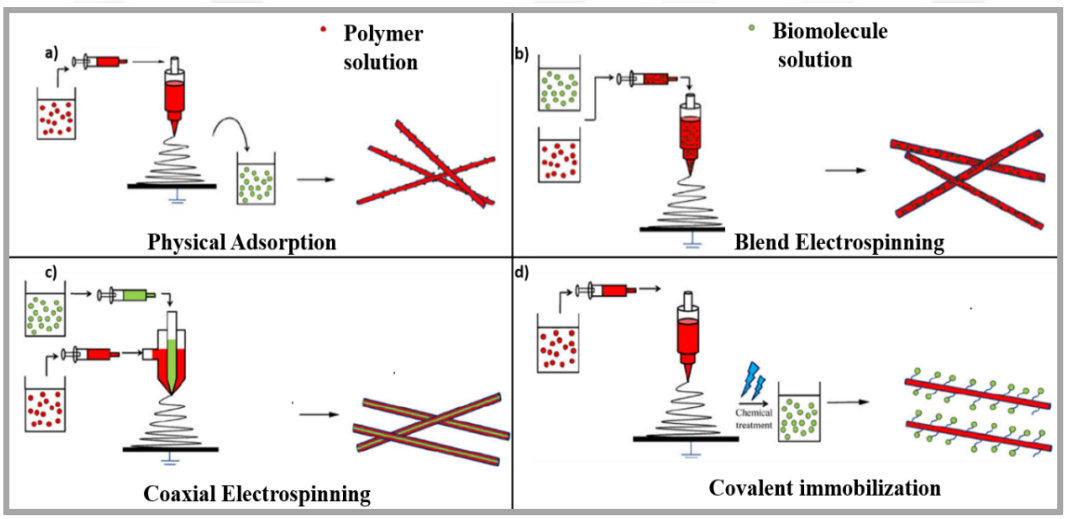

Figure 2.7 : Fabrication techniques of bio-composite electrospun nanofiber. a) physical adsorption; b) blend electrospinning; c) coaxial electrospinning; d) covalent immobilization [70]**.**

The fabrication techniques of bio-composite electrospun nanofiber has been briefly explained as follows.

- **Physical adsorption**: The nanofibers produced are immersed in an aqueous phase containing biomolecules, and the charged biomolecules are attached to the nanofibers by physical adsorption as a result of electrostatic forces [70].
- **Blend electrospinning:** Biomolecules are added to the polymer solution, then the obtained solution is used to produce a hybrid structure by electrospinning [71].
- **Coaxial electrospinning**: Two different solutions (i.e. polymer solution and other solution type) are coaxially and simultaneously electrospun through

different feed channels in one needle to produce composite nanofibers with core shell structures [72,73].

- **Covalent immobilization**: Biomolecules are immobilized onto the fiber surface via covalent bond, i.e., forming peptide bond through amino groups [74].

2.3.2.2 Solution blowing:

Solution blowing (SB) is one of the modern nanofiber production processes. In this process, the polymer solution is prepared and while it is fed through the inner nozzle at constant rate, gas flow with high velocity is sent simultaneously through the outer nozzle. Drag forces created at the gas/solution interface cause formation of multiple jets of polymer solution towards a collector. The jets are then attenuated using high speed air streams, which lead to a large decline in jet diameters. The carrier solvent evaporates rapidly. Eventually, randomly oriented fine nanofibers are deposited on the surface of the collector (Figure 2.8). SB is also about 10 times faster than traditional electrospinning (10 ml/h/nozzle vs. 1 ml/h/nozzle) [75]. So, it lets the production of nanofibers for industrial purposes [21,76].

SB does not require electric field and uses a simple apparatus. Therefore, the method is inexpensive, portable and easily applicable using hand-held equipment [77].

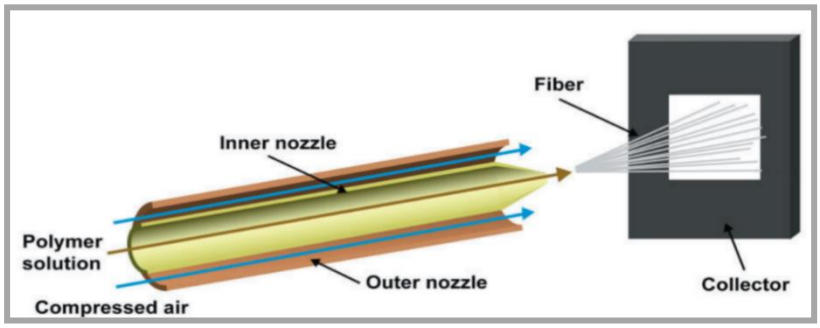

Figure 2.8 : Schematic presentation of solution blowing method [75].

As mentioned above, more than 100 different polymers have been successfully converted to nanofibers by electrospinning so far. Yet, nanofibers cannot be still fabricated from many polymer solutions due to the extremely high viscosity. Since the viscosity generally decreases with increasing temperature, this problem is overcome by using the SB method with the help of a hot air stream [25]. Moreover, in the SB method, there is no electrostatic restrictions and solvent limitation due to the dielectric constant and conductivity, and voltage sensitive polymers can also be

used [78,79]. Finally, we can say that SB is much safer than electrospinning due to not being dependent on high electric potential [75]. As one of the disadvantages of this method, formation of beads can be mentioned.

Nanofiber production in the SB method depends on; the solution variables such as molecular weight of the polymer, the concentration, surface tension and viscosity of the polymer solution; the process variables such as gas/air pressure and polymer solution feed rate and tip-to-collector distance; system variables nozzle diameter and geometry; and finally, the environmental variables such as ambient temperature, pressure and humidity. These parameters have a direct effect on the formation of a fiber-producing polymer jet [76,77].

2.3.2.3 Centrifugal spinning

Centrifugal spinning is also another modern nanofiber fabrication method. It is known as rotary jet spinning, rotor spinning, and force-spinning in literature [80].

In this method, the polymer solution is placed on a rotating spinning head. When the rotating speed reaches a critical value, the centrifugal force overcomes the surface tension of the polymer solution and liquid jets are ejected from the tip of the nozzles. Especially with effect of centrifugal force and air friction force, polymer jets are elongated and that leads to nanofiber formation. In addition, other forces such as rheological force, surface tension and gravity force also contribute to nanofiber formation. Stretched jets accumulate on the collector surface and form a non-woven mat from nanofibers (Figure 2.9) [81].

In centrifugal spinning method, high capacity for industrial production can be obtained with low power consumption.

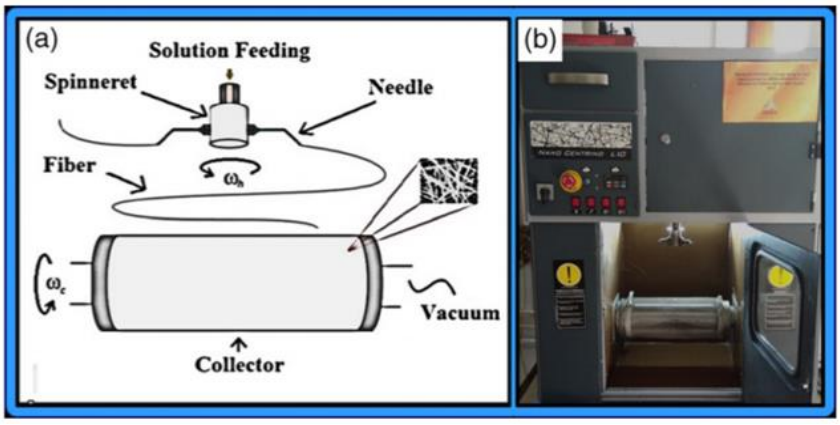

Figure 2.9 : (a) Schematic representation of the centrifugal spinning method and (b) The NanoCentrino L1.0 setup [82].

The diameter, porosity and morphology of nanofibers can be controlled by changing the process parameters such as nozzle geometry, rotation speed, orifice diameters; environmental parameters such as temperature and humidity; and properties of polymer solution (viscosity, polymer type and concentration, molecular weight of polymer, surface tension and evaporation rate of solvent). Highly aligned and defect-free nanofibers can be fabricated [77,82,83].

3. NANOFIBERS FOR FACE MASKS

3.1 Properties of Nanofibers Used as Air Filters

One of the promising filter materials is nanofibrous membranes because they have a high surface area/volume ratio, small fiber diameter and high porosity. By randomly overlapping the nanofibers, nanoscale pores can be obtained, thus allowing even micron and nano-aerosol filtration [85]. Furthermore, the nanofibrous filters have advantages such as low basis weight, thickness of nanofiber layer possible combinations with active chemical/functionality, and high permeability [86].

In addition, low pressure drop values can be obtained as a result of the air slip effect in nanofiber filters compared to microfiber filters [32]. In many studies, nanofibers have been shown to increase the efficiency of conventional materials used for filtering and separating particulate materials [87]. Gundogdu et al., have proved that nanofiber air filters show as much filtration efficiency as HEPA filters [88].

High filtration efficiency and low pressure drop are expected from the air filters [89]. Since high filtration efficiency generally causes high pressure drop, benefit-cost performance of filter is evaluated by quality factor (Q factor) [90,91]. It is well known for filtration application that as the fiber diameter decreases, filtration performance is greatly improved [92].

Pore size significantly affects the pressure drop of the filter. With smaller pore size, high filtration efficiency can be achieved, while air permeability and pressure drop of the filter are negatively affected. However, less pressure drop can be obtained if high porosity can be achieved simultaneously. Therefore, high-porous and low pore size nanofibers with small fiber diameters should be produced [3], and the desired properties can be obtained by electrospinning method by adjusting the relevant parameters.

Moreover, toxic gases and VOCs in the air can be adsorbed to the nanofiber surface by functionalizing the surface of the nanofiber filter. The specific surface area of the material, pore size distribution, and chemical affinity between adsorbents and VOC

pollutants are crucial for gas adsorption. Creating micro-meso pores (micropores, <2 nm; mesopores, 2-50 nm) on the nanofiber surface improves adsorption. For this, chemical and thermal methods can be used (activation and carbonization processes, addition of functional materials into nanofiber surface etc.) [10].

3.2 Properties of Nanofibers Used as Face Masks

Protective clothing such as face masks must have some characteristic features such as permeability specifications, resistance to diffusion by specific liquids, flammability, mechanical endurance, mechanical strength properties and wearer comfort [86].

There are five basic features that a typical protective medical face masks should have:

1. Bacterial filtration efficiency
2. Submicron particle filtration
3. Low differential pressure (an indicator of breathing comfort)
4. Liquid penetration resistance (to protect the user from blood contamination)
5. Flammability [86]

In order to provide strength and durability, nanofiber mats should be used in a layered structure with some support materials such as non-woven substrate. Therefore, the nanofiber mat should be flexible and provide good adhesion without delaminating and breaking from the substrate. For example, effective barrier materials such as protective clothes, face masks and filters against nanoparticulate aerosols, pesticides or chemical warfare agents are successfully produced by coating nonwovens with the electrospinning technique [55].

A nanofibrous composite face mask generally consists of an inner layer, one or more melt blown fiber layers, a porous film layer and an outer layer. Melt blown fiber layers provide aerosol filtration performance, while the porous film layer provides fluid resistance.

The remaining layers are used to minimize abrasion and increase the comfort of the user. Adsorptive materials can be incorporated into face mask to hold the toxic gases/chemical warfare agents [86].

While high filtration performance and resistance to liquid penetration are expected from face masks, they should also have features such as air permeability and water vapor transmission for the thermal comfort of the user [93].

According to Chinese National Standards, pressure drop in respiratory filters should be less than 147 Pa and it is very difficult to obtain this pressure drop value with high filtration efficiency [3]. Beyond that, there is still a need to investigate the durability and wearing comfort of nanofiber-based protective clothing [57,93].

3.3 Nanofiber Production Parameters and Nanofiber Properties Affecting the Air Filtration and Face Mask Performance

Main advantages of electrospinning for air-filter production is that the morphology and diameter of electrospun fibers can be adjusted. The morphology and size of nanofibers can significantly affect the filtration efficiency of the resulting filter [94].

The nanofiber diameter has a high impact on filtration efficiency. Also, the pressure drop in the nanofiber filter is lower than the microfiber filter due to its slip effect, which increases the air permeability of the filter. For this reason, nanofiber filters have started to be used frequently in filtration application. Smaller fiber diameter in a filter reduces pore size in the same thickness (Figure 3.1). As the pore size decreases, filtration efficiency and pressure drop increases [95].

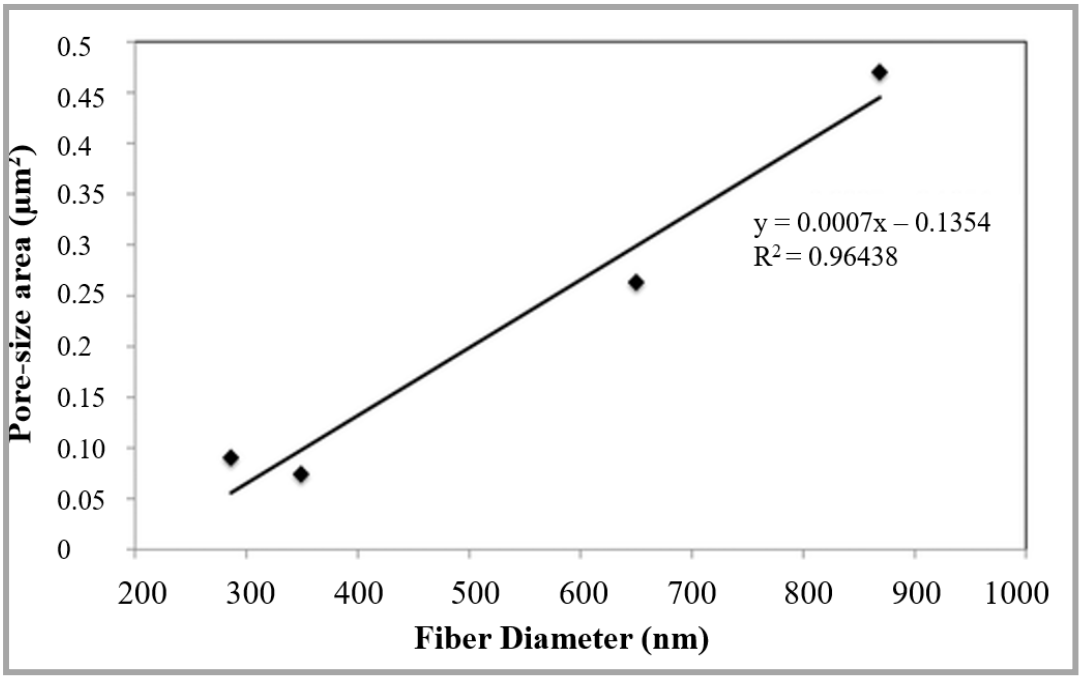

Figure 3.1 : Effect of fiber diameter on pore size [96].

As the fiber diameter decreases, particle capture ability increases. Further decrease in fiber diameter causes high pressure drop [57].

Givehchi et al., [59] have produced different PAN electrospun filters and showed the effect of fiber diameter on particle filtration. As the fiber diameter decreased, the increase in filtration efficiency was higher than the increase in pressure drop, so the quality factor value increased.

3.3.1 Effects of polymer concentration and solution viscosity

Polymer concentration and solution viscosity affect fiber morphology similarly. As the polymer concentration increases, the solution viscosity increases. According to that, the bead formation decreases and is not observed after sufficient increase in viscosity/polymer concentration (Figure 3.2).

If polymer concentration increases, the surface tension of droplet decreases, and the diameter of formed nanofiber become large. In order to obtain uniform fiber morphology without beads, the viscosity of solution and polymer concentration should be adjusted carefully (it must neither be high nor low) [56,57,97].

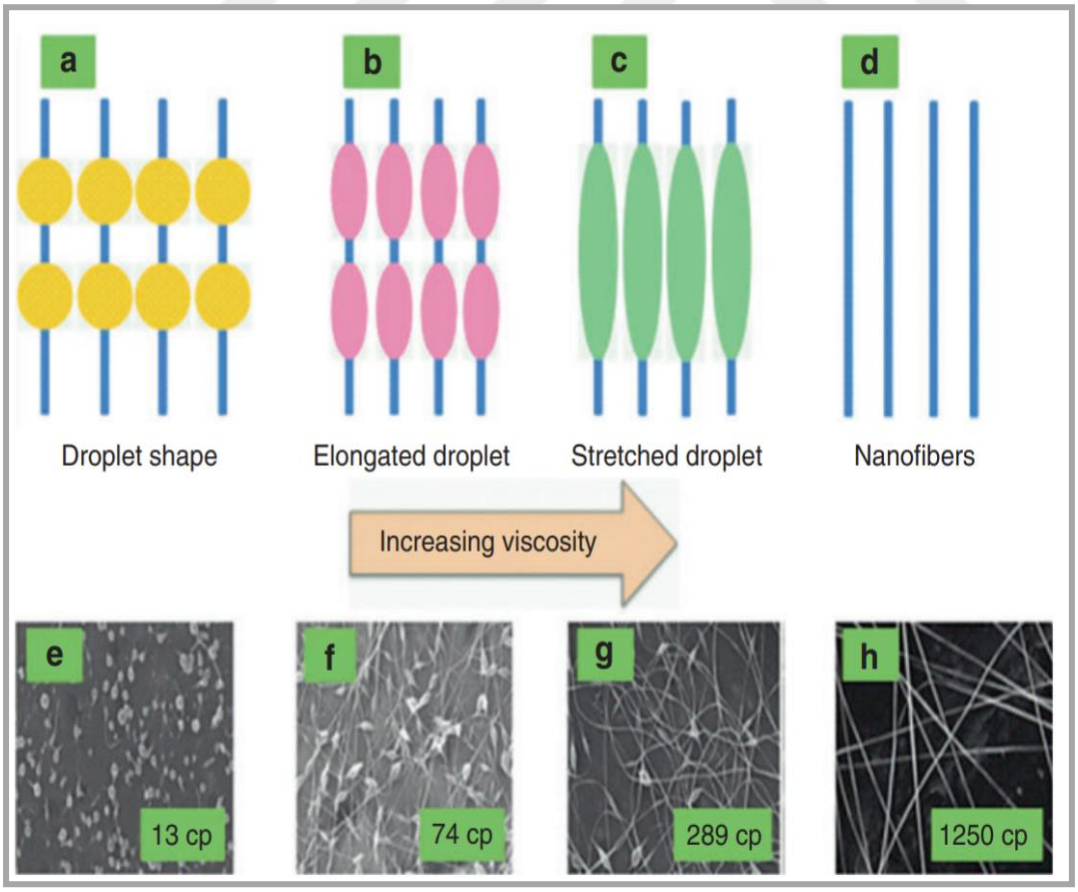

Figure 3.2 : Effects of increased viscosity on fiber morphology [79].

Effects of polymer concentration on fiber morphology is shown in Figure 3.3. It is clearly seen that the beaded fiber structure is obtained at low polymer concentration. These beads increase the distance between the nanofibers and facilitate the transport of air molecules.

In addition, meso- and macro-porosities on the bead surface also aid in the adsorption of airborne particles, enhancing filter performance [56]**.** As the polymer concentration increases, this leads to an increase in fiber diameter and disappearing of bead morphology (Figure 3.3) [21].

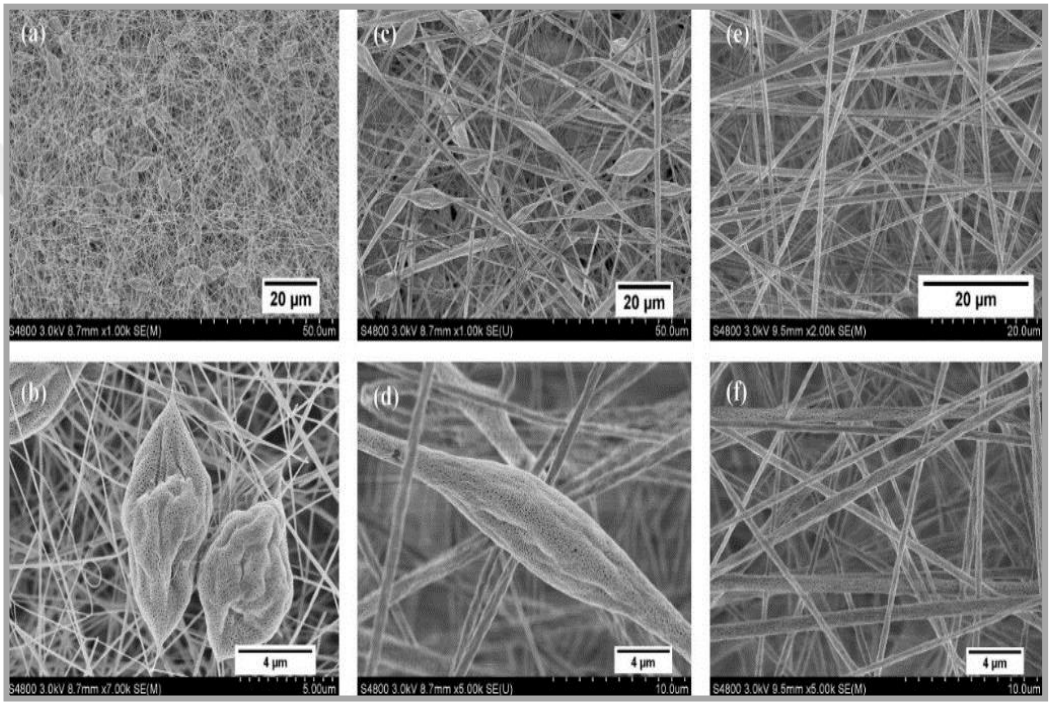

Figure 3.3 : SEM images of the PLA nanofiber at various concentrations: (a) 4.5, (c) 5.5, (e) 6wt% PLA solutions in DCM/DMAC (10/1, w/w). Highly magnified images corresponding to the membranes are shown in (b), (d), and (f), respectively [56].

3.3.2 Effects of ambient conditions (humidity and temperature)

Increased environmental temperature causes thinner nanofiber formation due to rapid evaporation of the solvent and reduced viscosity of the solution, thereby increasing filtration efficiency and also increasing pressure drop [66].

Casper et al., [67] have showed the effect of humidity on fiber morphology. Increased humidity causes an increase in the number, diameter and distribution of pores (Figure 3.4). It can also affect the evaporation rate of the solvent. If it can be adjusted to form small pores, filtration performance increases.

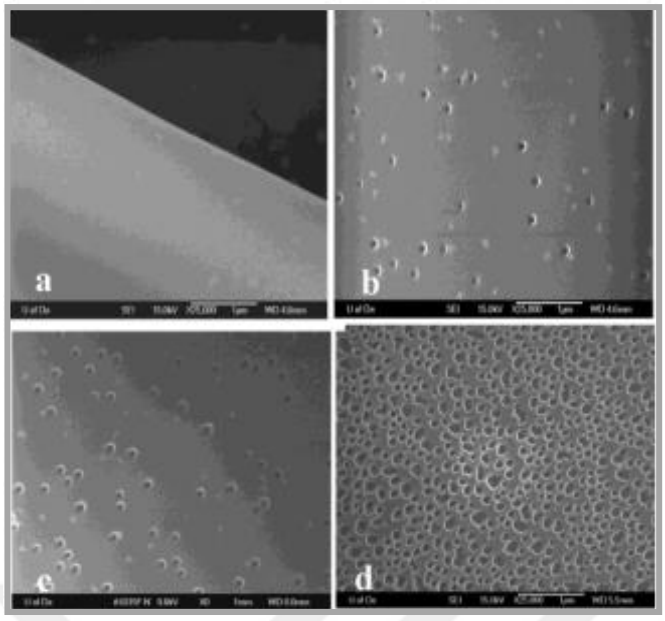

Figure 3.4 : The effect of humidity on morphology and pore size (PS/THF fibers electrospun under varying humidity: a)<25%, b)31-38%, c)40-45%, d)50-59%).

3.3.3 Effects of tip to collector distance

Givehchi et al., [59] have produced PAN nanofibers under varying tip-to-collector distances (10, 12.5, and 15 cm) while the voltage and operating time were constant. The mean fiber diameter decreased with increasing the tip-to-collector distance. The increase in the distance reduced the electric field intensity and increased the jet flight time. Longer distance provides more time for the fluid jet to sufficiently stretch and solvent to evaporate before the fibers deposit on the collector, resulting in finer nanofiber formation and hence higher filtration efficiency (Figure 3.5) [59].

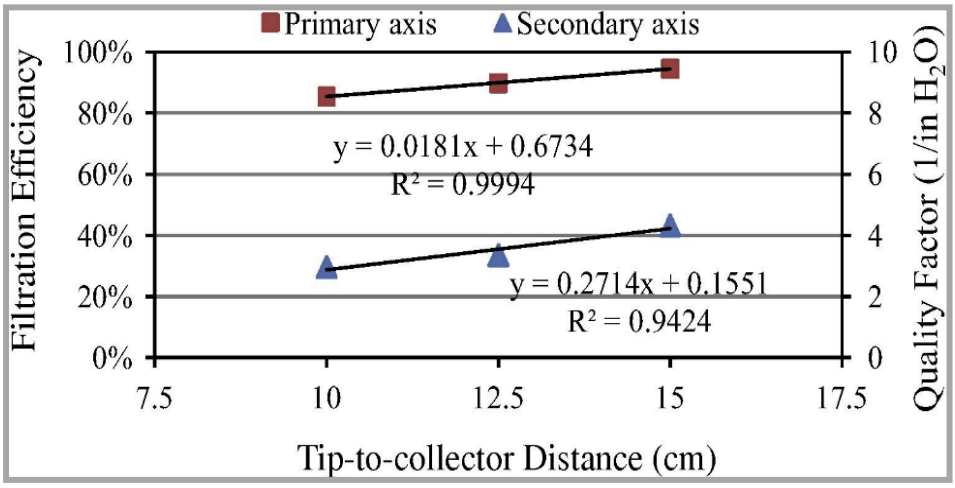

Figure 3.5 : Effect of tip-to-collector distance on filtration efficiency and quality factor [59].

3.3.4 Effects of solution flow rate

At low feed rates, the solvent will have enough time to evaporate until the fibers are deposited on the collector, and thinner and smoother fibers can be produced. High flow rate leads to the formation of beaded fibers caused by insufficient time to evaporate the solvent before reaching the collector and the nanofiber surface will be wet due to insufficient evaporation of solvent, which causes formation of ribbon-like (or flat) fibers [65,79].

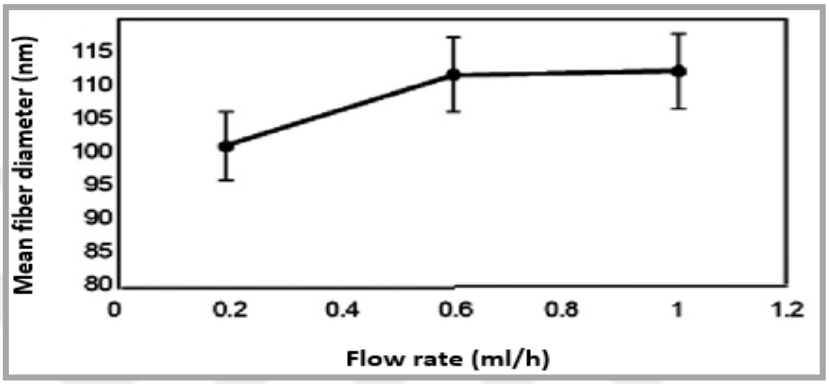

Figure 3.6 : Effect of flow rate of solution on fiber diameter [98].

As seen in the Figure 3.6, when the feed rate of solution increased, the diameter of fiber increased. So filtration efficiency of electrospun filter decreased and pressure drop decreased [66,98].

3.3.5 Effects of applied voltage

Effects of applied voltage on nanofiber diameter are not very clear. Some researchers say that as the voltage increases, the electrostatic repulsion and evaporation of solvent increases resulting in finer fibers but bead size also increases [60]**,** while others state that the increased voltage causes increase the solution volume ejected from the Taylor cone and thus increase the fiber diameter [63,64].

Effect of applied voltage can be associated with the type of jets formed. During electrospinning, the stretching force results from charges in the spinning jet in the electric field and that force contributes to the thinning of the spinning jet. Therefore, increasing the applied voltage has been shown to reduce the fiber diameter [99]. With higher voltage application, multiple jets form, which result in a smaller fiber diameter (Figure 3.7) [100]. However, beyond the optimum voltage, fiber diameter can start to increase due to the reduction in flight time [101].

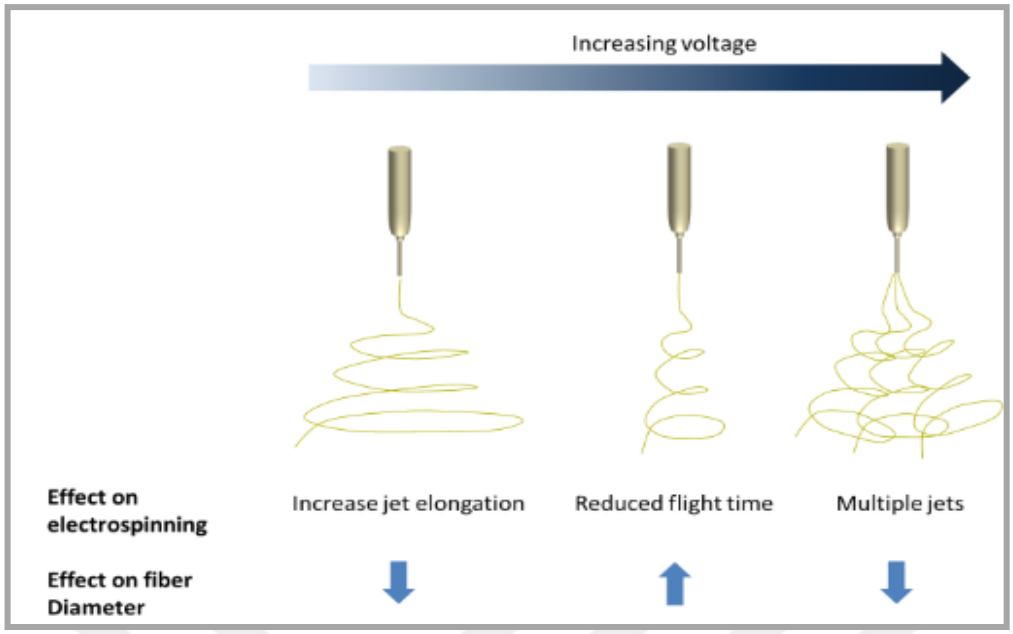

Figure 3.7 : Effect of applied voltage on diameter of nanofiber [101].

In the study done by Givehchi et al., [59] applied voltage causes increasing filter's solidity and thickness due to this effect both filtration efficiency and pressure drop across the filter increases (Figure 3.8).

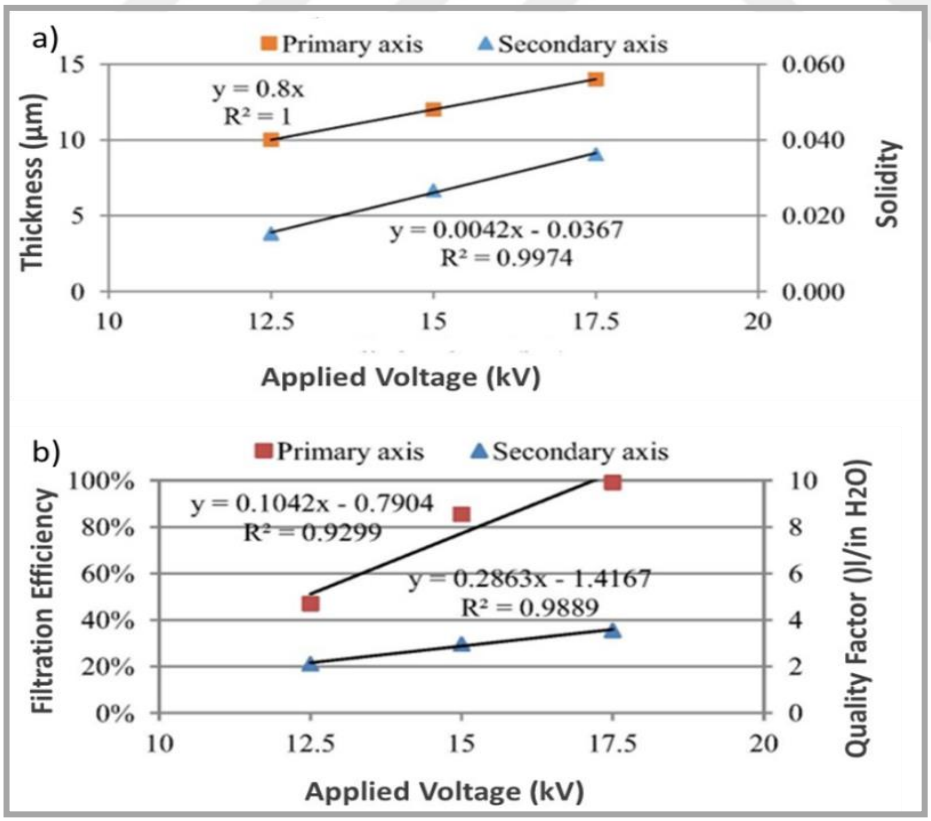

Figure 3.8 : Effect of applied voltage on a) thickness and solidity of filter, b) filtration efficiency and quality factor [59].

3.3.6 Effects of thickness and basis weight of filter

The thickness of the polyetherimide (PEI) electrospun filter (fully analyzed by measuring the basis weight of the filter) affects the removal efficiency (i.e. filtration efficiency) and pressure drop. Obviously, higher basis weight resulted in greater filtration efficiency and pressure drop (Figure 3.9a) [39].

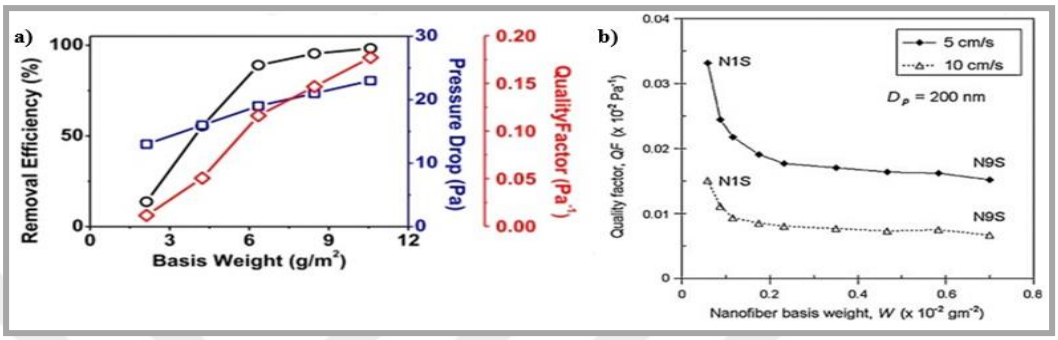

Figure 3.9 : Effect of basis weight on a) filtration performance [39], b) quality factor under face velocities of 5 and 10 cm s^{-1} [65].

In another study, the increased nanofiber basis weight caused higher pressure drop compared to higher filtration efficiency, it also resulted in a reduction of quality factor (Figure 3.9b) [65].

In another study to show the effect of electrospinning time on the performance of nanofibers, the fiber collection time was determined for 30, 60, 120, 180 and 240 minutes after the optimum conditions of electrospinning process were adjusted. Filtration efficiency and pressure drop increased with increasing operating time and thus filter thickness. Although the highest filtration efficiency was found to be 96% for the PA nanofiber filter of 240 minutes of run time (QF: 5.91 10^{-2} Pa^{-1}), it demonstrated lower quality factor than others due to the higher pressure drop. Thus, PA nanofibers with 30 minutes run time (QF: 7.02 10^{-2} Pa^{-1}), are more suitable for filtration applications because of demonstrating the highest quality factor [33]. Moreover, as the coating time increased, air permeability decreased [55].

3.4 Effects of Other Filtration Parameters on Particulate Filtration

3.4.1 Effects of face velocity

The face velocity is calculated by dividing the volumetric flow rate through the filter by the area of nanofiber that is utilized in filtration [102].

It is obviously seen in Figure 3.10 that as the face velocity increased, the pores are clogged rapidly and higher pressure drop observed and filtration performance decreased [58,103].

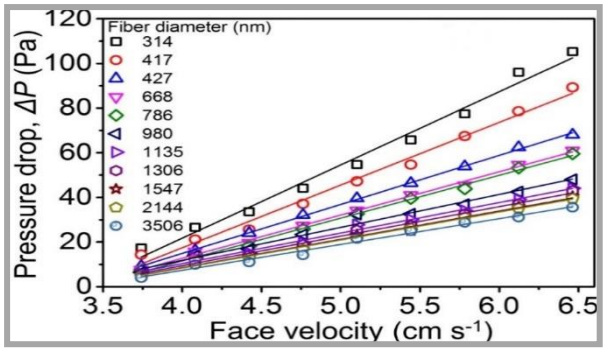

Figure 3.10 : Effect of face velocity on pressure drop of filter [103].

As the face velocity increased, filtration efficiency decreased especially as a result of exposure with particle below 100 nm. Due to the other particles reaching the filter surface and creating pressure, particles with small diameter are diffused into the filter, causing the filtration efficiency to decrease [65]**.**

3.4.2 Effects of particle size

Particulate filters hold the particles in the air owing to size, shape, and charge of the particles, depending on the surface, size, and charge characteristics of the fibrous filter. Interaction mechanism between particle and fiber is related to particle size. Brownian diffusion, interception, inertial impaction and gravitational settling are known as common interaction mechanisms (Figure 3.11).

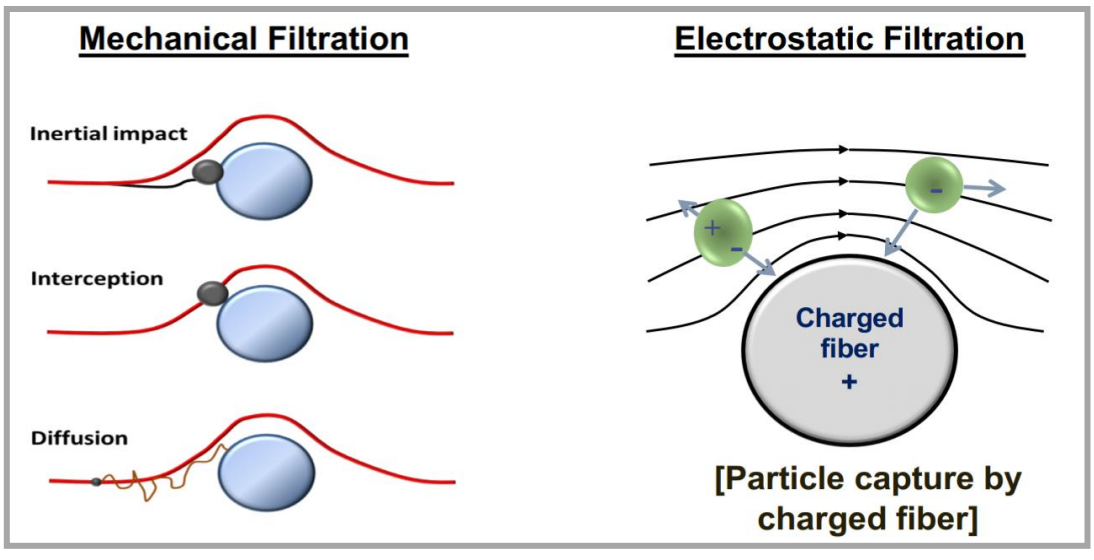

Figure 3.11 : Schematic representation of filtration mechanisms in nanofibers [104].

Particles larger than 10 μm are separated from the air stream before reaching the filter due to gravitational settling and very small particles (such as nanoparticles) can be easily captured due to Brownian diffusion. Particles ranging from 0.3 μm to 10 μm can be stopped by interception and inertial impaction (Figure 3.12) [94].

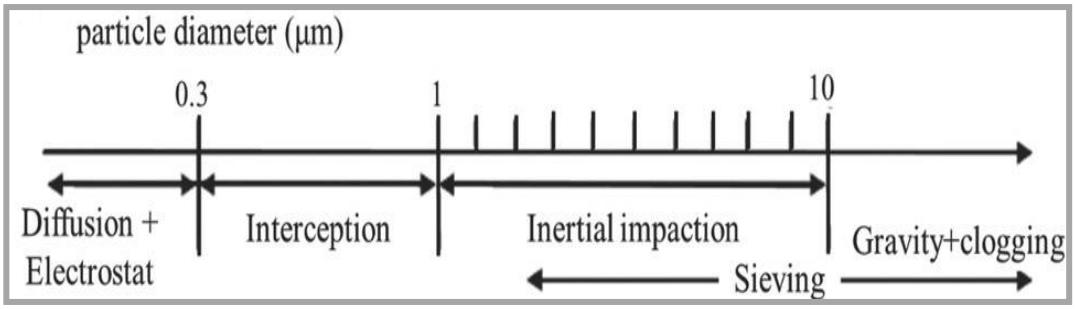

Figure 3.12 : Various capturing mechanisms related to particle size [94].

Other researchers showed effect of particle diameter and capturing mechanism on filtration. They used two different electrospun filters, charged and uncharged. In the case of particle size of between 80-100 nm, penetration of particle is lower in charged electrospun filter due to electrostatic capturing mechanism compared to uncharged filter (Figure 3.13) [62].

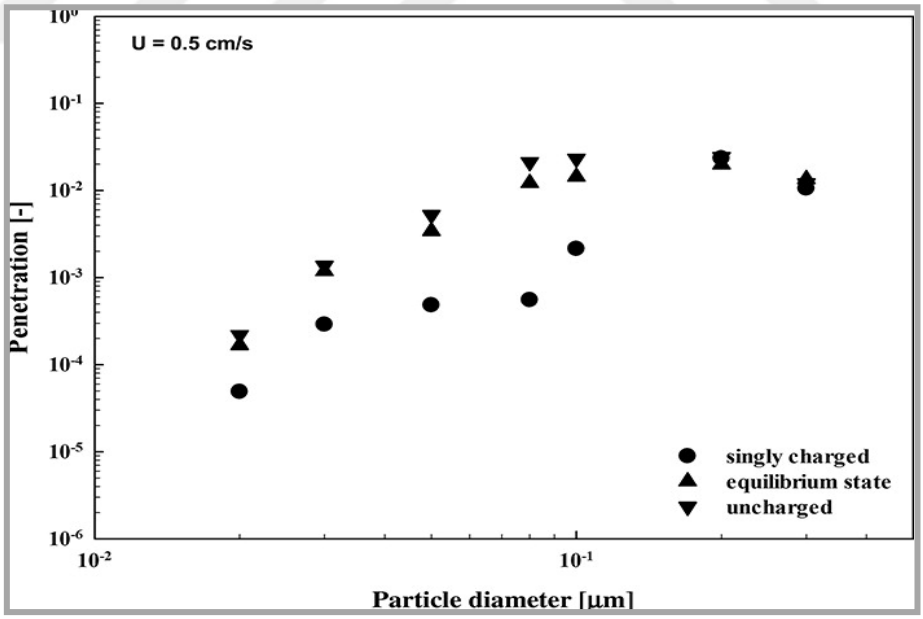

Figure 3.13 : Particle penetration of an electrospun filter of filters at face velocity of 0,5 cm/s [62].

As shown in the Figure 3.14, the particle size was larger than the electrospun fiber diameter, which demonstrates that interception was a predominant collection mechanism in nanofiber filtration [62].

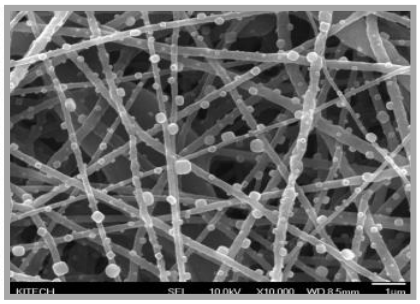

Figure 3.14 : SEM image of nanofiber filter after particulate filtration [62].

3.4.3 Effects of morphology

Different morphologies can be obtained by combining the nanofibers with different nanomaterials. The resulting composite structures not only improve the filtration performance of the filter, sometimes increase the antibacterial effect, sometimes gain hydrophobicity. They can also lead to improved mechanical and thermal properties. Different composite structure and their filtration performances can be seen from Table 3.1.

Table 3.1 : Characteristic filtration properties of various composite filters.

Composite Filters	Filtration Efficiency	Pressure Drop	Pore Size	Ave. Fiber Diameter	NaCl/KCl Size (nm)	Ref
PSU/TiO_2	99.997%	45.3 Pa	-	1150 nm	300-500	[90]
PA6/PAN/PA6	99.9998%	117.5 Pa	-	20-100-20 nm	300-500	[105]
Bilayer PAN NFs	96.8%	110 Pa	1.7 µm	400-200 nm	300-500	[106]
PA6-nonwowen substrate	99.33%	-	-	66-195 nm	15-300	[55]
PVA/PAA/SiO_2 /Ag NPs	98.85%	150 Pa	-	400 nm	300–500	[107]
PVA/PAA/SiO_2	75%	50 Pa	-	400 nm	300–500	[107]
Bead-on-string PLA	99.997%	165.3 Pa	-	-	260	[56]
PLA-N/PLA-P	99.999%	93.3 Pa	3.71 µm	-	260	[92]
PAN/TiO_2	89.6	120 Pa	2.7 µm	-	260	[91]
PVC/PU	99.5	144 Pa	3.52 µm	960 nm	300-500	[108]
PEO-PAN/PSU	99.992%	95 Pa	2 µm	270 nm-1,3 µm	300-500	[109]
PVDF–Ag-Al_2O_3	99.17%	-	0.36 µm	1.85 ± 0.19 µm	-	[110]
PVA /TiO_2	98%	-	-	-	>200 nm	[111]

Single and bilayer structures of PAN nanofibrous filters had compared for air filtration application. Also, the stacking order of the nanofibers in the two-layer structure was changed and compared. These changes altered the surface morphology of the nanofibers by affecting fiber diameter, pore size, and pore size distribution (Table 3.2) [106].

Table 3.2 : Details of single and bilayer nanofibrous structures [106].

Layers	Single Layer	Single Layer	Bilayer	Bilayer
PAN concentration (%, w/w)	8	10	8 and 10	8 and 10
Diameter of NFs	≈200	≈400	≈200 on top	≈400 on top
Layering order	200 nm	400 nm	200 nm 400 nm	400 nm 200 nm

The lowest pressure drop was observed in the sample stacked with approximately 400 nm fiber-diameter nanofiber layer on top and an average of 200 nm fiber-diameter nanofiber layer below. For this reason, two-layer structures significantly increased the quality factor compared to single-layer structures (Figure 3.15) [106].

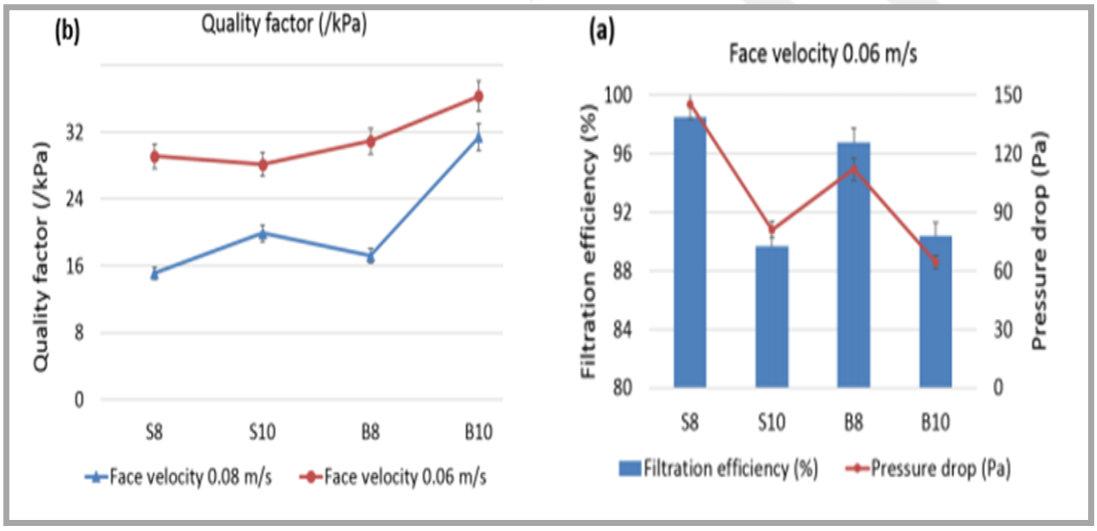

Figure 3.15 : Filtration performances of single and bilayer nanofibrous structures [106].

Porous bead-on string polylactic acid (PLA) nanofiber filters are produced by electrospinning. PLA fiber morphology, including fiber diameter, bead size, number of beads and surface structure of the beads can be closely controlled by adjusting the solvent compositions and concentrations of PLA solutions. Moderate bead size contributes to the low pressure drop, and the small fiber diameters and nanopores in

the beads help to increase the efficiency of filtration. In addition, nanofibrous filter from a 5wt% solution and a solvent mixture containing DCM/DMAC in a weight ratio of 10/1, exhibited excellent filtration efficiency (99.997%) and a low pressure drop [56].

Sandwich structured PA6/PAN/PA6 composite filter was formed for effective air filtration by sequential electrospinning (Figure 3.16). PAN bead-on-string fibers and 2D PA-6 nanonets were used. The resulting PA6/PAN/PA6 composite filters exhibit robust mechanical properties (tensile strength of 7,28 MPa, toughness of 1.77 MJ/m^3), high filtration efficiency of 99,9998%, low pressure drop of 117,5 Pa against 300–500 nm airborne particles. PA6 filter had been showed high filtration efficiency but pressure drop was so high, by adding the bead-on-string PAN nanofiber, cavity structure was formed and pressure drop reduced [105]**.**

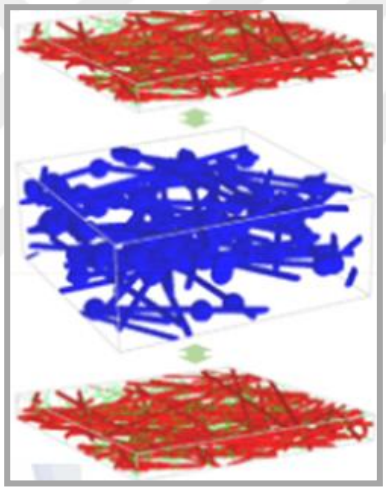

Figure 3.16 : Sandwich structure of PA6/PAN/PA6 composite filter [105].

A hierarchical structured PLA-N/PLA-P composite filters was produced via electrospinning by changing the relative humidity, and the nanopores on fiber surface played a key role in improving the specific surface area and filtration performance of the filters. The PLA-N/PLA-P double layer structured filter exhibited a relatively low pressure drop with 1/5 mass ratio and excellent air filtration efficiency, when face velocity was 5,3 cm/s [92]**.**

4. NANOFIBER FUNCTIONALISATION FOR FACE MASKS

4.1 Definition of Nanoparticles and Their Basic Properties

Nanoparticles are broad class of materials involving particulate matters generally defined as particles of at least one dimension less than 100 nm. As the size of the material changes, its physicochemical properties such as optical and electrical properties are affected. Any nanoparticle has an extremely high surface area/volume ratio; this is one of the reasons for some unusual features. However, this high surface area also means that the surface of the nanoparticle is a crucial component of the material [112,113].

In recent years, the use of nanoparticles in the textile field has been increasing rapidly. Thus, many functions such as fire resistance, stain resistance, antibacterial, UV resistance, water repellent, and mechanical resistance can be imparted to textile products (Table 4.1) [114].

It is difficult to keep the nanoparticles on the protective clothing such as face mask. Aggregation may be observed. Many nanoparticles lose their superb properties once they have aggregated. For this reason, they are added to the polymer solution and made composite by using device which produces nanofibers such as electrospinning. However, in this method, the nanoparticle surfaces are coated by the polymer and therefore the effectiveness in applications greatly reduced due to the insufficient amount of nanoparticles on the surface. So nanofiber production by electrospinning and the addition of nanoparticles by electrospraying to the surface of the fiber should realize simultaneously to improve effectiveness in applications [115].

Silver nanoparticles (NPs) are most often used to give antibacterial properties to any filter material. But Zinc Oxide (ZnO) NPs, Copper Oxide (CuO) NPs, Aluminum Oxide (Al_2O_3) and Magnesium Oxide (MgO) NPs can also be used. When ZnO NPs are impregnated to the filter material, it shows an excellent antibacterial activity against both gram-negative and gram-positive bacteria. ZnO NPs are more effective than Ag NPs in terms of cost, whiteness and UV blocking [116].

Table 4.1 : Nanomaterials, their applications and their properties that provide to textile products [117]**.**

Properties	Nanoparticle	Specific Application
Antibacterial	Silver Zinc oxide Copper oxide Magnesium oxide Aluminum oxide Silicon dioxide	Sportswear Medical textiles Filter materials
Fire resistance	Silicon dioxide Montmorillonite	Protective clothing Military clothing
UV protection	Zinc Oxide Titanium dioxide Magnesium oxide Aluminum oxide Clay nanoparticles	Summer clothing Sportswear
Heat conducting or insulating properties	Vanadium dioxide	Sportswear
Shielding electromagnetic radiation	Indium tin oxide	Protective clothing Military clothing
Self-cleaning- dirt repellent Hydrophobicity Oil repellent feature	Zinc Oxide Titanium dioxide	Home textile products Technical textiles
Increased durability	Silicon dioxide Nanoclay	Technical textiles Protective clothing Military clothing

Zinc oxide NPs firstly break down the cell membrane and then can penetrate the cell membrane because of their size smaller than the bacterial cells and they inhibit the growth of microorganisms. They accumulate in the cytoplasm where they interact with biomolecules that cause cell death.

Moreover, ZnO NPs cause ROS (Reactive Oxygen Species) production, thus putting cells under oxidative stress, which damages cellular components, namely lipids, proteins and DNA. ZnO NPs rapidly dissolve in the lysosome under acidic conditions (pH 4.5) and form Zn^{+2} ions, which are responsible for growth inhibition and finally the death of microbes. It is also known that the size of ZnO nanoparticles ranging from 50 to 500 nm has the same effect on bacterial growth inhibitihon [118].

The particle size of ZnO NPs has a significant effect on their antibacterial performance. It is known that antibacterial performance of ZnO increases as particle size of ZnO decreases. This is strongly related to the higher surface-to-volume ratio.

For this reason, small particles will interact more with the bacterial cell and show higher toxicity [119].

And shape of ZnO NPs effects their antibacterial performance as well. Papavlassopoulos et al., [120] demonstrated that ZnO tetrapods structure showed lower toxicity against mammalian fibroblast cells when compared to spherical ZnO.

MgO nanoparticles (NPs) are widely used in nanofibers as disruptive adsorbent through their high specific surface area, the high surface concentration of reactive sites [121].

Many functional groups such as acids, aldehydes, ketones, carboxylic groups and heteroatoms (S, N and P) containing chemicals are adsorbed exothermically on MgO metal oxide surfaces. The chemical reaction between MgO NPs and toxic substance is realized on the surface of the NPs and, then the substance may turn into a non-toxic form or a less toxic form than its original form. Disruptive adsorption ensures the irreversible degradation of toxics whereas physical adsorption ensure only reversible attachment of toxics. Desorption is mostly seen in the case of physical adsorption [115].

4.2 Effect of Nanoparticles on the Air Filtration Properties

Nanofiber/Nanoparticle composites are widely used for air filtration applications. The surface of the nanofibers can be functionalized by nanoparticles and they gain many excellent features.

Yusof et al., [122] also produced activated carbon nanofibers (ACNFs) embedded with MgO NPs. Addition of MgO onto ACNFs (198.80 m^2/g) brings about the higher specific surface area (SSA) than pure ACNFs (15.43 m^2/g). The obtained surface morphology is rough due to the distribution of MgO NPs onto the surface of the ACNFs. Furthermore, in the production of ACNFs, heat treatment is applied and during the heat treatment, CO and CO_2 gases form and these gases move away from the nanofiber structure because of the catalytic behavior of MgO NPs. Thus, it creates more micro- and meso-pores increasing the total SSA and adsorption performance on the surface of ACNFs. In that study, they found that Cd (II) adsorption on the MgO-ACNFs is higher than pure ACNFs and granular activated carbon (GAC).

Dadvar et al., [123] produced the ACNFs embedded with MgO NPs and investigated the effect over the adsorption of 2-chloroethyl ethyl sulfide (2-CEES) onto MgO NPs embedded into the ACNFs. As the amount and specific surface area of MgO NPs onto ACNFs increase, the 2-CEES adsorption rate of composite material increased. Compared to pure ACNFs, the adsorption rate of MgO embedded ACNFs is 2-4 times higher, depending on the specific surface area of MgO used. MgO NPs decontaminate of toxic chemicals such as 2-CEES from the environment due to their catalytic behavior.

In another work, composite filters of PSU/TiO_2 NPs were obtained in different TiO_2 content and the nanofiber morphology changed significantly and the roughness of the fiber surface increased. With the addition of TiO_2 nanoparticles, the pore size and fiber diameter between the fibers decreased, thereby increasing the filtration performance of the filter. However, a further increase in TiO_2 content causes the agglomeration of TiO_2 and the filtration performance and pressure drop decreased Composite filter exhibited improved filtration efficiency (99.997%) and pressure drop (45.3 Pa) in 5% TiO_2 NP content (Figure 4.1) [90].

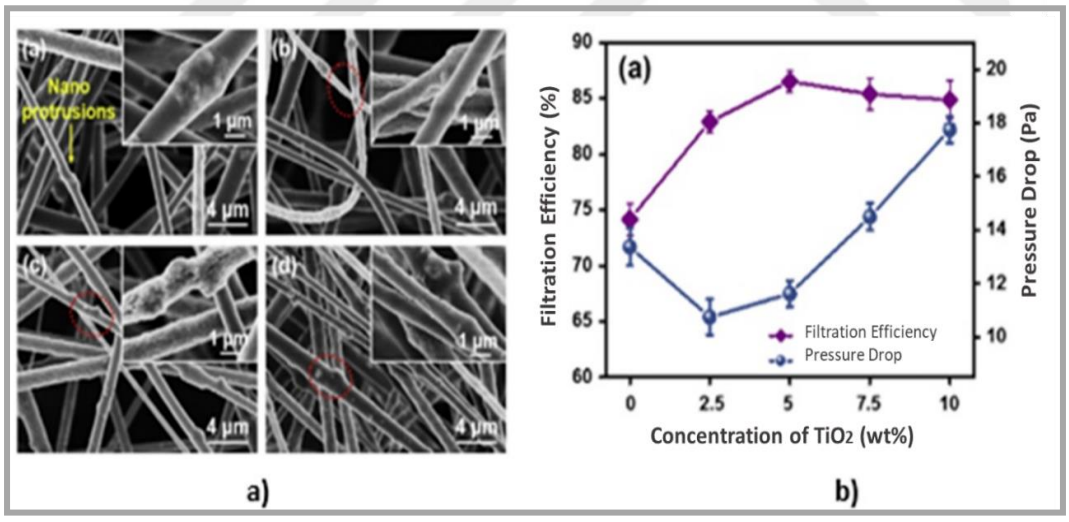

Figure 4.1 : a) SEM images of PSU/TiO_2 composite filters under increasing TiO_2 content (a to d), b) filtration performance of PSU/TiO_2 composite filters increasing TiO_2 content [90]**.**

Ag NPs are generally used in nanofiber filter to give antibacterial properties to the filter. Kang et al., [124] showed that Ag NPs have strong effect on bacteria and damage the membrane of bacteria and interact with bacterial DNA, which leads to lose its replication ability. Ag/PA6 and Ag/PA6 tree-like nanofiber filters showed

superior antibacterial properties against both *E. coli* and *S. aureus* compared with common pure PA6 nanofiber filters.

Lubasova and Barbora [125] used different nanoparticles with PVA nanofiber filter. They prepared TiO_2/PVA, ZnO/PVA, ZrO_2/PVA and SnO_2/PVA nanoparticle-nanofiber composite filters. They investigated bactericidal effect of these nanoparticles. At the end of the study, they found that SnO_2 and nanofiber filters showed antimicrobial properties only against *S. aureus*, and ZnO or ZrO_2 nanofiber filters exhibited antimicrobial properties against both bacteria (*E. coli* and *S. aureus*).

ZnO/PA6 nanofibers composite structure showed excellent antibacterial activity against both gram-negative *E. coli* and gram-positive *Bacillus cereus* (99.99%). It damaged the membrane of the bacteria and caused them to die [126].

4.3 Effects of Nanoparticles on Adsorption and Catalytic Behaviour

The pollution in the world is one of the serious problems for humanity. Many pollutants contaminate water, soil, and air and cause human health problems. Especially in wars, a myriad of toxic chemicals and biological warfare agents are released into the air. In that context, to be protected from them, protective clothes are preferable. If we look at the studies done before, we can see that metal ions or metal oxides such as MgO are commonly used in protective clothing as a catalyst in order to degrade hazardous substances. Metal oxide nanoparticles show higher catalytic behaviour owing to higher surface area, high amount of reactive edge and corner atom number, defects caused by anion and cation vacancies and more porosity than bulk metal oxides. Besides, surfaces properties such as morphology, particles size, size distribution, and aggregation tendency of NPs also have great significance.

The specific surface area (SSA) of MgO to be used here is critical. As the specific surface area of MgO increases, its chemical reactivity also increases and thus surface reactive oxide groups of the MgO NPs becomes more accessible [123]. In order to increase the catalytic efficiency, MgO is used with TiO_2 showing photocatalytic activity under UV light [115].

Al_2O_3 NPs are widely used metal oxide nanoparticles. Vanangamudi et al., [110] obtained PVDF–Ag–Al_2O_3 nanofibrous filters and they used Al_2O_3 nanoparticles to remove paraoxon which is a nerve agent simulant. As the concentration of Al_2O_3

increases, paraoxon detoxification increases. Besides, addition of the Al_2O_3 NPs cause that the average pore size of the filter reduced, and the thickness of the filter mat increased. Therefore, they contributed to increase the filtration performance.

ZnO/PA6 nanofibers composite structure exhibited a good detoxification activity (95%) against paraoxon, a highly toxic chemical. The amount of detoxified paraoxon increased as the content of ZnO in the nanofibrous filter increased. So, it is suitable for use as air filters [126].

In another study, Su et al., [91] used TiO_2 NPs and they obtained TiO_2/PAN composite filters. They used the photocatalytic effect of TiO_2 and, hence they improve the filter efficiency. TiO_2 was irradiated by xenon lamp. And they showed that conversion of toluene into CO_2 and water increased, with the increasing content of TiO_2 due to photocatalytic effect. So, one of the volatile organic compound toluene was detoxified (Figure 4.2).

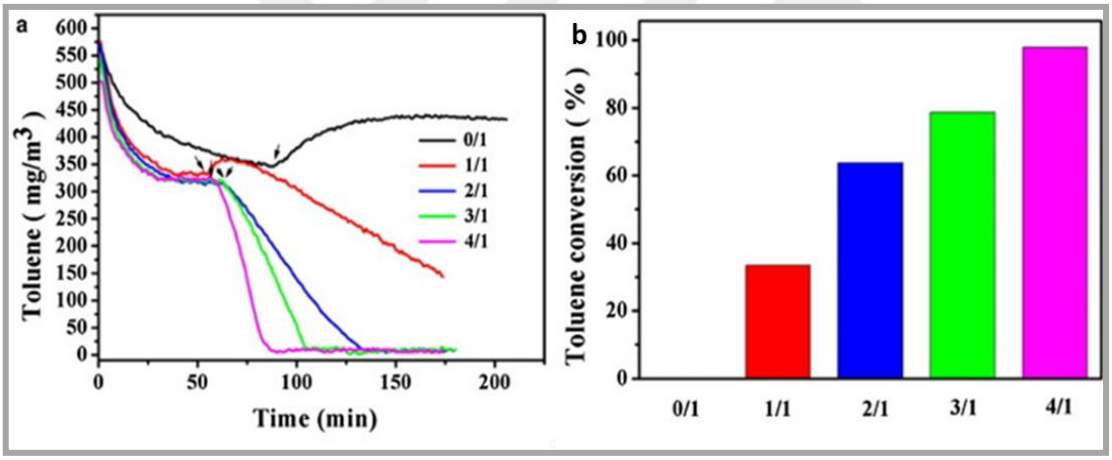

Figure 4.2 : a) Changes in the concentration of toluene throughout the test b) toluene conversion efficiency for the composite membranes with different TiO_2/PAN mass ratios [91]**.**

In another study, PVA/TiO_2 composite filter was irradiated by UV and the effects of exposure time (retention time) with UV and wavelength of UV were investigated for degradation of acetone. The results showed that the degradation efficiency increased with decreasing wavelength of UV and increasing retention time [111]**.**

5. EXPERIMENTAL STUDIES

5.1 Materials

The chemicals used throughout this study are listed in the Table 5.1. All chemicals except ZnO nanoparticle in water medium were used without any extra purification. DMF was added into mixing of ZnO/water and water was evaporated by Heidolph rotary evaporator until all water has been evaporated, thus obtaining ZnO/DMF mixture.

Table 5.1 : The used chemicals/products during experimental study and their suppliers.

Chemicals/Products	Supplier
Polyacrylonitrile (PAN) powder	AKKIM
N, N-dimethylformamide (DMF)	AKSA Chemical
MgO NPs (nanopowder, ≤50 nm particle size (BET), 98% purity)	Sigma Aldrich
ZnO NPs (<100 nm particle size (TEM), ≤40 nm ave. part. size (APS), 20 wt. % in H_2O)	Sigma Aldrich
Toluene	Merck
Methanol	Merck
Ethanol	Merck
Escherichia coli ATCC 8739	Gül Biyoloji Lab. San. ve Tic. Ltd
Staphylococcus aureus subsp. aureus ATCC® 6538	Gül Biyoloji Lab. San. ve Tic. Ltd
Bacteriological Pepton	Gül Biyoloji Lab. San. ve Tic. Ltd
Beef Extract (Meat Extract)	Gül Biyoloji Lab. San. ve Tic. Ltd
Bacteriological Agar (Agar agar)	Gül Biyoloji Lab. San. ve Tic. Ltd

5.2 Solution Preparation and Production of Nanofibers

5.2.1 MgO/PAN nanofibers production: First, the MgO NPs in the various contents (7wt%, 12wt%, 17wt%, 22wt%) was added into DMF, then the solution is stirred for 1 hour with the ultrasonic stirrer. Then, 13% wt of PAN powder (it kept constant for all solutions) was dissolved in the mixture solution of the DMF-MgO NPs by using magnetic stirrer for 6 hours.

5.2.2 ZnO/PAN nanofibers production: Firstly, 10 grams ZnO/water solution (2 at grams of ZnO in water) were taken and 15 grams DMF was added, then evaporated. 70℃ and 200 mbar in the rotary evaporator until total weight of the mixture decreased down to 15 grams. Then again 10 grams DMF was added to mixture and evaporated at 70℃ and 100 mbar in the rotary evaporator until total weight of the mixture decreased down to 10 grams. Finally, ZnO/DMF solution (20% (w/w) ZnO in DMF) was obtained (Figure 5.1).

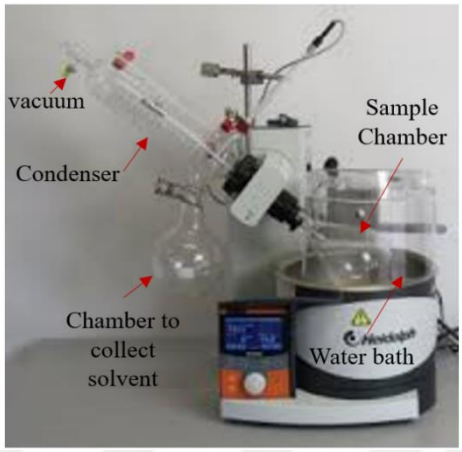

Figure 5.1 : Rotary Evaporator (Heidolph).

The ZnO/DMF solution was diluted or concentrated with DMF such that the total ZnO NP concentration in the solution was 7%, 12%, 17%, 22%, and 27% respectively. Then, the solution is stirred for 1 hour with the ultrasonic stirrer. Then, 13wt% of PAN powder (it kept constant for all solutions) was dissolved in the mixture solution of the DMF-ZnO NPs by using magnetic stirrer for 6 hours.

Figure 5.2 : NE300 model electrospinning device of Inovenso Technology Ltd.

The MgO/PAN and ZnO/PAN filters were fabricated onto a PP nonwoven substrate (25 gsm) by electrospinning device (The NE300 model, Inovenso Technology Ltd.**)** with 2 needles (Figure 5.2). The distance from the needle tip to the collector, the voltage, flow rate, homogeneity movement and drum speed were set at 23 cm, 26 kV, 2.2 ml/h, 20 mm/s-90 mm, and 200 rpm respectively.

Table 5.2 : The contents and preferred abbreviation of samples.

Sample	Content*		
20% MgO/PAN	7% MgO NP	13% PAN powder	80% DMF solvent
25% MgO/PAN	12% MgO NP	13% PAN powder	75% DMF solvent
30% MgO/PAN	17% MgO NP	13% PAN powder	70% DMF solvent
35% MgO/PAN	22% MgO NP	13% PAN powder	65% DMF solvent
20% ZnO/PAN	7% ZnO NP	13% PAN powder	80% DMF solvent
25% ZnO/PAN	12% ZnO NP	13% PAN powder	75% DMF solvent
30% ZnO/PAN	17% ZnO NP	13% PAN powder	70% DMF solvent
35% ZnO/PAN	22% ZnO NP	13% PAN powder	65% DMF solvent
40% ZnO/PAN	27% ZnO NP	13% PAN powder	60% DMF solvent

*Weight percentage is used for all samples.

5.3 Morphological Analysis

The fiber diameter, its distribution, surface roughness and surface morphology were investigated using Scanning Electron Microscope (SEM) (Tescan VEGA3), and quantitative chemical characterization of produced filters were made by Energy Dispersive X-ray Spectroscopy (EDX) (Figure 5.3). Before the SEM analysis of the produced filter, the samples were coated with gold/palladium.

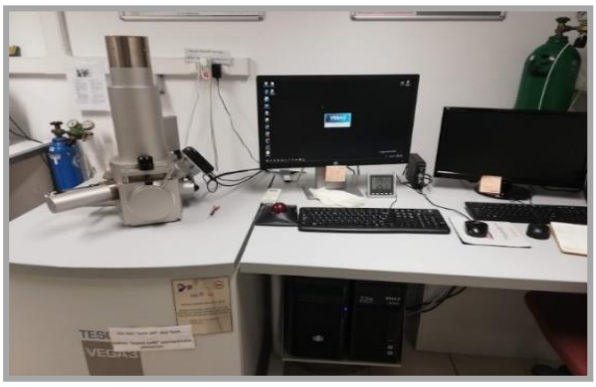

Figure 5.3 : Tescan VEGA3 SEM device with EDX equipment.

EDX is a technique in which characteristic X-rays produced from electron beam-sample interaction are analyzed to provide the elemental composition of the sample in the form of spectra. Each peak in the EDX spectrum correspond to the characteristic X-ray lines belonging the specific element. Thus, spectra provide quantitative chemical characterization of samples.

5.4 Particulate Filtration Test

An automated filter tester (TSI Model 8130A) (Figure 5.4) was used to evaluate the filtration performance of the MgO/PAN samples according to European EN 149 standard. Charge-neutralized monodisperse solid sodium chloride (NaCl) aerosol particles with diameter of 400 nm was used as an ultra-fine particle agent (Figure 5.4). The test parameters were adjusted so that the flow rate was 95 l/min, the analyzed area was 100 cm^2 and the face velocity was 15.7 cm/s. All samples were tested at room temperature.

Figure 5.4 : The Automated Filter Tester TSI Model 8130A.

5.5 Toluene Adsorption Test

Toluene gas adsorption studies were carried out using the test setup established in ITU Environmental Engineering Laboratory (Figure 5.5). The dry air generator was operated. Liquid toluene was put into gas washing bottle and placed into water bath. Its temperature was set at 50℃ to get toluene vapor. The produced membrane was cut round to a diameter of 4.7 cm and was placed into sterlitech (HP4750 Stirred Cell-the reactor that adsorption occurs). After the system stabilized, toluene vapor and dry air were sent to sterlitech at certain concentration. Here, dry air was used to

dilute toluene. The gases exiting from the reactor were collected into tube involving methyl alcohol of 5 ml for 1 minutes after certain adsorption time intervals (30 and 60 min) and sent to GC-MS (Agilent Technologies, 5975c series) (Figure 5.6) to determine the amount of toluene adsorption. It had also been investigated whether toluene was catalytically degraded and whether by-products such as H_2, CO and CO_2 were formed (Figure 5.6).

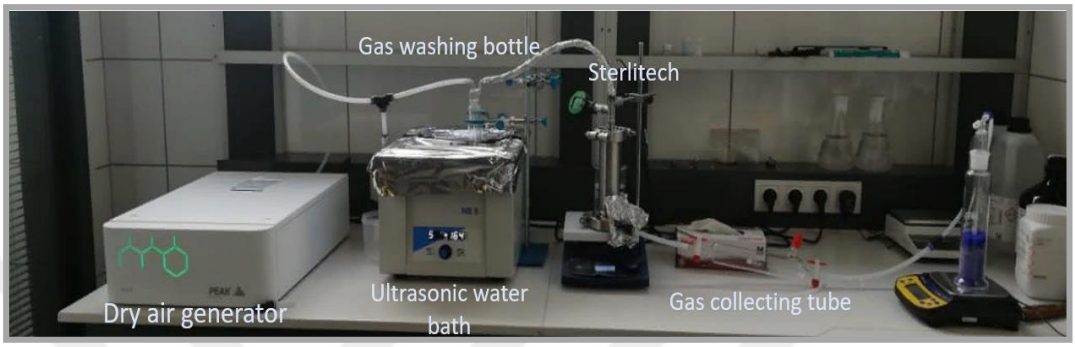

Figure 5.5 : Set-up of the toluene gas adsorption test.

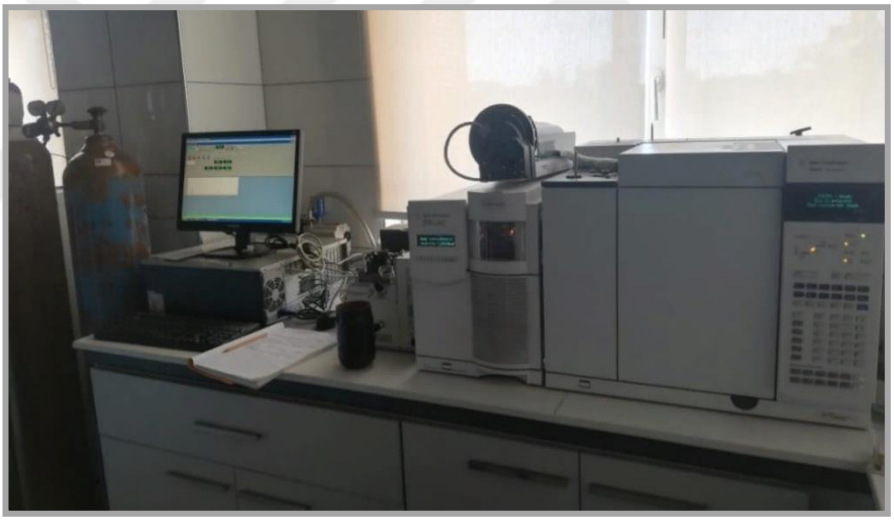

Figure 5.6 : GC-MS device.

5.6 Antibacterial Studies

Agar diffusion test was done to evaluate antibacterial efficacy against gram-negative bacterium *Escherichia coli* (ATCC 8739) and gram-positive bacterium *Staphylococcus aureus* (ATCC 6538).

After one bacterial colony was added to the broth medium, it was kept at 37°C for 24 hours to ensure enough reproduction in the incubation oven. According to the AATCC 147 test method, 100 µl of that broth medium in which bacteria had grown was taken and the bacteria were transferred to the agar medium homogeneously

using a glass stick by the spreading method. Then, the samples were cut at the 1 cm-1 cm in diameter and placed into agar medium and kept in an incubator at 37°C for 24 hours. In the experiment, 10 µl of 2wt% triclosan was used as reference material with antibacterial properties. The antibacterial effectiveness of the filter materials was determined by measuring the inhibition zones where there is no bacteria growth.

6. RESULTS AND DISCUSSION

6.1 Morphological Analysis Results

6.1.1 Morphologies of MgO/PAN Nanofibers

Morphological analyses of the produced samples are shown in the related figures.

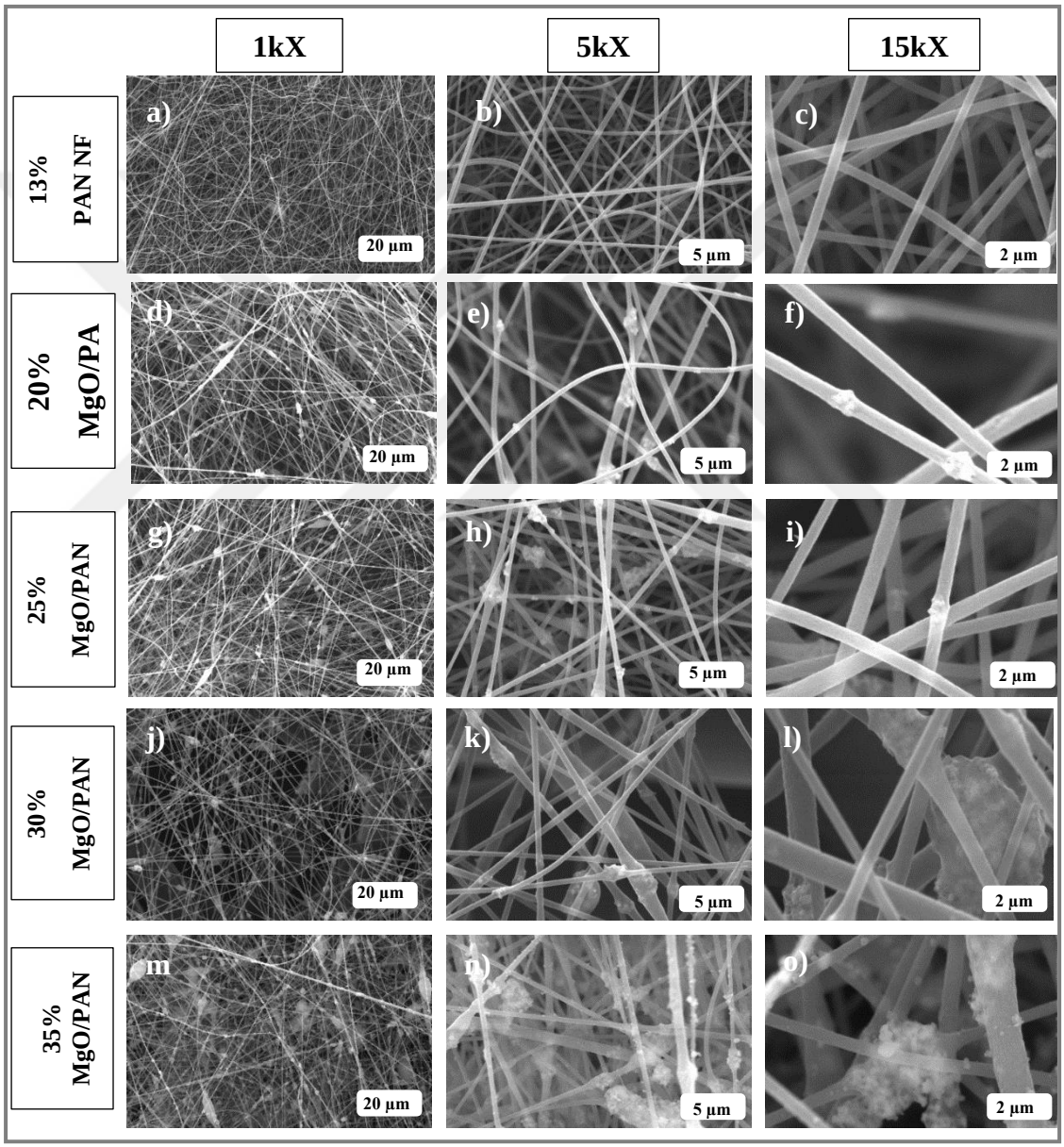

Figure 6.1 : Electrospinning time was kept constant (20 min) in all samples. For 13% PAN NF a) magnification: 1 kX; b) 5 kX; c) 15 kX. For 20% MgO/PAN NF d) 1 kX; e) 5 kX; f) 15 kX. For 25% MgO/PAN NF g) 1 kX; h) 5 kX; ı) 15 kX. For 30% MgO/PAN NF j) 1 kX; k) 5 kX; l) 15 kX. For 35% MgO/PAN NF m) 1 kX; n) 5 kX; o) 15 kX.

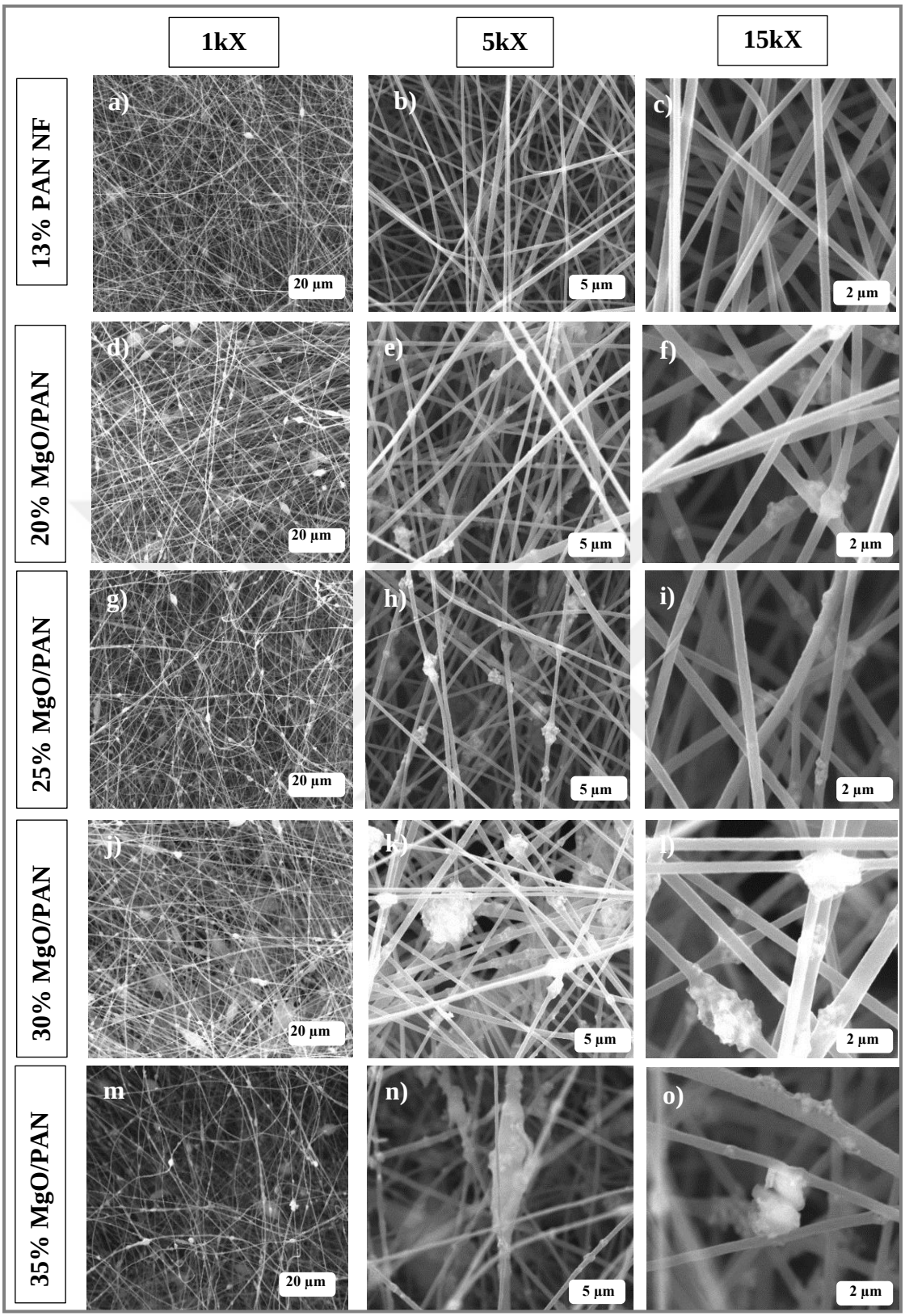

Figure 6.2 : Electrospinning time was kept constant (40 min) in all samples. For 13% PAN NF a) magnification (m):1 kX; b) m: 5 kX; c) m: 15 kX. For 20% MgO/PAN NF d) m: 1 kX; e) m: 5 kX; f) m: 15 kX. For 25% MgO/PAN NF g) m: 1 kX; h) m: 5 kX; ı) m: 15 kX. For 30% MgO/PAN NF j) m: 1 kX; k) m: 5 kX; l) m: 15 kX. For 35% MgO/PAN NF m) m: 1 kX; n) m: 5 kX; o) m: 15 kX.

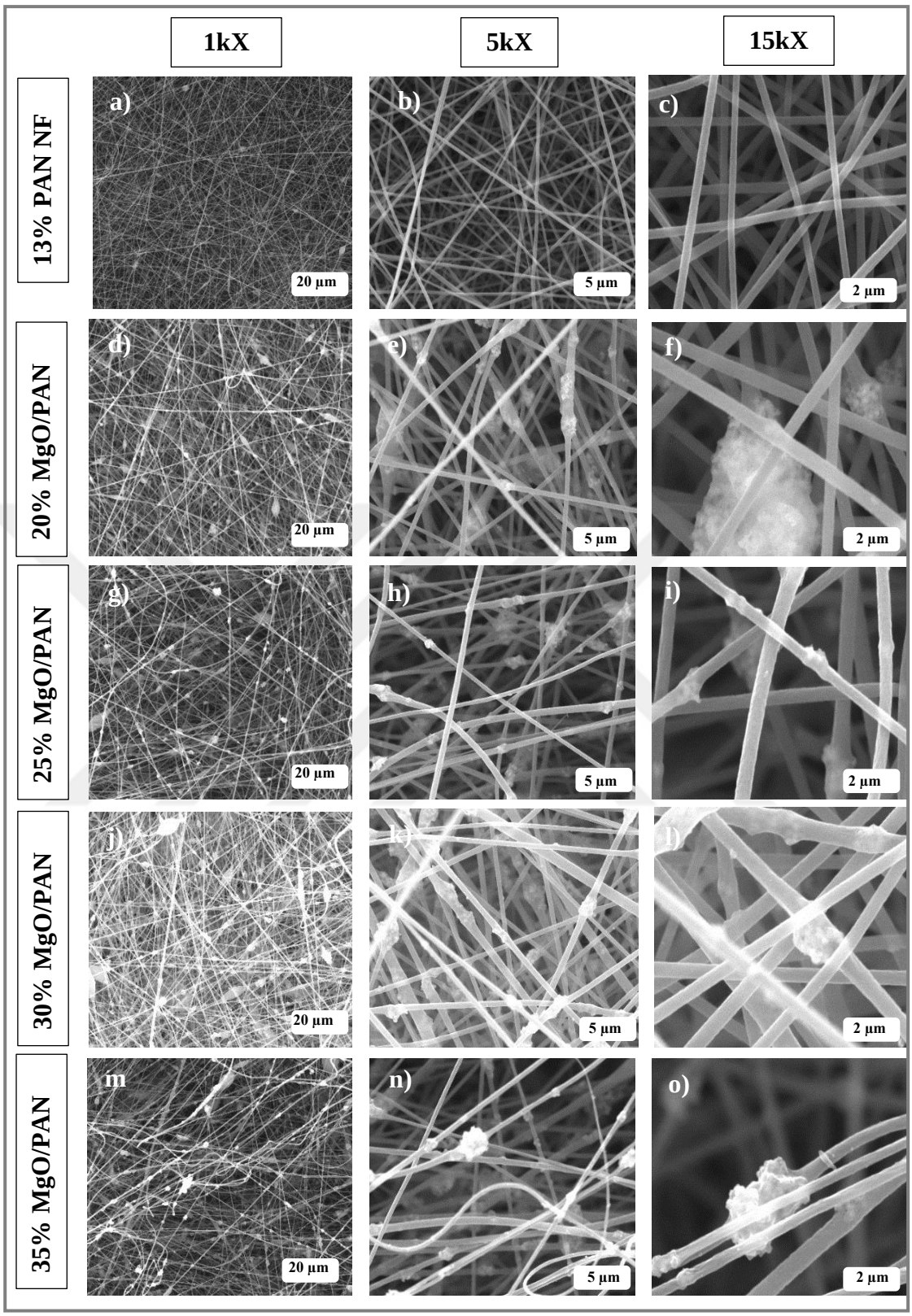

Figure 6.3 : Electrospinning time was kept constant (60 min) in all samples. For 13% PAN NF a) magnification (m):1 kX; b) m: 5 kX; c) m: 15 kX. For 20% MgO/PAN NF d) m: 1 kX; e) m: 5 kX; f) m: 15 kX. For 25% MgO/PAN NF g) m: 1 kX; h) m: 5 kX; ı) m: 15 kX. For 30% MgO/PAN NF j) m: 1 kX; k) m: 5 kX; l) m: 15 kX. For 35% MgO/PAN NF m) m: 1 kX; n) m: 5 kX; o) m: 15 kX.

As seen in Figure 6.1, 6.2 and 6.3, pure PAN nanofibers have smooth surface without any beads, regular and continuous fibrous structure. On the other hand, any presence of MgO NPs are clearly visible on the surfaces of nanofibers. As can be seen in the images, the presence of NPs caused to create a rough surface. Nanoparticles tend to come together/agglomerate by nature. The size of the agglomerate increased with increasing the nanoparticle concentration in the solution. The number of agglomerations and the size of agglomerate in samples of 20% and 25% MgO/PAN are less compared to the samples of 30% and 35% MgO/PAN. Moreover, the distribution of nanoparticles on the nanofiber surface is homogeneous. This interpretation was also confirmed by EDX analysis.

Electrospinning time or coating time did not affect nanofiber morphology and nanofiber diameter. But randomly overlapping nanofibers create a thicker active layer where particles can be captured, and gases can be adsorbed.

6.1.2 EDX analysis result

Elemental composition of 20% MgO/PAN NF was investigated by using an energy-dispersive X-ray spectrometer (EDX) to demonstrate the highly uniform disturibution of MgO NPs on the surface of PAN NF.

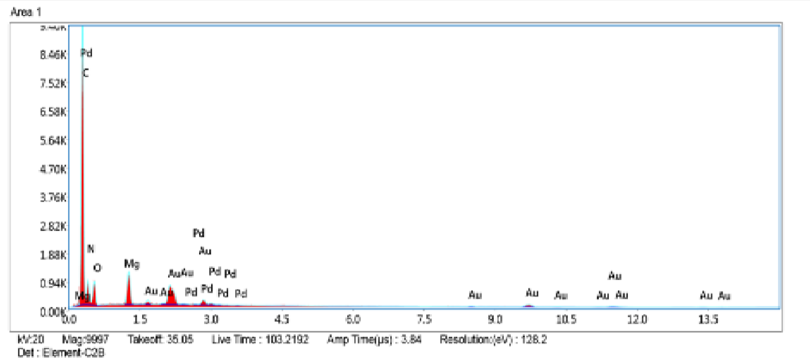

Element	Weight %	Atomic %	Error %
C K	53.60	66.40	6.00
N K	18.80	20.00	14.20
O K	11.00	10.30	14.20
Mg K	3.60	2.20	6.80
Pd L	1.50	0.20	19.70
Au L	11.40	0.90	16.60

Figure 6.4 : EDX analysis result of 20% MgO/PAN NF.

As seen in Figure 6.4, C atoms comes from PAN polymer and carbon coating. P atoms comes from PAN polymer. Mg and O atoms come from MgO NPs.

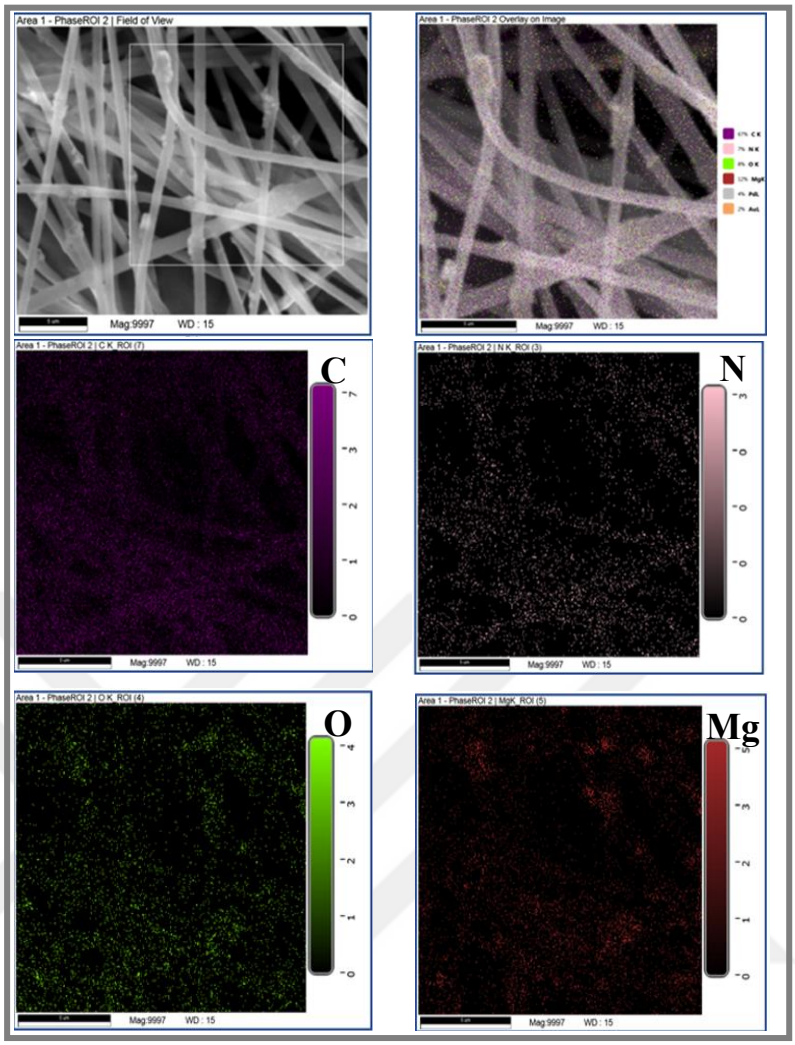

Figure 6.5 : EDX Mapping of 20% MgO/PAN NF.

As can be seen in Figure 6.5, Mg atoms were evenly distributed on the nanofiber surface.

6.1.3 Morphologies of ZnO/PAN nanofibers

Morphologies of 13% PAN NF and PAN NFs having various ZnO concentration under various electrospinning time of 20, 40 and 60 min were given in Figure 6.6, 6.7 and 6.8.

As seen in Figures 6.6, 6.7 and 6.8, pure PAN nanofibers have smooth surfaces with no beads, regular and continuous fiber structure. However, the presence of ZnO NPs on the fiber can be clearly seen and these NPs caused the formation of rough surface. Also, the distribution of nanoparticles on the nanofiber surface is homogeneous and agglomeration has not been observed. We can say that electrospinning time has no effect on nanofiber morphology and nanofiber diameter.

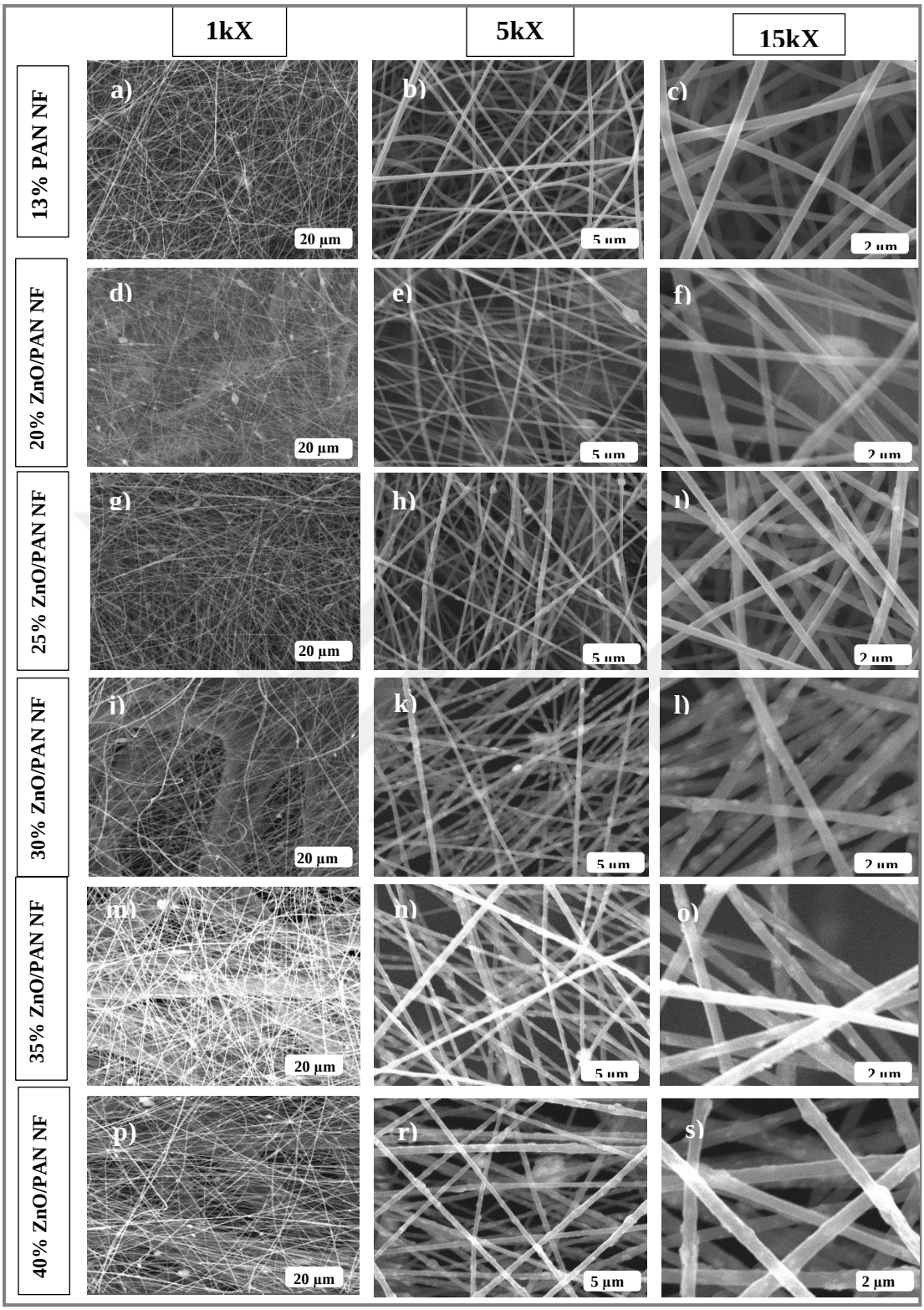

Figure 6.6 : Electrospinning time was kept constant (20 min) in all samples. For 13% PAN NF a) magnification (m):1 kX; b) m: 5 kX; c) m: 15 kX. For 20% MgO/PAN NF d) m: 1 kX; e) m: 5 kX; f) m: 15 kX. For 25% MgO/PAN NF g) m: 1 kX; h) m: 5 kX; ı) m: 15 kX. For 30% MgO/PAN NF j) m: 1 kX; k) m: 5 kX; l) m: 15 kX. For 35% MgO/PAN NF m) m: 1 kX; n) m: 5 kX; o) m: 15 kX. For 40% ZnO /PAN NF p) m: 1 kX; r) m: 5 kX; s) m: 15 kX.

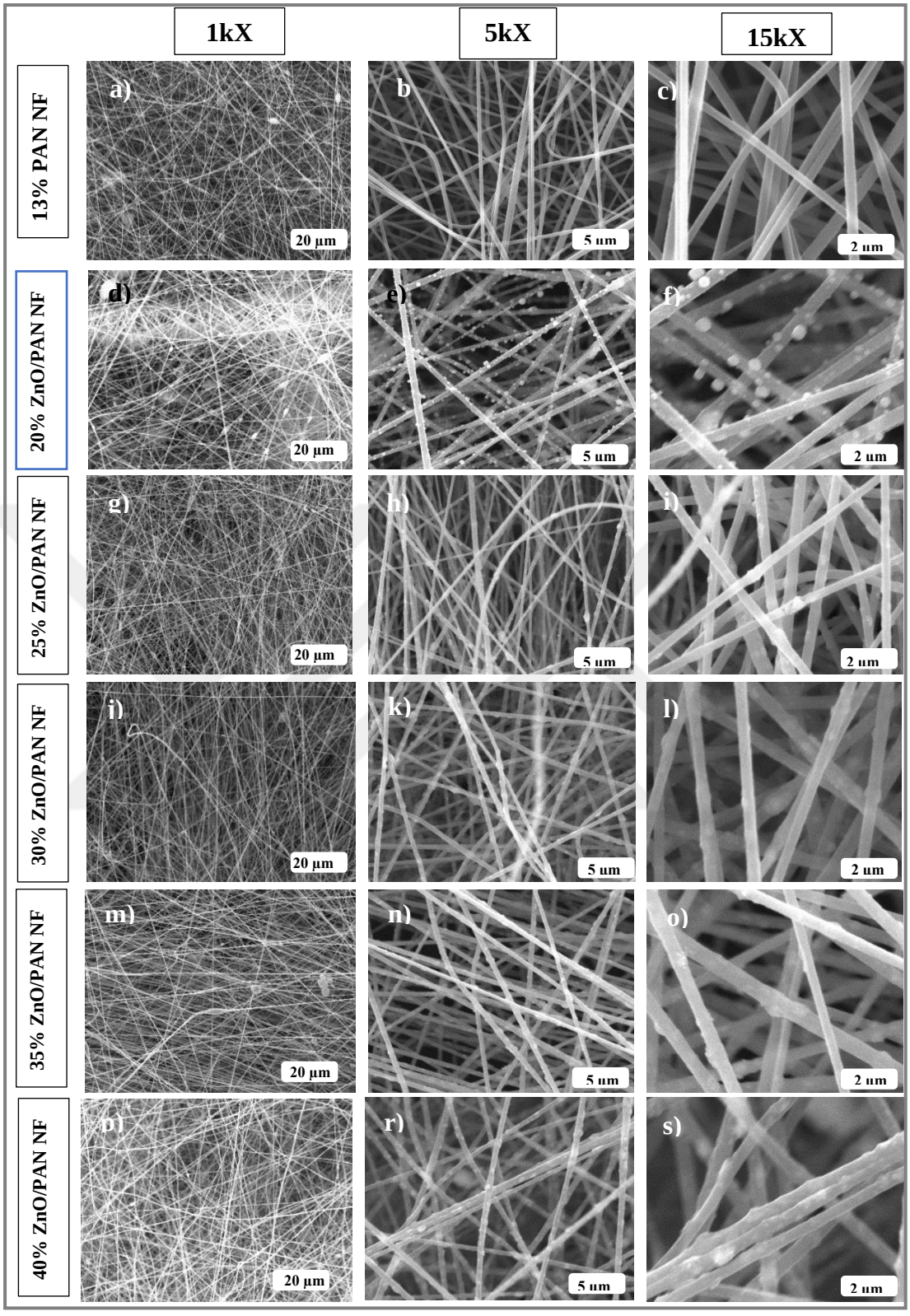

Figure 6.7 : Electrospinning time was kept constant (40 min) in all samples. For 13% PAN NF a) magnification (m):1 kX; b) m: 5 kX; c) m: 15 kX. For 20% MgO/PAN NF d) m: 1 kX; e) m: 5 kX; f) m: 15 kX. For 25% MgO/PAN NF g) m: 1 kX; h) m: 5 kX; ı) m: 15 kX. For 30% MgO/PAN NF j) m: 1 kX; k) m: 5 kX; l) m: 15 kX. For 35% MgO/PAN NF m) m: 1 kX; n) m: 5 kX; o) m: 15 kX. For 40% ZnO /PAN NF p) m: 1 kX; r) m: 5 kX; s) m: 15 kX.

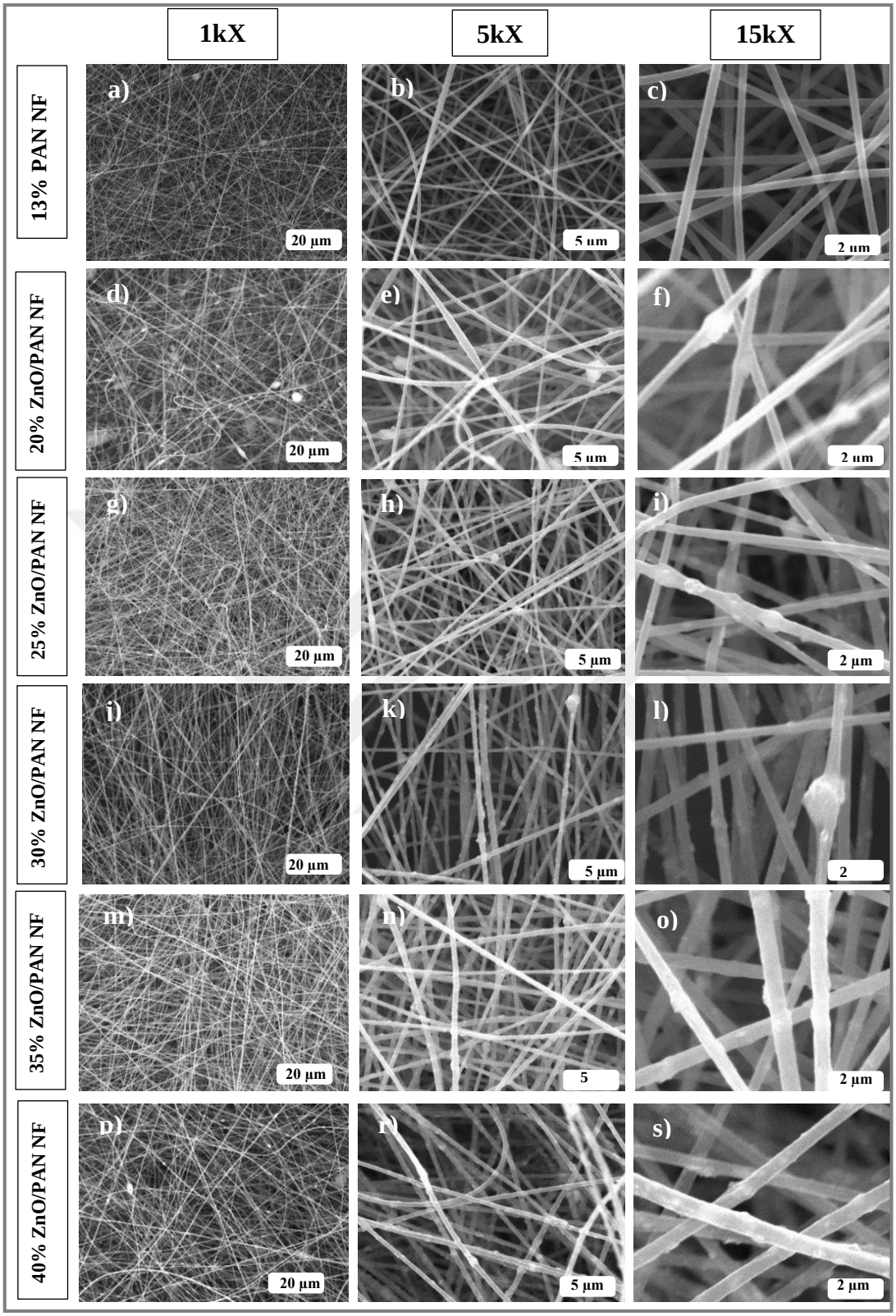

Figure 6.8 : Electrospinning time was kept constant (40 min) in all samples. For 13% PAN NF a) magnification (m):1 kX; b) m: 5 kX; c) m: 15 kX. For 20% MgO/PAN NF d) m: 1 kX; e) m: 5 kX; f) m: 15 kX. For 25% MgO/PAN NF g) m: 1 kX; h) m: 5 kX; ı) m: 15 kX. For 30% MgO/PAN NF j) m: 1 kX; k) m: 5 kX; l) m: 15 kX. For 35% MgO/PAN NF m) m: 1 kX; n) m: 5 kX; o) m: 15 kX. For 40% ZnO /PAN NF p) m: 1 kX; r) m: 5 kX; s) m: 15 kX.

The diameter of the nanofibers was measured using the ImageJ software (Figure 6.9 and Figure 6.10). Average fiber diameters were calculated using 20, 40 and 60-minute SEM images of each sample. Fiber diameter measurements were made from the smooth parts of the nanofiber where the nanoparticle is not deposited.

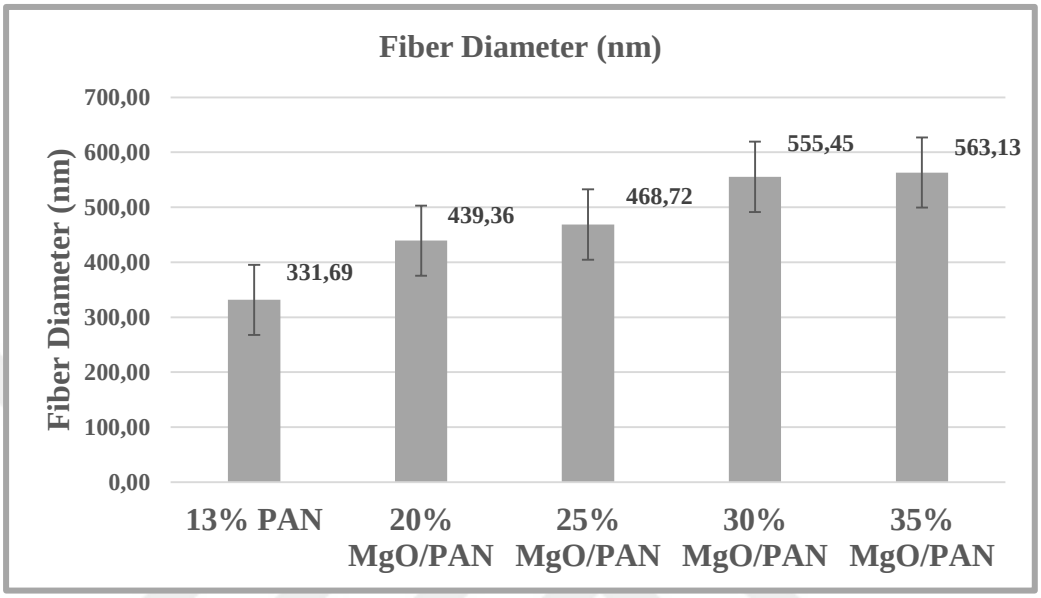

Figure 6.9 : Changes in fiber diameter with the addition of MgO NP.

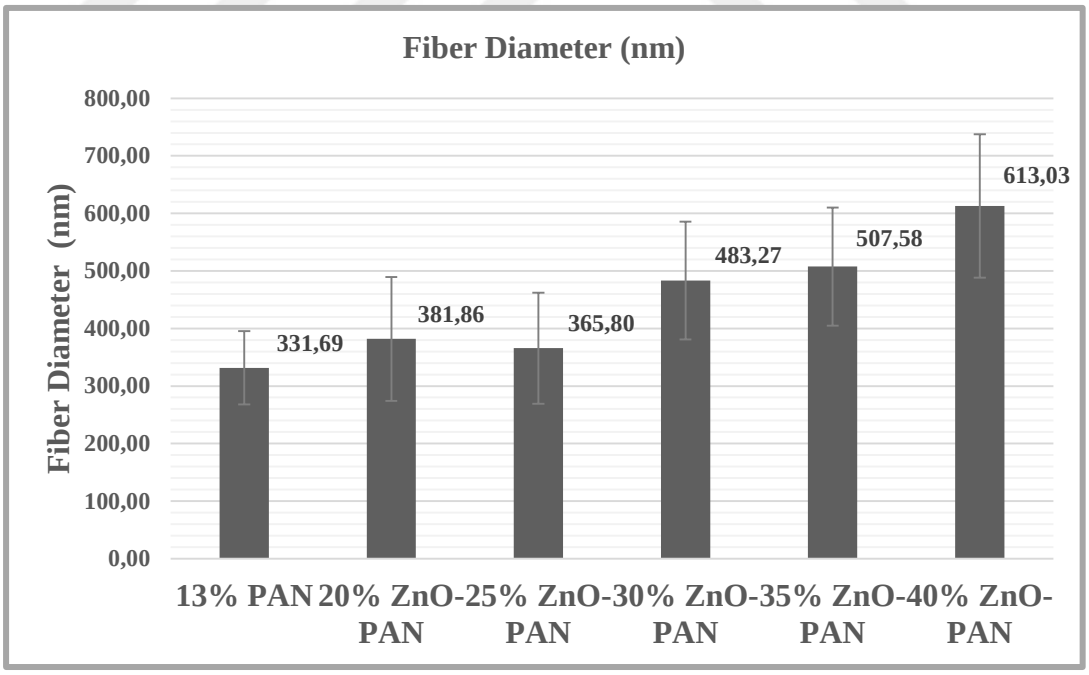

Figure 6.10 : Changes in fiber diameter with the addition of ZnO NP.

As can be seen in the Figure 6.9 and 6.10, the fiber diameter increased as the NP concentration in the solution increased. Increased NP concentration was thought to increase viscosity and therefore increased fiber diameter [127].

6.1.4 Morphology of MgO nanoparticles

To measure the size of the MgO NPs used, MgO NPs in the powder form were sprinkled onto the carbon tape and the SEM image was obtained. Particle sizes were measured from the SEM image (Figure 6.11).

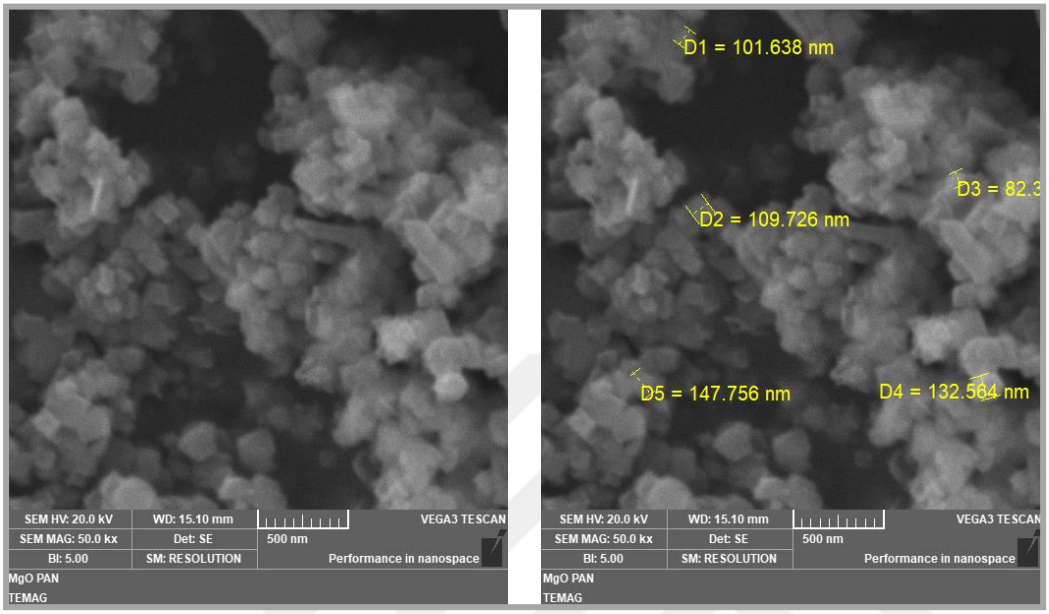

Figure 6.11 : SEM image and size measurement of MgO NPs

Although the product label of MgO NPs states that the MgO NPs have a particle size of 50 nm and smaller, particle sizes appear to be larger than the claimed values on the product label (Figure 6.11).

6.2 Air Filtration Test Results

According to the TS EN 149, the filtration test was performed with 2 different air velocities, 95 l/min and 32 l/min by using pure PAN NF and MgO/PAN NFs. The results are given in Table 6.1 and Figure 6.12-6.17 for 95 l/min. The results of air filtration test done at the air velocity of 32 l/min are given in the appendix.

The breathing resistance (pressure drop value) and filtration efficiency of face masks must comply with the values specified in EN 149+A1 Standard. The breathing resistance should be less than 2.1 mbar (0.21 kPa) when the filtration efficiency is greater than or equal to 80% for the FFP1 protection level, and the breathing resistance should be less than 2.4 mbar (0.24 kPa) when the filtration efficiency is then greater than or equal to 94% for the FFP2 protection level at a flow rate of 95 l/min as specified in EN 149+A1 Standard.

Table 6.1 : Particulate filtration test results of all produced nanofiber filters (the air velocity:95 l/min).

	Filtration Efficiency (%)					Pressure Drop (kPa)				
	13% PAN	**20% MgO/ PAN**	**25% MgO/ PAN**	**30% MgO/ PAN**	**35% MgO/ PAN**	**13% PAN**	**20% MgO/ PAN**	**25% MgO/ PAN**	**30% MgO/ PAN**	**35% MgO/ PAN**
20 min	94.6	86.3	82.5	44.2	50.0	0.225	0.101	0.080	0.036	0.051
40 min	97.3	90.2	95.8	85.7	74.7	0.361	0.146	0.213	0.120	0.117
60 min	98.9	95.7	97.6	96.2	93.0	0.451	0.207	0.215	0.253	0.256

	Quality Factor				
	13% PAN	**20% MgO/ PAN**	**25% MgO/ PAN**	**30% MgO/ PAN**	**35% MgO/ PAN**
20 min	0.013	0.0196	0.0218	0.0162	0.0137
40 min	0.010	0.0159	0.0149	0.0162	0.0117
60 min	0.010	0.0153	0.0174	0.0129	0.0104

In the light of this information, 20% and 25% MgO/PAN filters meet the standard, while the PAN filter not containing nanoparticles does not meet the standard due to the fact that pressure drop is rather above the acceptable limit despite its high filtration efficiency. Likewise, 30% and 35% MgO/PAN filters are not in accordance with the standard.

6.2.1 Effect of thickness on particulate filtration

As the thickness of the filter (depending on the coating time) increases, the pore size between the NFs decreases due to overlapping of the NFs. This situation leads to increase in both filtration efficiency and pressure drop (Figure 6.12 and 6.13). Although high filtration value is desired in face masks, high pressure value is not desired because in the case of higher pressure drop, air cannot pass through the filter and it becomes very difficult for the mask user to breathe.

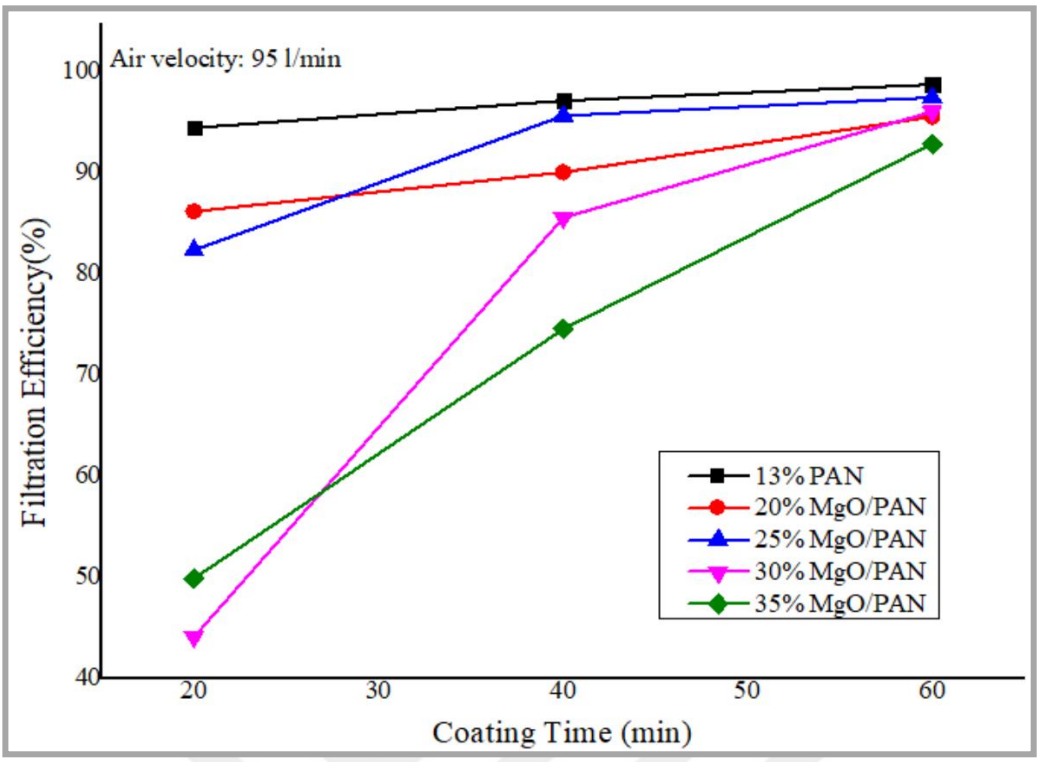

Figure 6.12 : Effect of thickness on filtration efficiency for all related samples produced.

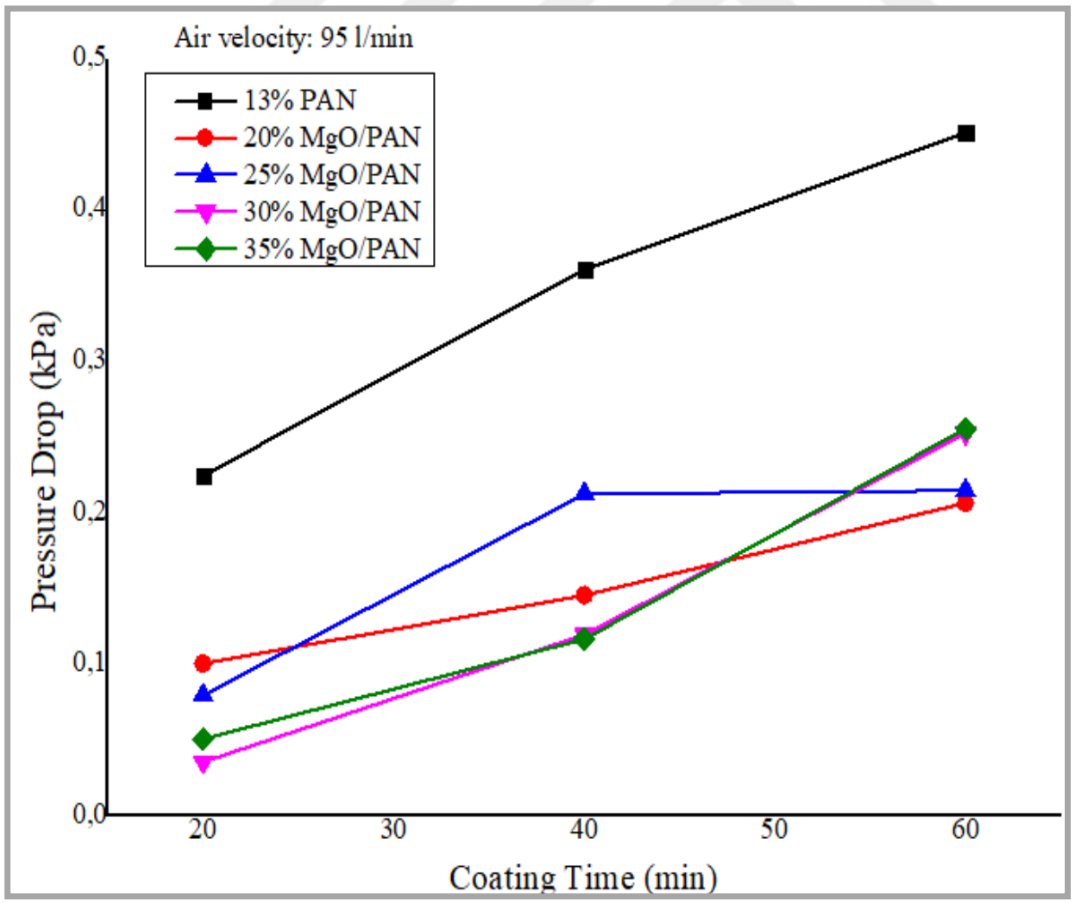

Figure 6.13 : Effect of thickness on pressure drop for all related samples produced.

6.2.2 Effect of nanoparticle concentration on particulate filtration

The results of the tests performed to examine effect of nanoparticle concentration on particle filtration were given in the graphics below. Filtration performance results of samples prepared in three different coating times for each MgO/PAN with different concentrations were shown in Figures 6.14 and 6.15, and the quality factor values calculated using these data were shown in Figure 6.16.

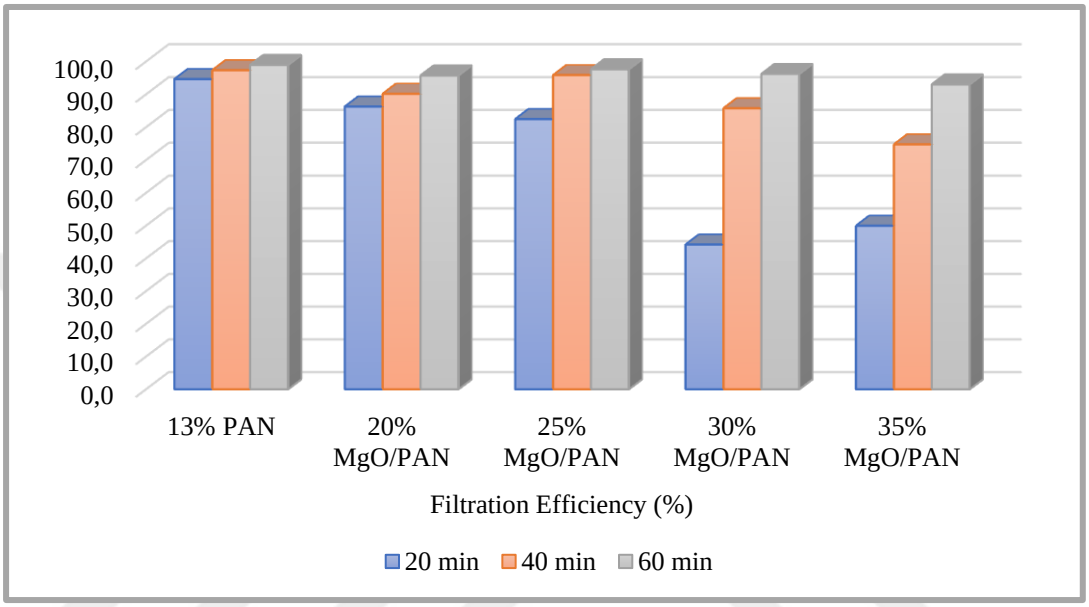

Figure 6.14 : Effect of nanoparticle concentration on filtration efficiency for all related samples produced.

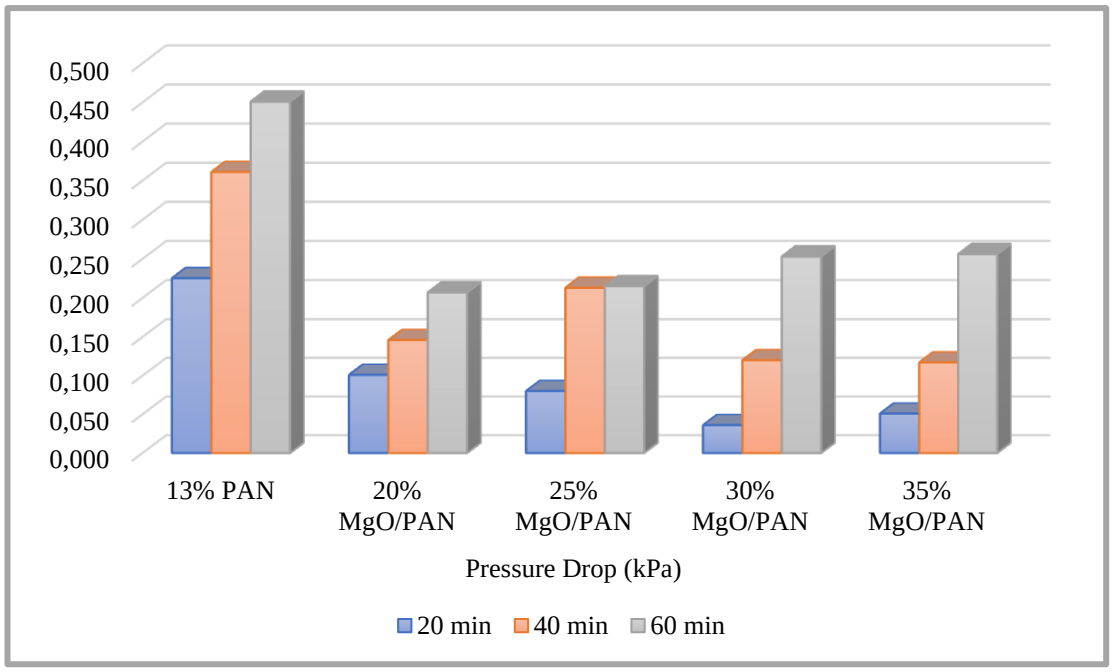

Figure 6.15 : Effect of nanoparticle concentration on pressure drop for all related samples produced.

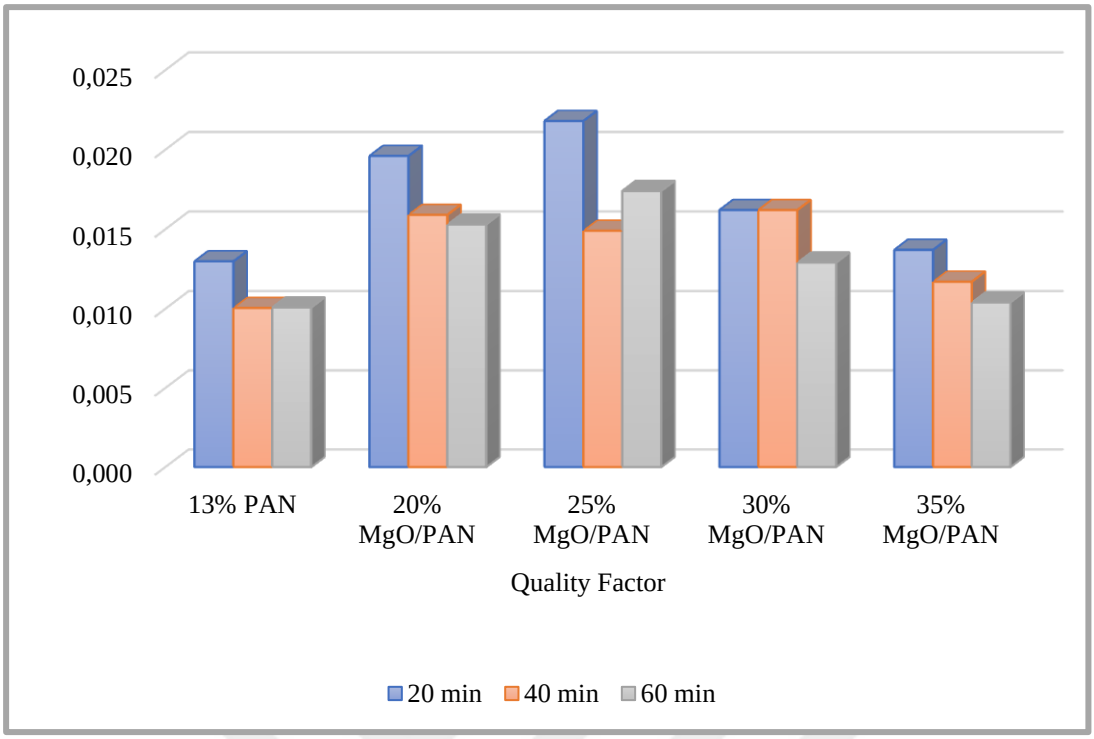

Figure 6.16 : Effect of nanoparticle concentration on quality factor for all related samples.

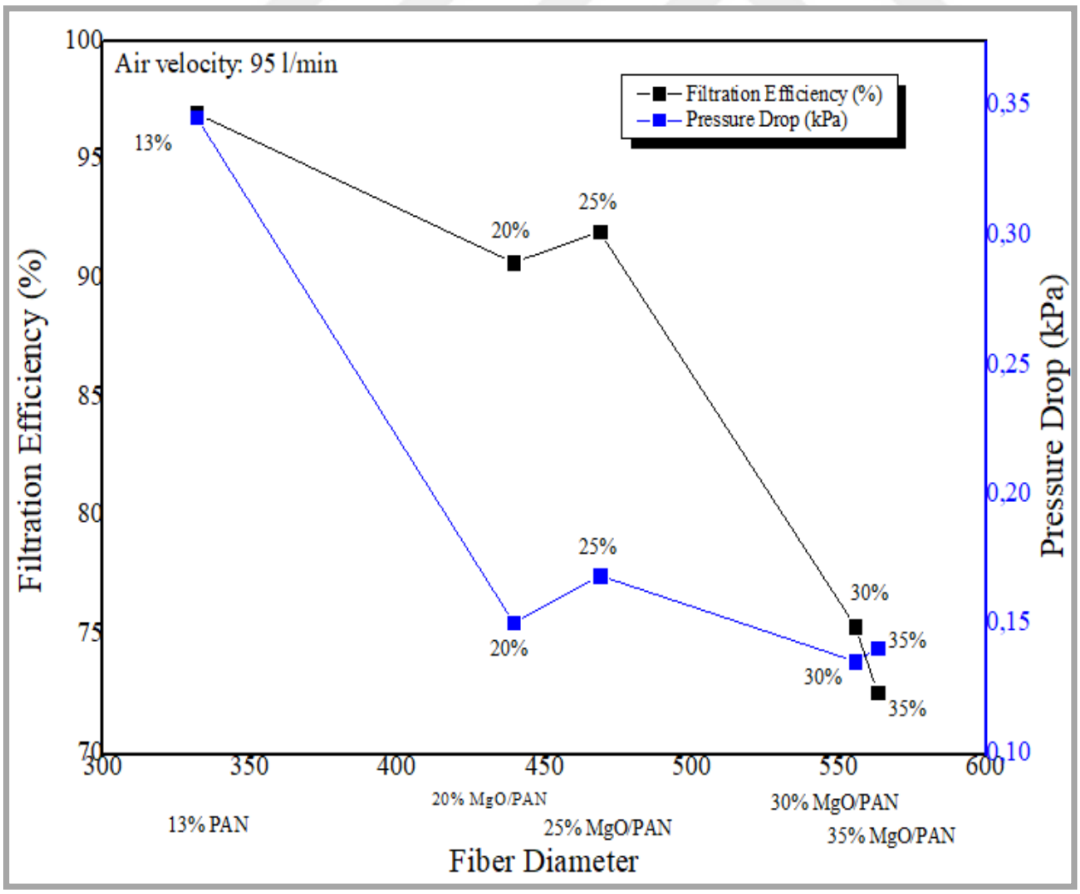

Figure 6.17 : Filtration efficiency and pressure drop of nanofibers with various fiber diameter under an air velocity of 95 l/min.

The graph in Figure 6.17 was drawn to show effect of nanoparticle concentration and fiber diameter on particulate filtration. Average fiber diameter and average filtration performance values were used for each MgO/PAN concentration to avoid complexity.

As seen in the graph, 13% PAN sample with the smallest fiber diameter had the highest filtration efficiency and pressure drop value. According to the literature, as the fiber diameter increases, the pore size increases among the fibers, thereby reducing filtration efficiency and pressure drop.

For 20% and 25% MgO/PAN samples, despite the increased fiber diameter and therefore increased the pore sizes among the fibers, an slight decrease in filtration efficiency was observed because of the homogeneously dispersed MgO NPs on the nanofiber surface. The particles must have adsorbed to MgO NPs. With the addition of MgO nanoparticle, there was a slight decrease in filtration efficiency, while the pressure drop was significantly reduced, thus producing filters with high quality factors. With the addition of MgO nanoparticle, there was a slight decrease in filtration efficiency, while the pressure drop decreased dramatically and thus filters with high quality factor were produced.

In the 30% and 35% MgO/PAN samples, the lowest filtration efficiency and pressure drop were observed due to both high fiber diameter and MgO NP agglomeration. 25% MgO/PAN sample showed the best result in terms of filtration performance.

6.3 Toluene Adsorption Test Results

As the Figure 6.18, 6.19 and 6.20 indicated, the increased amount of NPs (30% and 35% MgO/PAN) have inevitably resulted in agglomeration of NPs and their particulate filtration performance has been found rather low. So, just only the samples of 20% and 25% MgO/PAN showing uniform nanoparticle distribution on nanofiber surface with less agglomeration compared to others were used for our toluene test. Unfortunately, during the adsorption test, we have obtained inconsistent adsorption results that may result from not being stable of the toluene test set up, and we have only utilized the acceptable and reasonable results. To repeat the experiments by using other adsorption methods will be beneficial for the accuracy of the data.

6.3.1 Effect of thickness and adsorption time on toluene adsorption

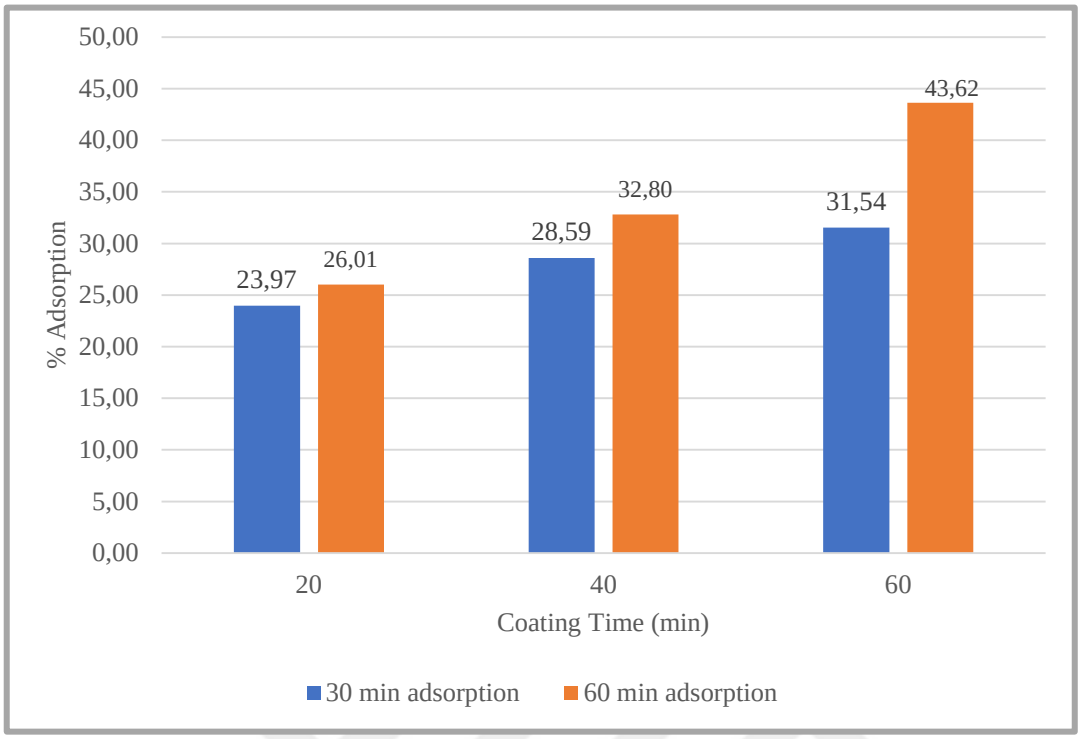

Figure 6.18 : Effect of coating time and adsorption time on toluene adsorption for 20% MgO/PAN sample.

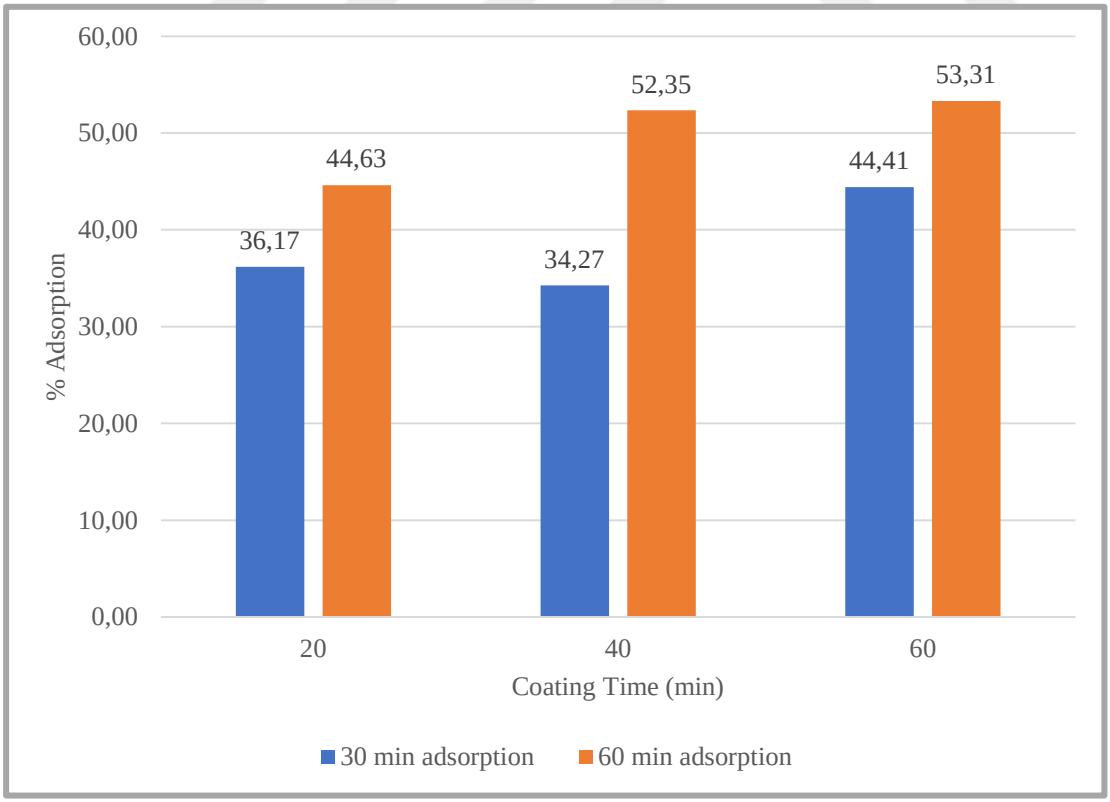

Figure 6.19 : Effect of coating time and adsorption time on toluene adsorption for 25% MgO/PAN sample.

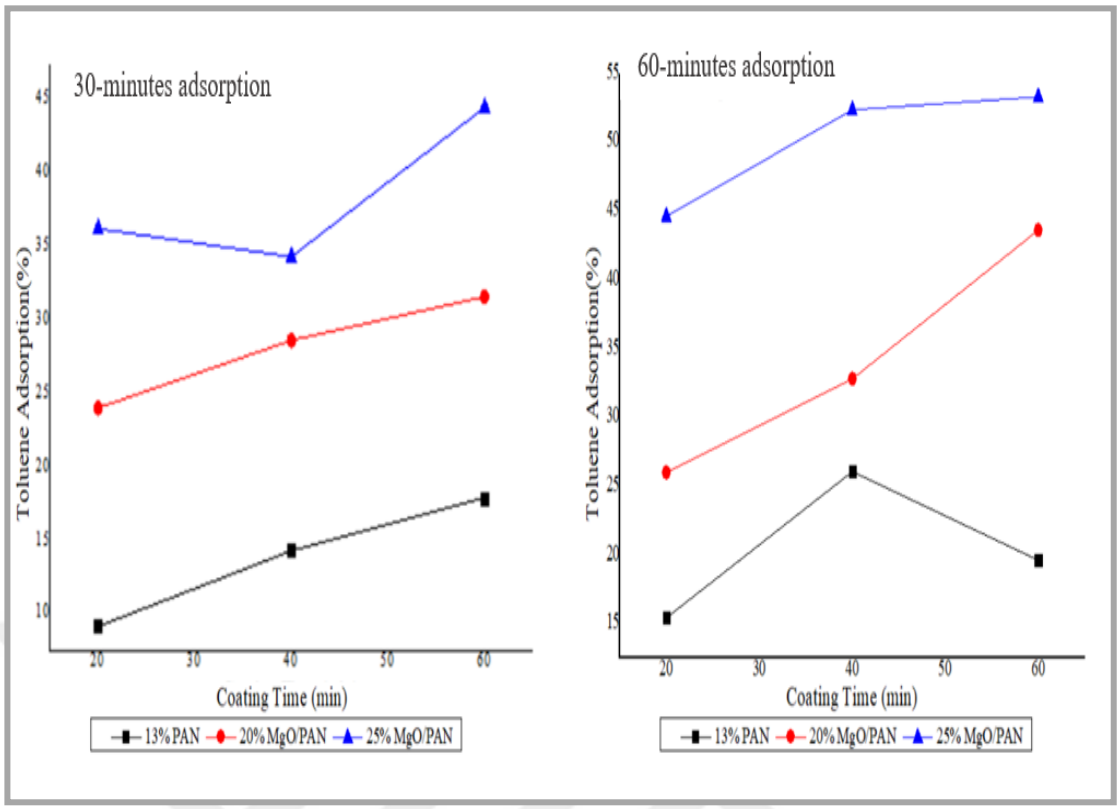

Figure 6.20 : Effect of coating time and adsorption time on toluene adsorption for all samples analyzed.

As the thickness of the filter (depending on the coating time) increases, the pore size between the NFs decreases due to overlapping of the NFs, so that toluene gas can be trapped by the classical molecular sieving technique and adsorbed to the MgO NPs inside the nanofiber layer.

As the adsorption time increased, the amount of toluene gas adsorbed increased. In other words, there were still regions where toluene could be adsorbed. Slowing down in the adsorption amount is due to the reduction of available open sites that adsorption occurs (Figure 6.18-6.20).

When the adsorption time was 30 minutes, with increasing coating time the slight reduction in toluene adsorption was observed for 25% MgO/PAN sample. It was probably due to the instability of the test process. Because when the adsorption time was 60 minutes, toluene adsorption increased with increasing coating time for the same 25% MgO/PAN sample.

The decrease in the toluene adsorption for 13% PAN sample in 60 minutes adsorption time could be arise from weak physical adsorption between PAN and toluene. A similar result was obtained in the study done by Behnam et al [128].

6.3.2 Effect of nanoparticle concentration on toluene adsorption

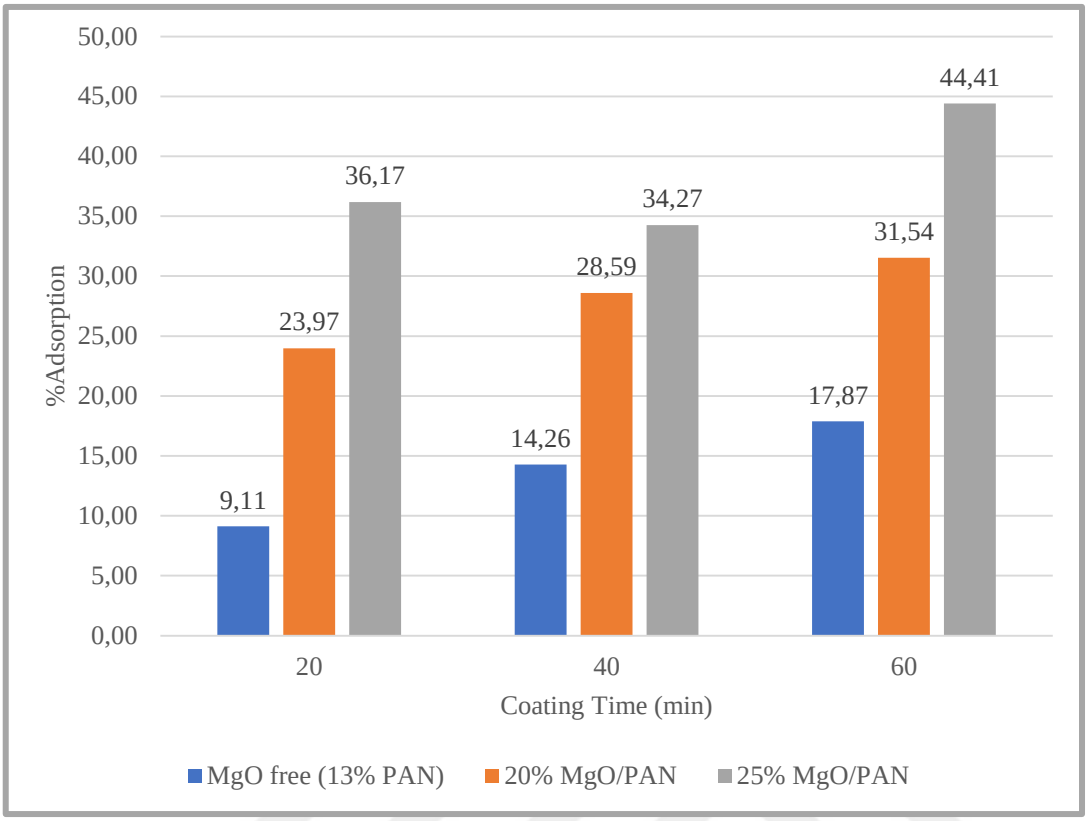

Figure 6.21 : Effect of nanoparticle concentration on toluene adsorption for 30 minutes adsorption time.

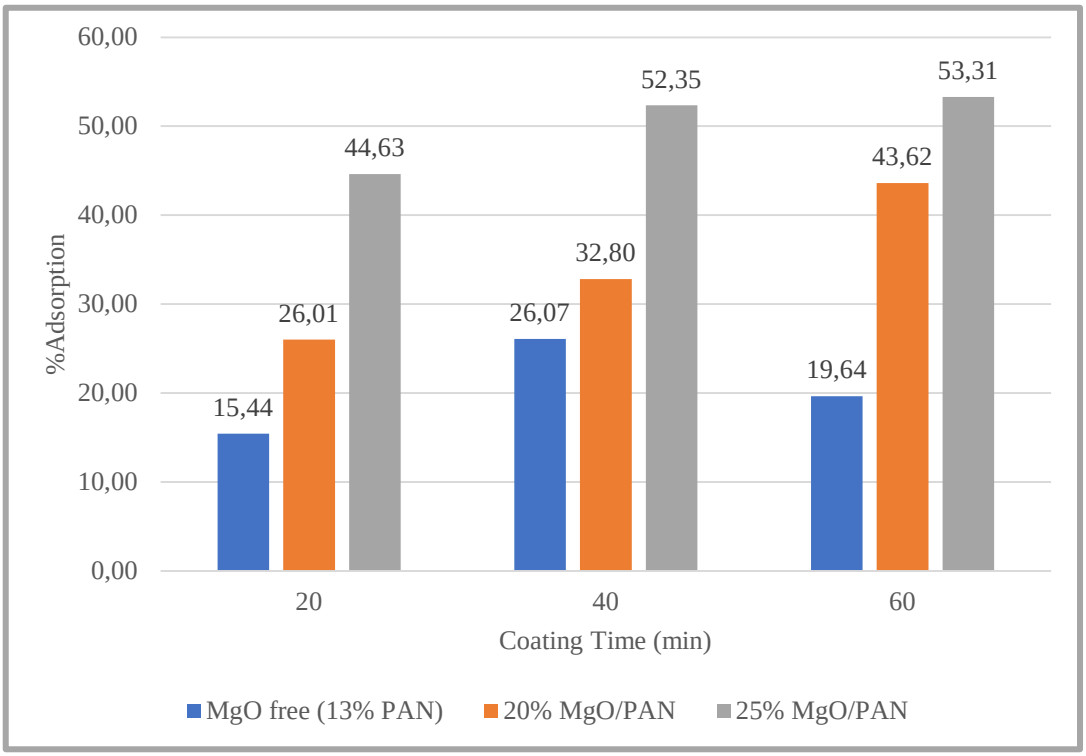

Figure 6.22 : Effect of nanoparticle concentration on toluene adsorption for 60 minutes adsorption time.

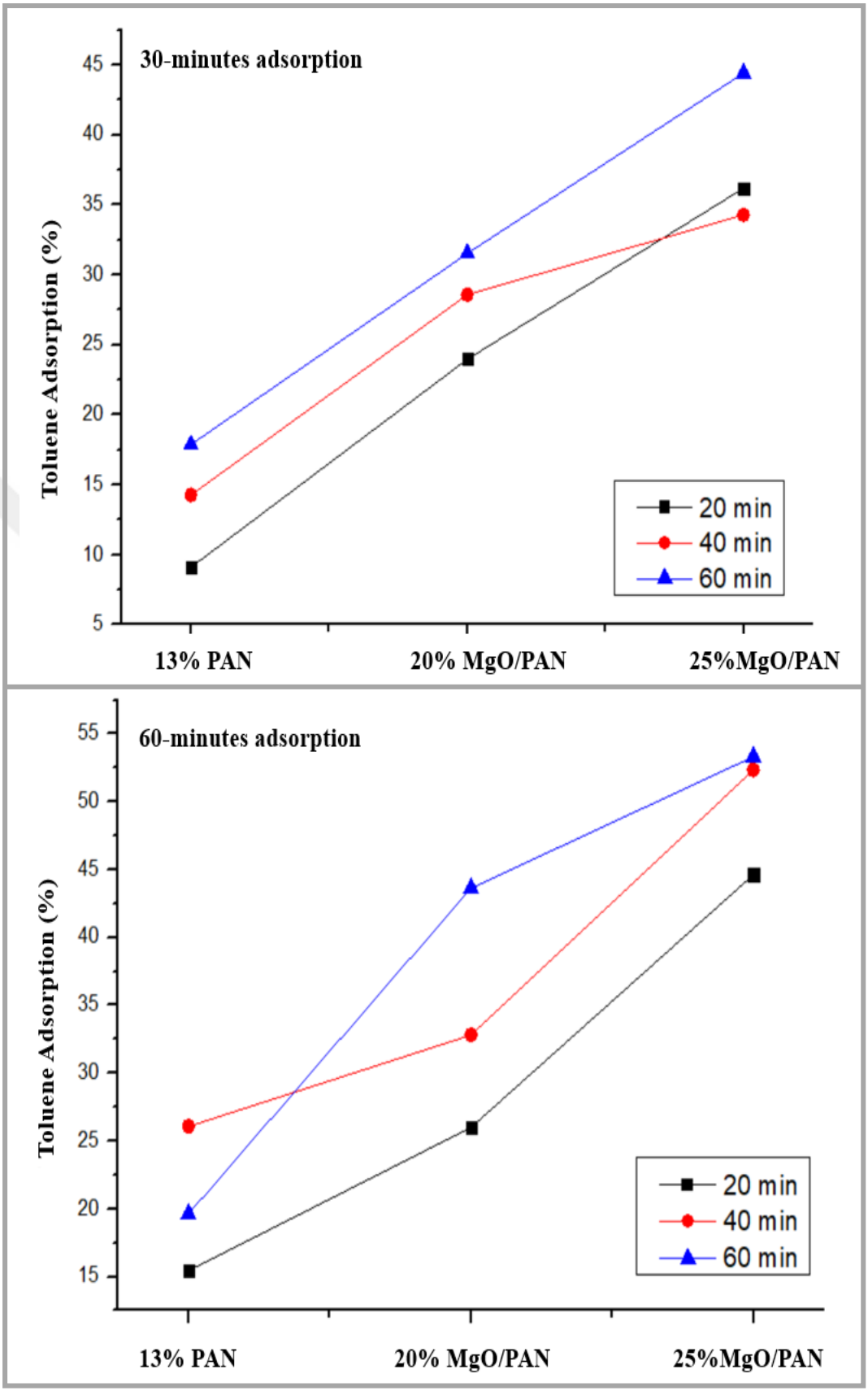

Figure 6.23 : Effect of nanoparticle concentration on toluene adsorption for all samples analyzed for both 30 and 60 minutes adsorption time.

The toluene adsorption of PAN NFs containing MgO NPs is higher than that of neat PAN NFs. It is clear that MgO NPs have a great effect on the adsorption ability of PAN NF.

The percentage of adsorbed toluene increased as the amount of MgO NP onto PAN NF increased (Figure 6.21-6.23).Because of the surface oxide, magnesium and hydroxide ions of MgO NPs can be physically bound to toluene gas through hydrogen bonds, ion-dipole and dipole-dipole interactions.

Moreover, defect sites and low-coordinated atoms of NPs can be covalently bound with toluene. As the concentration of MgO NPs increases, the total ion concentrations of MgO NPs surface increases, so chemical affinity between the MgO NPs and the toluene gas rise and result in higher toluene adsorption [127–129].

As it has been mentioned in the section 4.3, MgO NPs have catalytic behavior, but this feature could not have been observed in any of our test results. It was not observed another component except toluene in GC-MS analyses, after treatment of toluene with MgO/PAN NFs. If the toluene catalytic decomposition occurred, the formation of by-products such as H_2, CO, CO_2 would have been expected. This may be due to coating of MgO NPs with PAN polymer, which leads to a decrease in effectiveness of MgO NPs.

Other reasons may be that the particle size of the MgO NPs used is not small enough and hence agglomeration problem was occurred. According to the literature, as the nanoparticle size decreases, number of low-coordinated atoms that are more reactive increased and some defects are formed in the corner and edge sites of the crystalline structure of MgO , which can react with toxic gases and decompose them [127–129].

6.4 Antibacterial Test Results

ZnO NPs were expected to give antibacterial properties to the produced nanofiber filter. For this purpose, ZnO/PAN nanofibers were used in various ZnO concentrations against for gram-negative *Escherichia coli* and gram-positive *Staphylococcus aureus*.

Agar diffusion test results of produced samples against *S. aureus* were shown in Figure 6.24, against *E. coli* were shown in Figure 6.25. The effect of increasing ZnO NP on antibacterial activity was investigated.

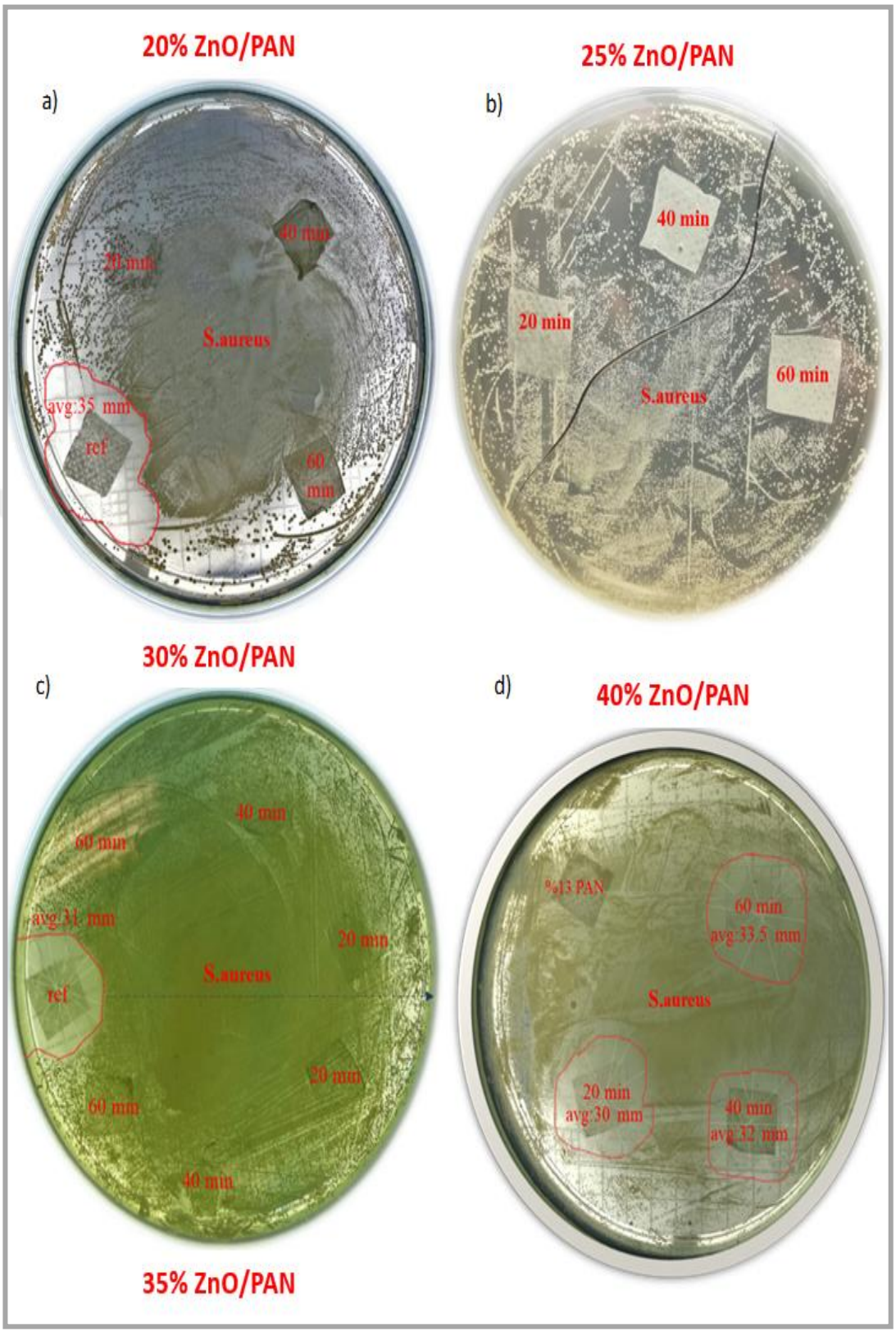

Figure 6.24 : Agar diffusion test results of various ZnO/PAN nanofibers with varying coating times of 20 minutes, 40 minutes and 60 minutes against *Staphylococcus aureus*, a gram positive bacteria; a) 20% ZnO/PAN, b) 25% ZnO/PAN, c) 30% ZnO/PAN (top) and 35% ZnO/PAN (bottom), d) 40% ZnO/PAN.

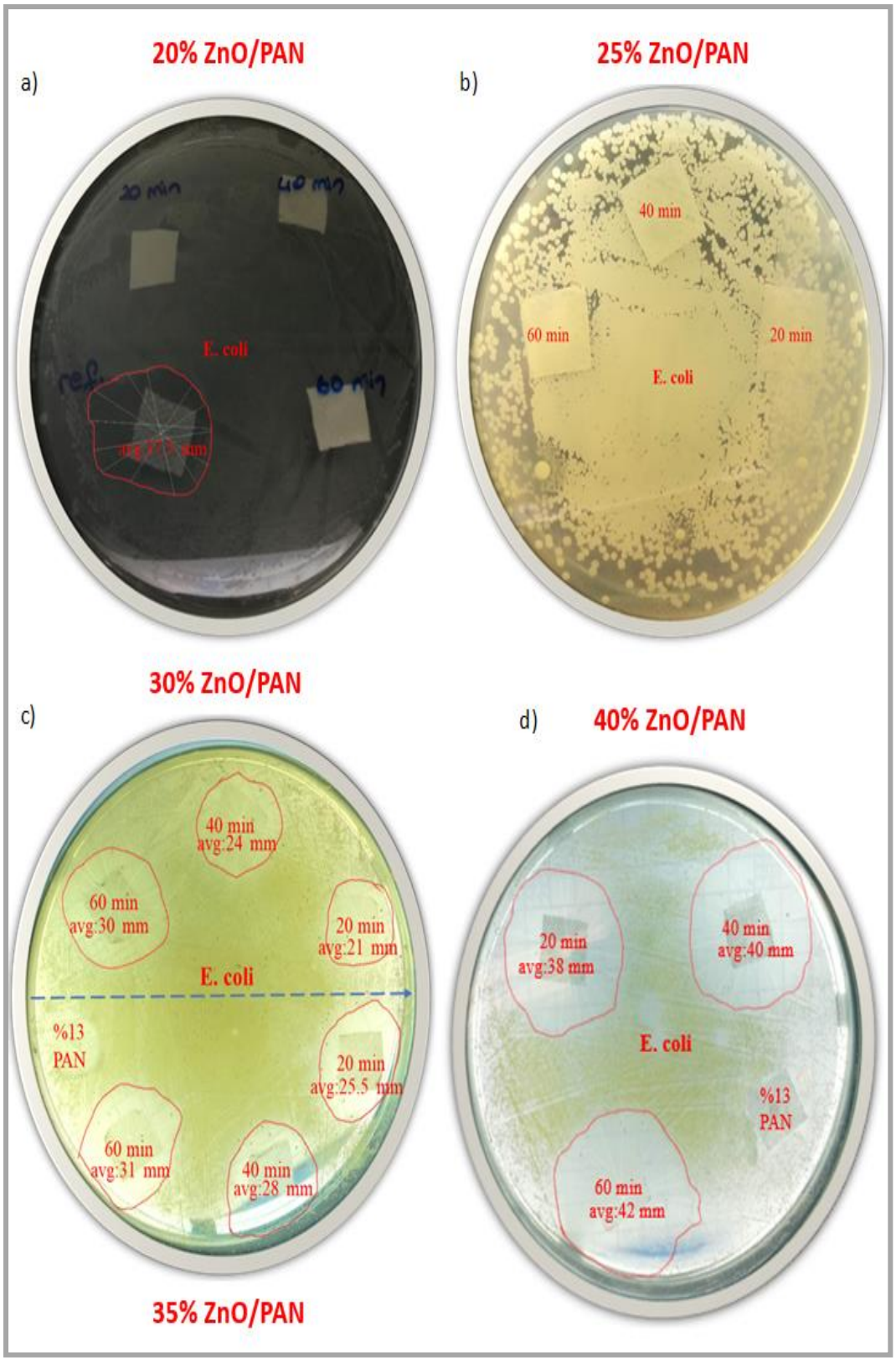

Figure 6.25 : Agar diffusion test results of various ZnO/PAN nanofibers with varying coating times of 20 minutes, 40 minutes and 60 minutes against *Escherichia coli*, a gram negative bacteria; a) 20% ZnO/PAN, b) 25% ZnO/PAN, c) 30% ZnO/PAN (top) and 35% ZnO/PAN (bottom), d) 40% ZnO/PAN.

6.4.1 Discussion on antibacterial test results

According to Figure 6.24, it can be concluded that an inhibition zone formed only in the sample of 40% ZnO/PAN (27wt% of ZnO NPs in solution). No antibacterial effect was observed at lower ZnO NPs concentration, which was not enough to prevent bacterial growth. In addition, as the thickness of the filter produced, that is, the coating time increased (from 20 min to 60 min), the inhibition zone also increased (from 30 mm to 33.5 mm) in the sample of 40% ZnO/PAN. This must be associated with an increase in the amount of ZnO NP in the sample.

According to Figure 6.25, the first inhibition zone was observed in the sample of 30% ZnO/PAN with 20 min coating time, and as the both ZnO concentration and coating time of samples increased, the zone diameter increased and reached to 42 mm.

While antibacterial activity against both gram-positive and gram-negative bacteria was not observed in the sample of 13wt% PAN that did not consist of any nanoparticle, 10 µl of 2wt% triclosan, whose antibacterial efficacy was previously known and used as reference material, showed antibacterial activity against both type of bacteria.Moreover, it is obvious that the antibacterial efficiency of ZnO NPs is higher against to gram-negative bacterium *E. coli* compared to gram-negative bacterium *S. aureus* due to differences in cell membrane of bacteria. Due to this difference in the cell wall, gram-positive bacteria seemed to be more resistant to ZnO nanoparticles than gram-negative bacteria.

In gram-negative bacteria such as *Escherichia coli*, bacterial cells are wrapped with a layer of lipopolysaccharide (1-3 µm thick) and peptitoglycans (~8 nm thick) as seen in Figure 6.26. This structure may ease to enter of ions released from the ZnO NPs into the cell. As a consequence of the physical interaction between ZnO NPs and the cell wall of bacterium, the cell wall of the bacterium is damaged. This damage is greater in gram-negative bacteria because the peptidoglycan layer, which has possibly protective properties, is thinner compared to gram-positive bacteria. Another reason may be that the Gram-negative bacteria are coated with lipopolysaccharide molecules carrying a negative charge. Because these negatively charged molecules have a higher attraction to the released positively charged ions, so the gram-negative bacteria cell will be destroyed more quickly.

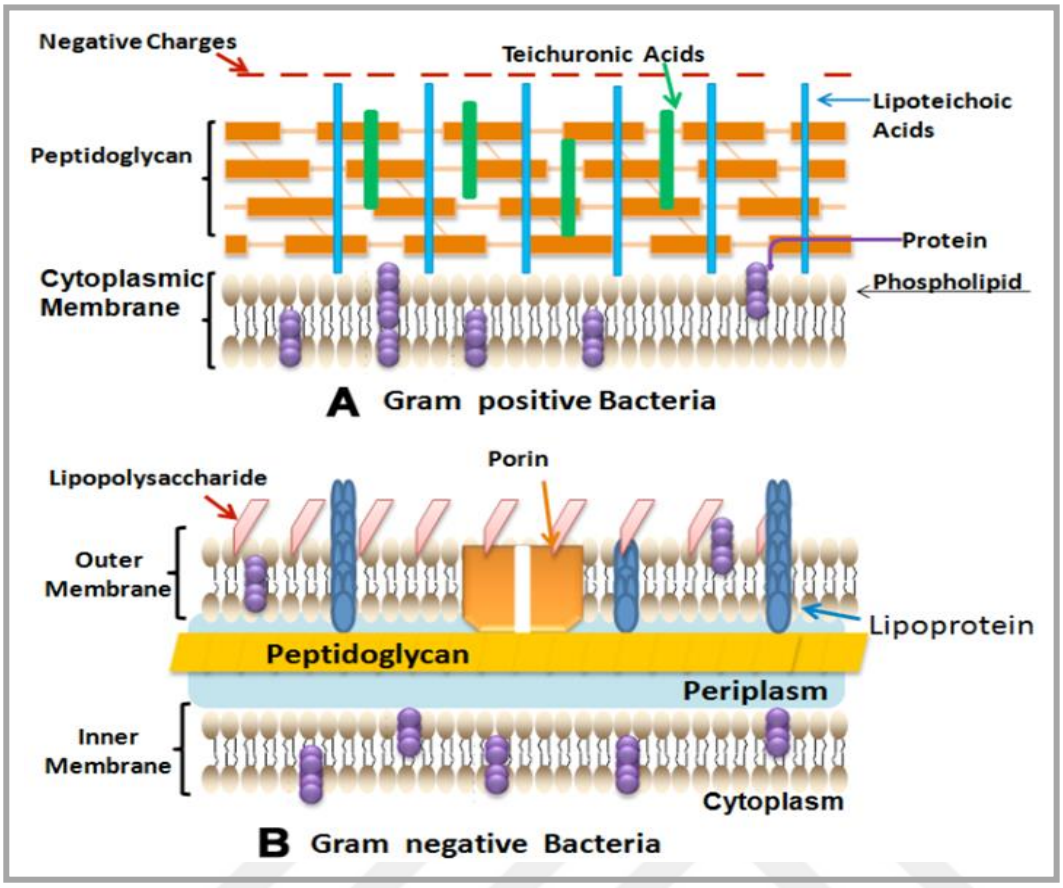

Figure 6.26 : A) Gram positive bacterial cell consisting of porous peptidoglycan layer and single lipid bilayer B) Gram negative bacterial cell consisting of peptidoglycan layer between bilayer lipid layers and an outer lipopolysaccharide layer [130].

7. CONCLUSIONS AND SUGGESTIONS FOR FURTHER WORK

Air quality has been decreasing day by day because of increasing industrialization, growing population and inadequate filtering systems used. Toxic gases, ultra-fine particles especially called PM10 and PM2.5 and biological pollutants such as bacteria and viruses in the air affect human health negatively. For this purpose, PAN nanofiber filters functionalized by MgO NP or ZnO NP have been produced, which have antibacterial properties, can adsorb toluene that is one of the toxic gases in the air, and can hold ultra-fine particles.

The PAN polymer was used because of its polar nature with a greater dipole moment compared to many polymers. Thus, PAN NF can easily capture particulate pollutants from the environment. To functionalize the nanofiber filter, MgO NP is preferred due to its high catalytic properties, while ZnO NP is preferred due to its high killing impact on bacteria.

With the addition of MgO NPs into PAN NF, the nanofiber morphology has become rough and nanofiber diameter increased. Normally, the filtration performance decreases as the nanofiber diameter increased. In this study filtration performance of produced filters increased in the case of distributing MgO NPs onto nanofiber surface homogeneously and without agglomeration (for 20% and 25% MgO/PAN filters) although nanofiber diameter increased. Since the nanofiber diameter increased, the pore size among nanofibers increased and so, pressure drop increased. By the means of oxide and hydroxyl groups on the nanofiber surface, particles were attracted to surface of NPs. So, filtration efficiency of filter did not decrease dramatically although nanofiber diameter increased.

It was also shown that nanofiber morphology is very important for particulate filtration performance. More addition of MgO NPs into polymer solution caused to agglomeration problem and, filtration performance of produced filters decreased dramatically (for 30% and 35% MgO/PAN filters). In this study, 25% MgO/PAN filter have showed high filtration efficiency of 97,6% and low pressure drop of 215 Pa, which meet the standard of EN149+A1.

We have also evaluated the impact of thickness of the nanofiber layer on particulate filtration. As the thickness of the filter increases, the pore size among NFs decreases due to overlapping of the NFs. This situation led to increase in both filtration efficiency and pressure drop. Although high filtration efficiency is desired in face masks, high pressure value is not desired because in the case of higher pressure drop, air molecules can not pass through the filter and it becomes very difficult for us to breathe.

We have also achieved a high amount of toluene adsorption (53.31%). The number of reactive surface ions of MgO NPs increases as the concentration of MgO NPs increases, so chemical affinity between the MgO NPs and the toluene gas increase and hence, result in higher toluene adsorption.

Moreover, we have observed that as the adsorption time increases, the amount of toluene gas adsorbed increases. In other words, there were still regions where toluene could be adsorbed. Slowing down in the adsorption amount is due to the reduction of available open sites that adsorption occurs.

The amount of toluene adsorbed increased when we used the more thicker nanofiber layer. This indicates that the toluene gas is adsorbed to the MgO NPs both at the surface and inside of nanofiber layer. Also, it was observed that pure 13% PAN NFs could adsorb toluene gas. This indicates that the pore sizes between nanofibers are small enough to adsorb gas molecules and toluene gas is captured by the classical molecular sieving technique.

We know from the literature that MgO NPs have catalytic behavior, but we have not seen this feature in any of our test results. This may be due to coating of MgO NPs with PAN polymer, which leads to a decrease in effectiveness of MgO NPs. Other reasons may be that the particle size of the MgO NPs used is not small enough and agglomeration problem.

We have also obtained antibacterial filter that produced from ZnO/PAN. While antibacterial activity against *E. coli* was first seen in the 30% ZnO/PAN filter, antibacterial activity against *S. aureus* was seen in the 40% ZnO/PAN filter containing higher ZnO NP. The other filters with lower ZnO concentration did not show any antibacterial effect. Namely, it is obvious that the antibacterial efficiency of ZnO NPs is higher against to gram-negative bacteria *E. coli* compared to gram-

positive bacteria *S. aureus* due to differences in cell membrane of bacteria. Due to this difference in the cell wall, gram-positive bacteria seemed to be more resistant to ZnO nanoparticles than gram-negative bacteria.

Suggestions:

As a future study, repeating the toluene gas adsorption test using one of the other adsorption methods will be useful to prove the accuracy of the data we found. Also, the adsorption test can be repeated using MgO NPs with a small enough particle size to see the catalytic activity of MgO NPs.

The particle filtration test and VOC (toluene) adsorption test can be repeated using ZnO/PAN filters to compare the filtration and adsorption performances of MgO/PAN and ZnO/PAN.

As a further study, it should be inserted the XRD or RAMAN characterization technique to prove the MgO or ZnO crystallinity and, to show the effective cooperation between metal oxide NPs and polymer.

REFERENCES

[1]**Keleş, R., Hamamcı, C. & Çoban, A.** (2012). *Çevre politikası*. (İmge Kitabevi).

[2]**Yerramilli, A., Dodla, V. B. R. & Yerramilli, S.** (2011). Air pollution, modeling and GIS based decision support systems for air quality risk assessment. *Advance air pollution* 295–324.

[3]**Kadam, V. V., Wang, L. & Padhye, R.** (2018). Electrospun Nanofibre Materials to Filter Air Pollutants – A Review. *Journal of Industrial Textiles*, 47. **8**: 2253-2280.

[4]**Kampa, M. & Castanas, E.** (2008). Human health effects of air pollution. *Environmental Pollution* **151**, 362–367.

[5]**Xing, Y.-F., Xu, Y.-H., Shi, M.-H. & Lian, Y.-X.** (2016). The impact of PM2.5 on the human respiratory system. *J Thorac Dis* **8**, E69–E74.

[6]**Anderson, J. O., Thundiyil, J. G. & Stolbach, A.** (2012). Clearing the Air: A Review of the Effects of Particulate Matter Air Pollution on Human Health. *J. Med. Toxicol.* **8**, 166–175.

[7]**Pöschl, U.** (2005). Atmospheric Aerosols: Composition, Transformation, Climate and Health Effects. *Angewandte Chemie International Edition* **44**, 7520–7540.

[8]**Khan, F. I. & Kr. Ghoshal, A.** (2000). Removal of Volatile Organic Compounds from polluted air. *Journal of Loss Prevention in the Process Industries* **13**, 527–545.

[9] **Sarigiannis, D. A., Gotti, A., & Karakitsios, S. P.** (2019). Indoor Air and Public Health. *In Management of Emerging Public Health Issues and Risks* (pp. 3-29). Academic Press. doi:10.1016/B978-0-12-813290-6.00001-9.

[10]**Kim, J. M., Kim, J. H., Lee, C. Y., Jerng, D. W. & Ahn, H. S.** (2018). Toluene and acetaldehyde removal from air on to graphene-based adsorbents with microsized pores. *Journal of Hazardous Materials* **344**, 458–465.

[11]**Li, L., Sun, Z., Li, H. & Keener, T. C.** (2012). Effects of activated carbon surface properties on the adsorption of volatile organic compounds. *Journal of the Air & Waste Management Association* **62**, 1196–1202.

[12]**Zhang, X., Gao, B., Creamer, A. E., Cao, C. & Li, Y.** (2017). Adsorption of VOCs onto engineered carbon materials: A review. *Journal of Hazardous Materials* **338**, 102–123.

[13] **US EPA, O.** (2014). Biological Pollutants' Impact on Indoor Air Quality. *US EPA*. https://www.epa.gov/indoor-air-quality-iaq/biological-pollutants-impact-indoor-air-quality.

[14] **Singh, S. B., Young, K. & Silver, L. L.** (2017). What is an "ideal" antibiotic? Discovery challenges and path forward. *Biochemical Pharmacology* **133**, 63–73.

[15] **Wertheim, H. F.** (2005). The role of nasal carriage in Staphylococcus aureus infections. *The Lancet Infectious Diseases* **5**, 751–762.

[16] **Clarke, S. C., Haigh, R. D., Freestone, P. P. E. & Williams, P. H.** (2002). Enteropathogenic Escherichia coli infection: history and clinical aspects. *British Journal of Biomedical Science* **59**, 123–127.

[17] **Dust Mask Ratings: FFP1 vs FFP2 vs FFP3- The Ultimate Guide.** ***Xamax Workplace Solutions*** https://www.xamax.co.uk/blog/how-to-pick-a-dust-mask-rating-p1-vs-p2-vs-p3.html (22.11.2019).

[18] **Toz Maskesi- Gaz Maskesi | MFA® Maske.** https://www.mfamask.com/sayfa-detay-onemli-bilgiler-10.aspx.

[19] **isgtedbir. Solunum Koruyucular & Maskeler.** https://isgtedbir.com/diger/solunum-koruyucular/ (2016).

[20] **Chirkin, A. V. & Kaptsov, V. A.** (2013). Proper use of gas masks as prevention of occupational diseases. *Gig Sanit* 42–45.

[21] **Valipouri, A.** (2017). Production Scale Up of Nanofibers: A Review. *Journal of Textıles and Polymers* **5**, 9.

[22] **Wei, Q.** (2012). *Functional Nanofibers and their Applications*. (Elsevier).

[23] **Jeevanandam, J., Barhoum, A., Chan, Y. S., Dufresne, A. & Danquah, M. K.** (2018). Review on nanoparticles and nanostructured materials: history, sources, toxicity and regulations. *Beilstein J Nanotechnol* **9**, 1050–1074.

[24] **Tiwari, J. N., Tiwari, R. N. & Kim, K. S.** (2012). Zero-dimensional, one-dimensional, two-dimensional and three-dimensional nanostructured materials for advanced electrochemical energy devices. *Progress in Materials Science* **57**, 724–803.

[25] **Burger, C., Hsiao, B. S. & Chu, B.** (2006). Nanofibrous Materials and Their Applications. *Annual Review of Materials Research* **36**, 333–368.

[26] **Barhoum, A., Rasouli, R., Yousefzadeh, M., Rahier, H. & Bechelany, M.** (2018). Nanofiber Technology: History and Developments. In *Handbook of Nanofibers* (eds. Barhoum, A., Bechelany, M. & Makhlouf, A.) 1–42 (Springer International Publishing).

27] **Jirsák, O. and Dao, T. A.** (2009). Production, Properties and End-Uses of Nanofibres. In *Nanotechnology in Construction 3* (eds. Bittnar, Z., Bartos, P. J. M., Němeček, J., Šmilauer, V. & Zeman, J.) 95–99 (Springer Berlin Heidelberg). doi:10.1007/978-3-642-00980-8_11.

[28] **Beglou, M. J. & Haghi, A. K.** Electrospun Biodegradable and Biocompatible Natural Nanofibers: A Detailed Review. *Cellulose Chemistry & Technology*, *42*(9), 441.

[29] **Bhattarai, N., Li, Z., Edmondson, D. & Zhang, M.** (2006). Alginate-Based Nanofibrous Scaffolds: Structural, Mechanical, and Biological Properties. *Advanced Materials* **18**, 1463–1467.

[30] **Amalorpava Mary, L.** Senthilram T. Suganya S. Nagarajan L. Venugopal J. Ramakrishna S. Giri Dev V. R. (2013). Centrifugal spun ultrafine fibrous web as a potential drug delivery vehicle. *Express Polymer Letters* **7**, 238–248.

[31] **Kumbar, S. G., James, R., Nukavarapu, S. P. & Laurencin, C. T.** (2008). Electrospun nanofiber scaffolds: engineering soft tissues. *Biomedical materials* **3**, 034002.

[32] **Zhang, Q., Welch, J., Park, H., Wu, C. Y., Sigmund, W., and Marijnissen, J. C. M.** (2010). Improvement in nanofiber filtration by multiple thin layers of nanofiber mats. *Journal of Aerosol Science* **41**, 230–236.

[33] **Aliabadi, M.** (2017). Effect of electrospinning parameters on the air filtration performance using electrospun polyamide-6 nanofibers. *Chemical Industry and Chemical Engineering Quarterly* **23**, 441–446.

[34] **Huang, Z.-M., Zhang, Y. Z., Ramakrishna, S. & Lim, C. T.** (2004). Electrospinning and mechanical characterization of gelatin nanofibers. *Polymer* **45**, 5361–5368.

[35] **Boakye, M. A. D., Rijal, N. P., Adhikari, U. & Bhattarai, N.** (2015). Fabrication and Characterization of Electrospun PCL-MgO-Keratin-Based Composite Nanofibers for Biomedical Applications. *Materials* **8**, 4080–4095.

[36] **Costa, L. M. M., de Olyveira, G. M., Cherian, B. M., Leão, A. L., de Souza, S. F., Ferreira, M.** (2013). Bionanocomposites from Electrospun PVA/Pineapple Nanofibers/Stryphnodendron Adstringens Bark Extract for Medical Applications. *Industrial Crops and Products* **41**, 198–202.

[37] **Dadvar, S., Tavanai, H. & Morshed, M.** (2011). UV-Protection Properties of Electrospun Polyacrylonitrile Nanofibrous Mats Embedded with Mgo and Al_2O_3 Nanoparticles. *Journal of Nanoparticle Research* **13**, 5163–5169.

[38] **Pattanshetti, V. V., Shashidhara, G. M. & Veena, M. G.** (2018). Dielectric and thermal properties of magnesium oxide/poly(aryl ether ketone nanocomposites. *Science and Engineering of Composite Materials* **25**, 915–925.

[39] **Cheng, Y., Wang, C., Zhong, J., Lin, S., Xiao, Y., Zhong, Q., Hulin, J., Nan, W., Wenbo, L., Shuwen, C., Bo, W., Yingying, Z., Jun, Z.** (2017). Electrospun polyetherimide electret nonwoven for bi-functional smart face mask. *Nano Energy* 34: 562-569.

[40] **Sharma, N. and Kakkar, R.** (2013). Recent Advancements on Warfare Agents/Metal Oxides Surface Chemistry and Their Simulation Study. *Advanced Materials Letters* **4**, 508–521.

[41] **Homaeigohar, S. and Elbahri, M.** (2014). Nanocomposite Electrospun Nanofiber Membranes for Environmental Remediation. *Materials* **7**, 1017–1045.

[42] **Wang, X. and Li, B.** (2014). Electrospun Nanofibrous Sorbents and Membranes for Carbon Dioxide Capture. B, Ding, J. Yu (Eds.), In *Electrospun*

Nanofibers for Energy and Environmental Applications (pp. 249–263) Berlin, Heidelberg, Springer. doi:10.1007/978-3-642-54160-5_10.

[43] **Sahoo, T. R.** (2017). Polymer Nanocomposites for Environmental Applications. D.K. Tripathy, B.P. Sahoo (Eds.), In *Properties and Applications of Polymer Nanocomposites: Clay and Carbon Based Polymer Nanocomposites* (pp. 77-106). Berlin, Heidelberg, Springer. doi:10.1007/978-3-662-53517-2_5.

[44] **Yoon, K., Hsiao, B. S. & Chu, B.** (2008). Functional nanofibers for environmental applications. *Journal of Materials Chemistry* **18**, 5326–5334.

[45] **Sundarrajan, S. & Ramakrishna, S.** (2007). Fabrication of Nanocomposite Membranes from Nanofibers and Nanoparticles for Protection against Chemical Warfare Stimulants. *Journal of Materials Science* **42**, 8400–8407.

[46] **Wang, C., Wang, J., Zeng, L., Qiao, Z., Liu, X., Liu, H., Zhang, J., Ding, J.** (2019). Fabrication of Electrospun Polymer Nanofibers with Diverse Morphologies. *Molecules* **24**, 834.

[47] **Nanofibers Market Size | Industry Research Report, 2024.** https://www.grandviewresearch.com/industry-analysis/nanofibers-market, date retrieved 22.11.2019.

[48] **Alghoraibi, I. & Alomari, S.** (2018). Different Methods for Nanofiber Design and Fabrication. In *Handbook of Nanofibers* (eds. Barhoum, A., Bechelany, M. & Makhlouf, A.) 1–46 (Springer International Publishing). doi:10.1007/978-3-319-42789-8_11-2.

[49] **Nune, S. K., Rama, K. S., Dirisala, V. R. & Chavali, M. Y.** (2017). Chapter 11- Electrospinning of collagen nanofiber scaffolds for tissue repair and regeneration. In *Nanostructures for Novel Therapy* (eds. Ficai, D. & Grumezescu, A. M.) 281–311 (Elsevier). doi:10.1016/B978-0-323-46142-9.00011-6.

[50] **Kulkarni, A. A. & Rao, P. S.** (2013). Synthesis of polymeric nanomaterials for biomedical applications. In *Nanomaterials in Tissue Engineering* 27–63 (Elsevier).

[51] **Garg, T., Rath, G. & Goyal, A. K.** (2015). Biomaterials-based nanofiber scaffold: targeted and controlled carrier for cell and drug delivery. *Journal of drug targeting* **23**, 202–221.

[52] **Bezir, N. Ç., Evcin, A. & Oktay, A.** (2014). Seryum Katkılı $T\dot{I}O_2$ Nanofiberlerin Üretim ve Karakterizasyonu. *Afyon Kocatepe Üniversitesi Fen ve Mühendislik Bilimleri Dergisi*, **14(3)**, 315-318.

[53] **Vinh, N. & Kim, H.-M.** (2016). Electrospinning Fabrication and Performance Evaluation of Polyacrylonitrile Nanofiber for Air Filter Applications. *Applied Sciences* **6**, 235.

[54] **Yamaguchi, S., Yamamoto, E., Mannen, T., Nagamune, T. & Nagamune, T.** (2013). Protein refolding using chemical refolding additives. *Biotechnol J* **8**, 17–31.

[55] **Gonçalves, R.** (2015). Magnetoelectric $CoFe_2O_4$/polyvinylidene fluoride electrospun nanofibres. *Nanoscale* **7**, 8058–8061. doi: 10.1039/C5NR00453E

[56] **Mit- uppatham, C., Nithitanakul, M. & Supaphol, P.** (2004). Ultrafine Electrospun Polyamide-6 Fibers: Effect of Solution Conditions on Morphology and Average Fiber Diameter. *Macromolecular Chemistry and Physics* **205**, 2327–2338.

[57] **Faccini, M., Vaquero, C. & Amantia, D.** (2012). Development of Protective Clothing Against Nanoparticle Based on Electrospun Nanofibers. *J. Nanomaterials* **2012**, 18:1–18:9.

[58] **Wang, Z., Zhao, C. & Pan, Z.** (2015). Porous Bead-on-String Poly(lactic acid) Fibrous Membranes for Air Filtration. *Journal of Colloid and Interface Science* **441**, 121–129.

[59] **Bhardwaj, N. & Kundu, S. C.** (2010). Electrospinning: A Fascinating Fiber Fabrication Technique. Biotechnology Advances 28, 325–347. https://doi.org/10.1016/j.biotechadv.2010.01.004

[60] **Asiri, A. M. & Mohammad, A.** (2018). Applications of nanocomposite materials in drug delivery. (Woodhead Publishing).

[61] **Givehchi, R., Li, Q. & Tan, Z.** (2016). Quality factors of PVA nanofibrous filters for airborne particles in the size range of 10–125 nm. *Fuel* **181**, 1273–1280.

[62] **Şener, A. G., Altay, A. S. & Altay, F.** (2011). Effect of Voltage on Morphology of Electrospun Nanofibers. In *2011 7th International Conference on Electrical and Electronics Engineering (ELECO)* 324–328.

[63] **Zhang, C., Yuan, X., Wu, L., Han, Y. & Sheng, J.** (2005). Study on morphology of electrospun poly (vinyl alcohol) mats. *European polymer journal* **41**, 423–432.

[64] **Choi, H. J., Kim, S. B., Kim, S. H. & Lee, M. H.** (2014). Preparation of electrospun polyurethane filter media and their collection mechanisms for ultrafine particles: *Journal of the Air & Waste Management Association*.

[65] **Zargham, S., Bazgir, S., Tavakoli, A., Rashidi, A. S. & Damerchely, R.** (2012). The Effect of Flow Rate on Morphology and Deposition Area of Electrospun Nylon 6 Nanofiber. *Journal of Engineered Fibers and Fabrics* **7**, 155892501200700400.

[66] **Zhang, S., Shim, W. S. & Kim, J.** (2009). Design of ultra-fine nonwovens via electrospinning of Nylon 6: Spinning parameters and filtration efficiency. *Materials & Design* **30**, 3659–3666.

[67] **Leung, W. W.-F., Hung, C.-H. & Yuen, P.-T.** (2010). Effect of face velocity, nanofiber packing density and thickness on filtration performance of filters with nanofibers coated on a substrate. *Separation and purification technology* **71**, 30–37.

[68] **Yamaguchi, S., Yamamoto, E., Mannen, T., Nagamune, T., Nagamune, T.** (2009). The effect of temperature and humidity on electrospinning. *J Mater Sci* **44**, 1357–1362.

[69] **Casper, C. L., Stephens, J. S., Tassi, N. G., Chase, D. B. & Rabolt, J. F.** (2004). Controlling Surface Morphology of Electrospun Polystyrene Fibers: Effect of Humidity and Molecular Weight in the Electrospinning Process. *Macromolecules* **37**, 573–578.

[70] **Ji, W., Sun, Y., Yang, F., van den Beucken, J., Fan, M., Chen, Z., Jansen, J.** (2010). Bioactive Electrospun Scaffolds Delivering Growth Factors and Genes for Tissue Engineering Applications. *Pharmaceutical research* **28**, 1259–72.

[71] **Bhattarai, R. S., Bachu, R. D., Boddu, S. H. S. & Bhaduri, S.** (2018). Biomedical Applications of Electrospun Nanofibers: Drug and Nanoparticle Delivery. *Pharmaceutics* **11**.

[72] **Rubert, M., Dehli, J., Li, Y.-F., Taskin, M. B., Xu, R., Besenbacher, F., Chen, M.** (2014). Electrospun PCL/PEO coaxial fibers for basic fibroblast growth factor delivery. *J. Mater. Chem. B* **2**, 8538–8546.

[73] **Suk Choi, J., Ho Choi, S. & Sang Yoo, H.** (2011). Coaxial electrospun nanofibers for treatment of diabetic ulcers with binary release of multiple growth factors. *Journal of Materials Chemistry* **21**, 5258–5267.

[74] **Zhang, L. G., Khademhosseini, A. & Webster, T.** (2016). *Tissue and Organ Regeneration: Advances in Micro- and Nanotechnology*. (CRC Press).

[75] **Polat, Y., Calisir, M., Gungor, M., Sagirli, M. N., Atakan, R., Akgul, Y., Demir, A., Kiliç, A.** (2019). Solution blown nanofibrous air filters modified with glass microparticles. *Journal of Industrial Textiles* doi:10.1177/1528083719888674.

[76] **Daristotle, J. L., Behrens, A. M., Sandler, A. D. & Kofinas, P. A** (2016). Review of the Fundamental Principles and Applications of Solution Blow Spinning. *ACS Applied Materials & Interfaces* **8**, 34951–34963.

[77] **Stojanovska, E., Canbay, E., Pampal, E. S., Calisir, M. D., Agma, O., Polat, Y., Simsek, R., Gundogdu, N. A. S., Akgul, Y., Kilic, A.** (2016). A review on non-electro nanofibre spinning techniques. *RSC Advances* **6**, 83783–83801.

[78] **Medeiros, E. S., Glenn, G. M., Klamczynski, A. P., Orts, W. J. & Mattoso, L. H. C.** (2009). Solution blow spinning: A new method to produce micro- and nanofibers from polymer solutions. *Journal of Applied Polymer Science* **113**, 2322–2330.

[79] **Zahmatkeshan, M., Adel, M., Bahrami, S., Esmaeili, F., Rezayat, S. M., Saeedi, Y., Mehravi, B., Jameie, S. B., Ashtari, K.** (2018). Polymer Based Nanofibers: Preparation, Fabrication, and Applications. In *Handbook of Nanofibers* (eds. Barhoum, A., Bechelany, M. & Makhlouf, A.) 1–47 (Springer International Publishing). doi:10.1007/978-3-319-42789-8_29-2.

[80] **Rogalski, J. J., Bastiaansen, C. W. M. & Peijs, T.** (2017). Rotary jet spinning review – a potential high yield future for polymer nanofibers. *Nanocomposites* **3**, 97–121.

[81] **Zhang, X. & Lu, Y.** (2014). Centrifugal Spinning: An Alternative Approach to Fabricate Nanofibers at High Speed and Low Cost. *Polymer Reviews* **54**, 677–701.

[82] **Tepekıran, B., Calisir, M., Polat, Y., Akgul, Y. & Kilic, A.** (2019). Centrifugally Spun Silica (SiO_2) Nanofibers for High-Temperature Air Filtration. *Aerosol Science and Technology* **53**, 1–13.

[83] **Calisir, M. D. & Kilic, A.** (2020). A comparative study on SiO2 nanofiber production via two novel non-electrospinning methods: Centrifugal spinning vs solution blowing. *Materials Letters* **258**, 126751.

[84] **Gungor M., Calisir, M. D., Akgul, Y., Selcuk, S., Ali, D., Kilic, A.** (2019). Submicron aerosol filtration performance of centrifugally spun nanofibrous polyvinylpyrrolidone media. *Journal of Industrial Textiles.* doi:10.1177/1528083719865041.

[85] **Vincent, J. H.** (1995). Air filtration: An integrated approach to the theory and applications of fibrous filters. *JAerS* **26**, 171.

[86] **Graham, K., Gogins, M. & Schreuder-Gibson, H.** (2004). Incorporation of Electrospun Nanofibers into Functional Structures. *International Nonwovens Journal* **os-13**, 1558925004os–1300209.

[87] **Barhate, R. S. & Ramakrishna, S.** (2007). Nanofibrous filtering media: Filtration problems and solutions from tiny materials. *Journal of Membrane Science* **296**, 1–8.

[88] **Gundogdu, N. S., Akgul, Y. & Kilic, A.** (2018). Optimization of centrifugally spun thermoplastic polyurethane nanofibers for air filtration applications. *Aerosol Science and Technology* **52**, 515–523.

[89] **Vitchuli, N., Shi, Q., Nowak, J., McCord, M., Bourham, M., Zhang, X.** (2010). Electrospun ultrathin nylon fibers for protective applications. *Journal of Applied Polymer Science* **116**, 2181–2187.

[90] **Wan, H., Wang, N., Yang, J., Si, Y., Chen, K., Ding, B., Sun, G., El-Newehy, M., Al-Deyab, S. S., Yu, J.** (2014). Hierarchically structured polysulfone/titania fibrous membranes with enhanced air filtration performance. *Journal of Colloid and Interface Science* **417**, 18–26.

[91] **Su, J., Yang, G., Cheng, C., Huang, C., Xu, H., Ke, Q.** (2017). Hierarchically structured TiO_2/PAN nanofibrous membranes for high-efficiency air filtration and toluene degradation. *Journal of colloid and interface science* **507**, 386–396.

[92] **Wang, Z. & Pan, Z.** (2015). Preparation of hierarchical structured nano-sized/porous poly(lactic acid) composite fibrous membranes for air filtration. *Applied Surface Science* **356**, 1168–1179.

[93] **Lee, S. & Obendorf, S. K.** (2016). Use of Electrospun Nanofiber Web for Protective Textile Materials as Barriers to Liquid Penetration: *Textile Research Journal.* doi:10.1177/0040517507080284.

[94] **Zhu, M., Han, J., Wang, F., Shao, W., Xiong, R., Zhang, Q., Pan, H., Yang, Y., Samal, S. K., Zhang, F., Huang, C.** (2017). Electrospun

Nanofibers Membranes for Effective Air Filtration. *Macromolecular Materials and Engineering* **302**, 1600353.

[95] **Choi, H.-J., Kumita, M., Hayashi, S., Yuasa, H., Kamiyama, M., Seto, T., Tsai, C.-J., Otani, Y.** (2017). Filtration Properties of Nanofiber/Microfiber Mixed Filter and Prediction of its Performance. *Aerosol and Air Quality Research* **17**, 1052–1062.

[96] **Nelson, M. T., Keith, J. P., Li, B.-B., Stocum, D. L. & Li, J.** (2012). Electrospun composite polycaprolactone scaffolds for optimized tissue regeneration. *Proceedings of the Institution of Mechanical Engineers, Part N: Journal of Nanoengineering and Nanosystems* **226**, 111–121.

[97] **Nezarati, R. M., Eifert, M. B. & Cosgriff-Hernandez, E.** (2013). Effects of Humidity and Solution Viscosity on Electrospun Fiber Morphology. *Tissue Engineering Part C: Methods* **19**, 810–819.

[98] **Choi, H.-J., Kumita, M., Hayashi, S., Yuasa, H., Kamiyama, M., Seto, T., Tsai, C.-J., Otani, Y.** (2015). Fabrication of PEO/chitosan/PCL/olive oil nanofibrous scaffolds for wound dressing applications. *Fibers Polym* **16**, 1201–1212.

[99] **Lee, J. S., Choi, K. H., Ghim, H. D., Kim, S. S., Chun, D. H., Kim, H. Y., Lyoo, W. S.** (2004). Role of molecular weight of atactic poly(vinyl alcohol) (PVA) in the structure and properties of PVA nanofabric prepared by electrospinning. *Journal of Applied Polymer Science* **93**, 1638–1646.

[100] **Jet Shaping Nanofibers and the Collection of Nanofiber Mats in Electrospinning**- Open Access Library. http://www.oalib.com/paper/1533982, date retrieved 22.11.2019.

[101] **Abdel-Hady, F., Alzahrany, A. & Hamed, M.** (2011). Experimental Validation of Upward Electrospinning Process. *ISRN Nanotechnology* **2011**, 1–14.

[102] **McDade, C. E., Dillner, A. M. & Indresand, H.** (2009). Particulate Matter Sample Deposit Geometry and Effective Filter Face Velocities. *Journal of the Air & Waste Management Association* **59**, 1045–1048.

[103] **Rajak, A., Hapidin, D. A., Iskandar, F., Munir, M. M. & Khairurrijal, K.** (2019). Controlled morphology of electrospun nanofibers from waste expanded polystyrene for aerosol filtration. *Nanotechnology* **30**, 425602.

[104] **Hinds, W. C.** (1999). Aerosol Technology: Properties, Behavior, and Measurement of Airborne Particles. (John Wiley & Sons).

[105] **Yang, Y., Zhang, S., Zhao, X., Yu, J. & Ding, B.** (2015). Sandwich structured polyamide-6/polyacrylonitrile nanonets/bead-on-string composite membrane for effective air filtration. *Separation and Purification Technology* **152**, 14–22.

[106] **Kadam, Truong, Y., Kyratzis, I. L., Wang, L. & Padhye, R.** (2017). Bilayer Electrospun Nanofibre Structures to Improve Quality Factor in Air Filtration. doi:10.11159/icnfa17.120.

[107] **Zhu, M., Hua, D., Pan, H., Wang, F., Manshian, B., Soenen, S. J., Xiong, R., Huang, C.** (2018). Green electrospun and crosslinked poly (vinyl alcohol)/poly (acrylic acid) composite membranes for antibacterial effective air filtration. *Journal of colloid and interface science* **511**, 411–423.

[108] **Wang, N., Raza, A., Si, Y., Yu, J., Sun, G., Ding, B.** (2013). Tortuously structured polyvinyl chloride/polyurethane fibrous membranes for high-efficiency fine particulate filtration. *Journal of Colloid and Interface Science* **398**, 240–246.

[109] **Zhang, S., Liu, H., Yin, X., Yu, J. & Ding, B.** (2016). Anti-deformed Polyacrylonitrile/Polysulfone Composite Membrane with Binary Structures for Effective Air Filtration. *ACS Appl. Mater. Interfaces* **8**, 8086–8095.

[110] **Vanangamudi, A., Hamzah, S. & Singh, G.** (2015). Synthesis of hybrid hydrophobic composite air filtration membranes for antibacterial activity and chemical detoxification with high particulate filtration efficiency (PFE). *Chemical Engineering Journal* **260**, 801–808.

[111] **Chuang, Y.-H., Hong, G.-B. & Chang, C.-T.** (2014). Study on particulates and volatile organic compounds removal with TiO_2 nonwoven filter prepared by electrospinning. *Journal of the Air & Waste Management Association* **64**, 738–742.

[112] **Khan, I., Saeed, K. & Khan, I.** (2019). Nanoparticles: Properties, applications and toxicities. *Arabian Journal of Chemistry* **12**, 908–931.

[113] **Christian, P., Von der Kammer, F., Baalousha, M. & Hofmann, Th.** (2008). Nanoparticles: structure, properties, preparation and behaviour in environmental media. *Ecotoxicology* **17**, 326–343.

[114] **Rivero, P. J., Urrutia, A., Goicoechea, J. & Arregui, F. J.** (2015). Nanomaterials for Functional Textiles and Fibers. *Nanoscale Res Lett* **10**, 501.

[115] **Sundarrajan, S., Chandrasekaran, A. R. & Ramakrishna, S.** (2010). An Update on Nanomaterials-Based Textiles for Protection and Decontamination: An Update on Nanomaterials-Based Textiles. *Journal of the American Ceramic Society* **93**, 3955–3975.

[116] **Sirelkhatim, A., Mahmud, S., Seeni, A., Kaus, N. H. M., Ann, L. C., Bakhori, S. K. M., Hasan, H., Mohamad, D.** (2015). Review on Zinc Oxide Nanoparticles: Antibacterial Activity and Toxicity Mechanism. *Nanomicro Lett* **7**, 219–242.

[117] **Use of Nanomaterials in Textiles.** https://www.umweltbundesamt.de/sites/default/files/medien/376/publikationen/datenblatt_nanoprdukte_textilien_e.pdf 22.11.2019.

[118] **Siddiqi, K. S., ur Rahman, A., Tajuddin & Husen, A.** (2018). Properties of Zinc Oxide Nanoparticles and Their Activity Against Microbes. *Nanoscale Res Lett* **13**.

[119] **Zakharova, O. & Kolesnikov E, V. E.** (2019). Antibacterial activity of ZnO nanoparticles: dependence on particle size, dispersion media and

storage time. In *IOP Conf. Series: Earth and Environmental Science* vol. 226 012062.

[120] **Papavlassopoulos, H., Mishra, Y. K., Kaps, S., Paulowicz, I., Abdelaziz, R., Elbahri, M., Maser, E., Adelung, R., Röhl, C.** (2014). Toxicity of Functional Nano-Micro Zinc Oxide Tetrapods: Impact of Cell Culture Conditions, Cellular Age and Material Properties. *PLOS ONE* **9**, e84983.

[121] **Li, Y. X., Koper, O., Atteya, M. & Klabunde, K. J.** (1992). Adsorption and decomposition of organophosphorus compounds on nanoscale metal oxide particles. In situ GC-MS studies of pulsed microreactions over magnesium oxide. *Chemistry of Materials* **4**, 323–330.

[122] **Dadvar, S., Tavanai, H., Morshed, M. & Ghiaci, M. A** (2013). Study on the Kinetics of 2-Chloroethyl Ethyl Sulfide Adsorption onto Nanocomposite Activated Carbon Nanofibers Containing Metal Oxide Nanoparticles. *Separation and Purification Technology* **114**, 24–30.

[123] **Yusof, N.** (2016). Adsorption of Cadmium (Ii) Ions by Polyacrylonitrile-Based Activated Carbon Nanofibers/Magnesium Oxide as Its Adsorbents. *Malaysian Journal of Analytical Science* **20**, 1467–1473.

[124] **Kang, W., Ju, J., Zhao, H., Li, Z., Ma, X., Cheng, B.** (2016). Characterization and antibacterial properties of Ag NPs doped nylon 6 tree-like nanofiber membrane prepared by one-step electrospinning. *Fibers Polym* **17**, 2006–2013.

[125] **Daniela, L. & Barbora, S.** (2014). *Antibacterial efficiency of nanofiber membranes with biologically active nanoparticles*. (IAAST).

[126] **Vitchuli, N., Shi, Q., Nowak, J., Kay, K., Caldwell, J. M., Breidt, F., Bourham, M., McCord, M., Zhang, X.** (2011). Multifunctional ZnO/Nylon 6 Nanofiber Mats by an Electrospinning–Electrospraying Hybrid Process for Use in Protective Applications. *Science and technology of advanced materials* **12**, 055004.

[127] **Rahman, M. & Asiri, A. M.** (2016). *Nanofiber Research: Reaching New Heights*. (BoD – Books on Demand).

[128] **Behnam, R., Morshed, M., Tavanai, H. & Ghiaci, M.** (2013). Destructive Adsorption of Diazinon Pesticide by Activated Carbon Nanofibers Containing Al_2O_3 and MgO Nanoparticles. *Bulletin of Environmental Contamination and Toxicology* **91**, 475–480.

[129] **Michalkova, A., Ilchenko, M., Gorb, L. & Leszczynski, J.** (2004). Theoretical Study of the Adsorption and Decomposition of Sarin on Magnesium Oxide. *The Journal of Physical Chemistry B* **108**, 5294–5303.

[130] **Bindhu, M. R., Umadevi, M., Kavin Micheal, M., Arasu, M. V. & Abdullah Al-Dhabi, N.** (2016). Structural, morphological and optical properties of MgO nanoparticles for antibacterial applications. *Materials Letters* **166**, 19–22.

[131] **Kakkar, R., Kapoor, P. N. & Klabunde, K. J.** (2004). Theoretical Study of the Adsorption of Formaldehyde on Magnesium Oxide Nanosurfaces:

Size Effects and the Role of Low-Coordinated and Defect Sites. *J. Phys. Chem. B* **108**, 18140–18148.

APPENDICES

APPENDIX A: Air filtration test results at 32 l/min air velocity

APPENDIX A

Table A.1 : Particulate filtration test results of all produced nanofiber filters (the air velocity:32 l/min)

	Filtration Efficiency (%)					Pressure Drop (kPa)				
	13% PAN	20% MgO/ PAN	25% MgO/ PAN	30% MgO/ PAN	35% MgO/ PAN	13% PAN	20% MgO/ PAN	25% MgO/ PAN	30% MgO/ PAN	35% MgO/ PAN
20 min	94,80	89,49	90,18	54,23	59,48	0,073	0,036	0,026	0,011	0,016
40 min	98,75	92,69	98,90	93,71	78,79	0,129	0,052	0,075	0,039	0,039
60 min	99,29	93,36	98,18	97,92	95,01	0,164	0,059	0,069	0,084	0,086

	Quality Factor				
	13% PAN	20% MgO/ PAN	25% MgO/ PAN	30% MgO/ PAN	35% MgO/ PAN
20 min	0,040	0,063	0,090	0,069	0,056
40 min	0,034	0,050	0,060	0,070	0,040
60 min	0,030	0,046	0,058	0,046	0,035

Effect on Thickness on Particulate Filtration

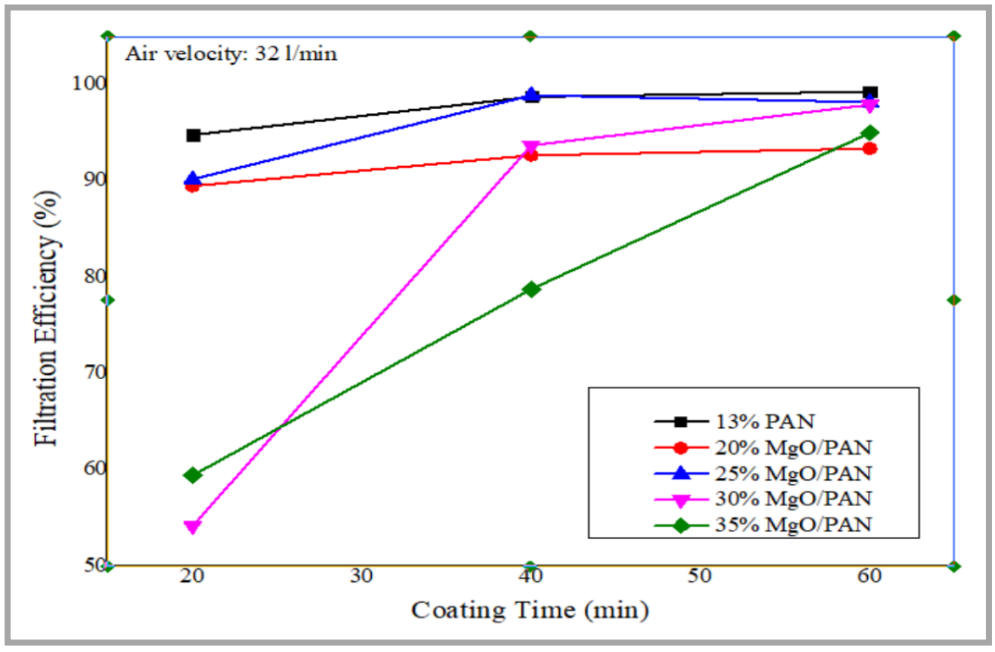

Figure A.1 : Effect of thickness on filtration efficiency for all related samples produced.

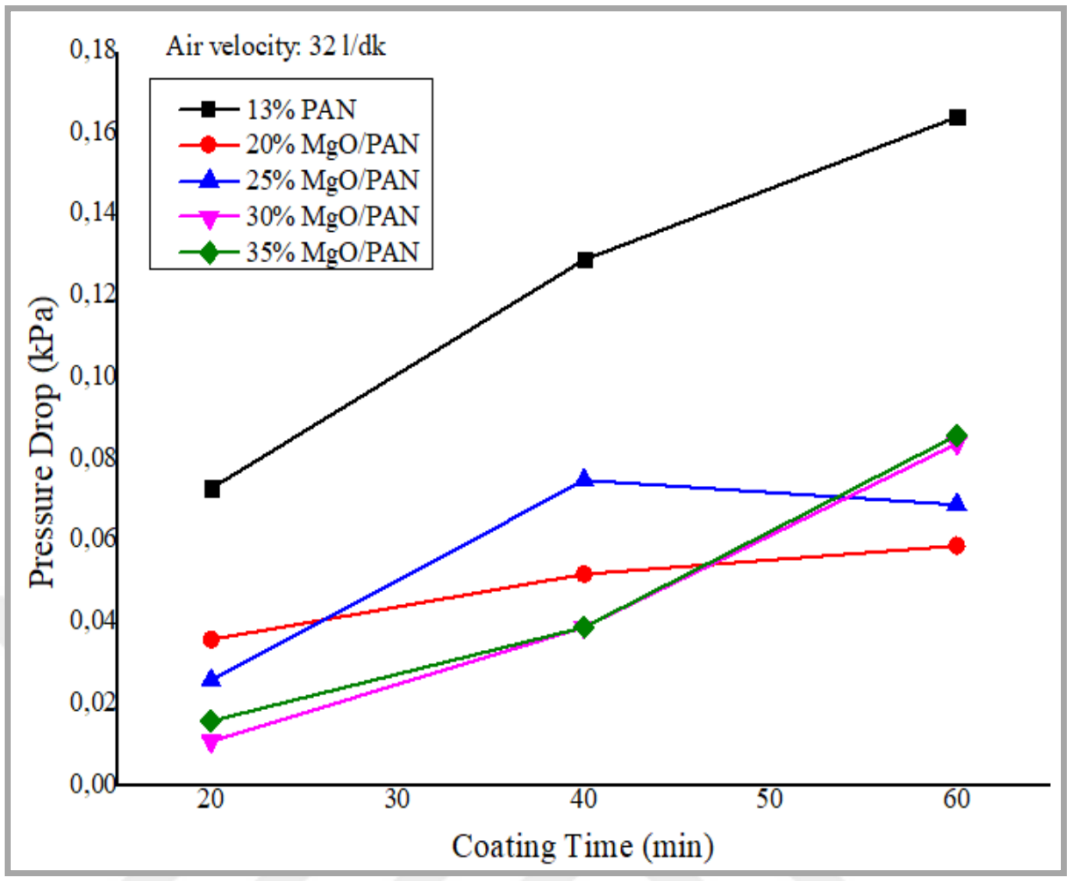

Figure A.2 : Effect of thickness on pressure drop for all related samples produced.

Effect of Nanoparticle Concentration on Particulate Filtration

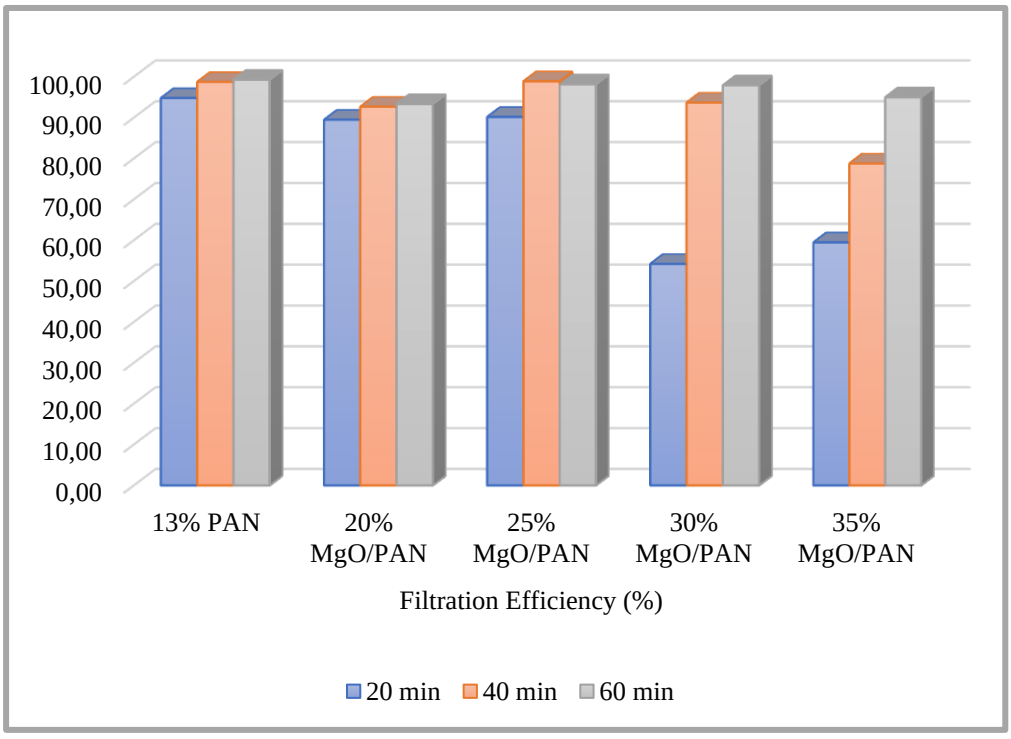

Figure A.3 : Effect of nanoparticle concentration on filtration efficiency for all related samples produced.

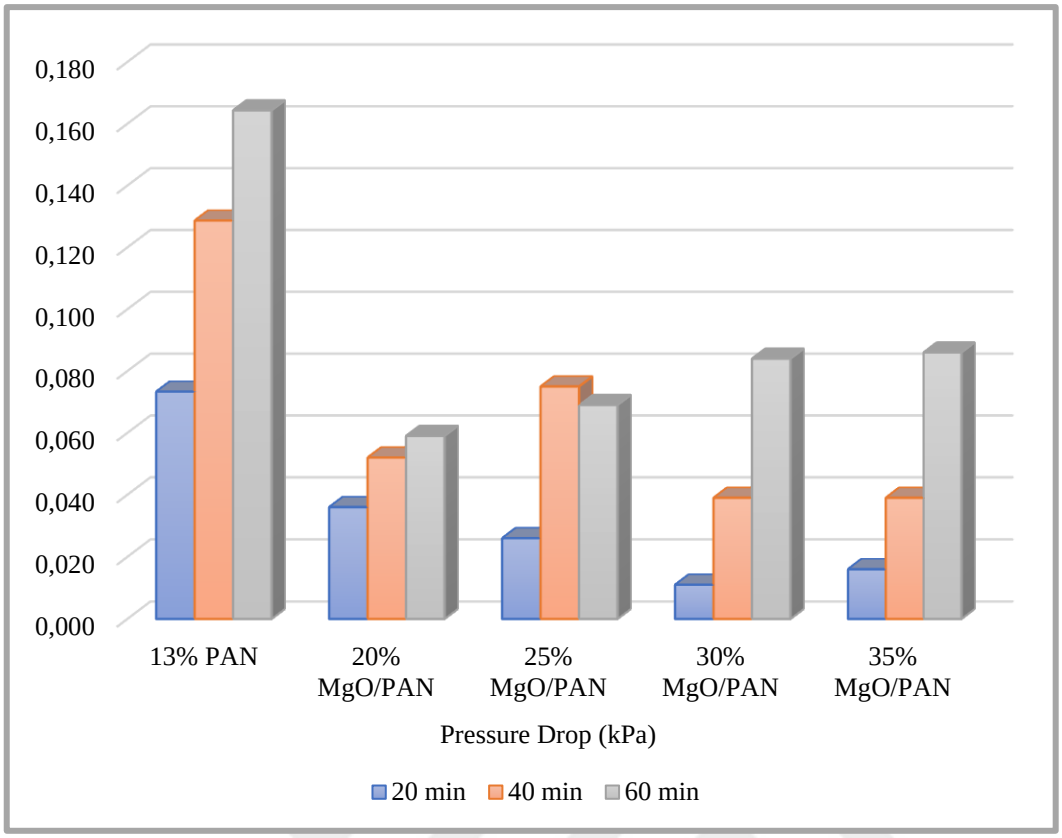

Figure A.4 : Effect of nanoparticle concentration on pressure drop for all related samples produced.

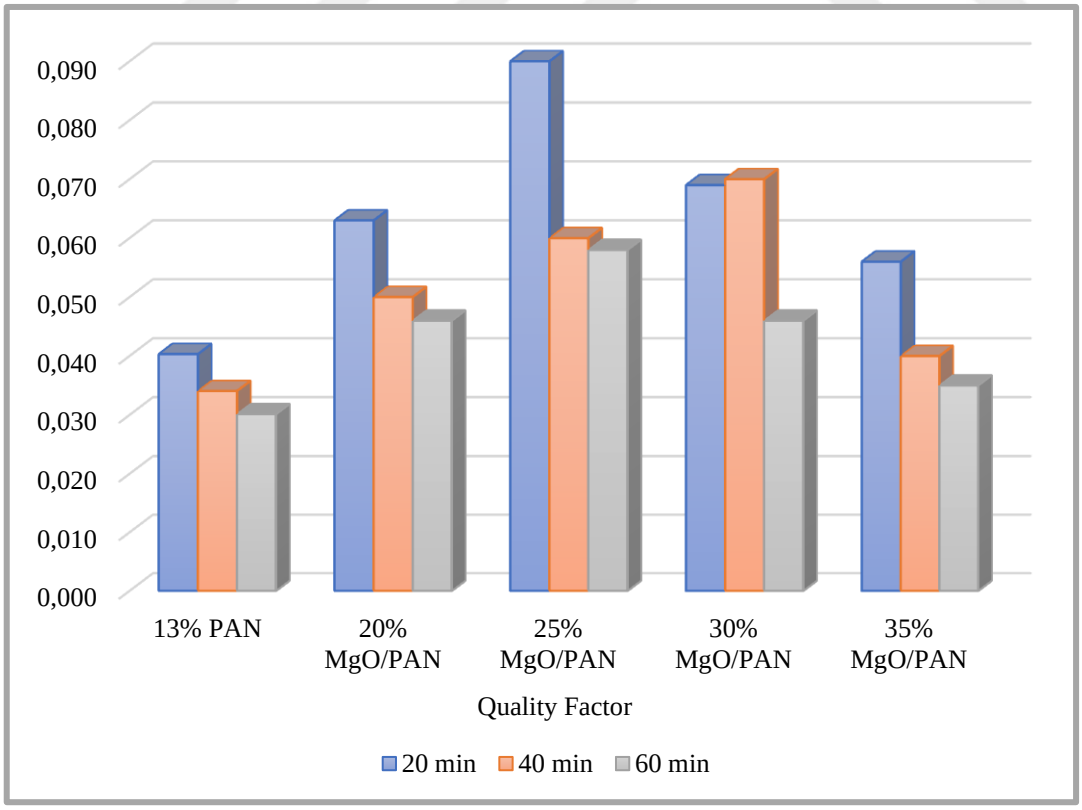

Figure A.5 : Effect of nanoparticle concentration on quality factor for all related samples.

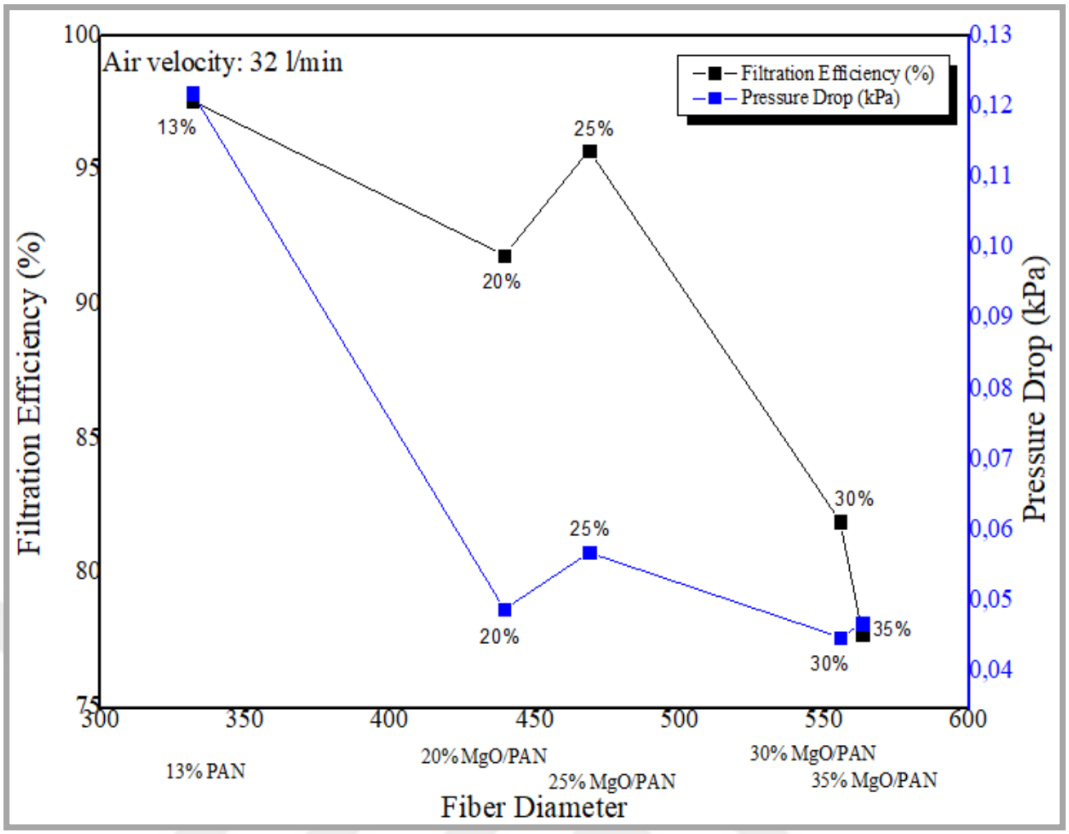

Figure A.6 : Filtration efficiency and pressure drop of nanofibers with various fiber diameter under an air velocity of 32 l/min.

Since nano-size aerosols were delivered at a lower air velocity, filtration efficiencies were higher and pressure drops were lower compared to results at an air velocity of 95 l/min. When the effect of nanofiber layer thickness and nanoparticle concentration on particulate filtration have examined, similar interpretations can be made with the filtration test results performed at an air speed of of 95 l/min.

CURRICULUM VITAE

Name and Surname **:** Tugba Baysal

Date of Birth and Place **:** 14/03/1994 – Istanbul

E-mail **:** tugbabaysal94@gmail.com

EDUCATION:

B.Sc. **:** 2017, Yıldız Technical University, Faculty of Chemical and Metallurgical Engineering, Department of Chemical Engineering.

PROFESSIONAL EXPERIENCE:

- 01/2018-11/2019 : Research Assistant in Mehmet Akif Ersoy University
- 01/2020- Present : Research Assistant in Gebze Technical University

PUBLICATIONS, PRESENTATIONS AND PATENTS ON THE THESIS:

- **Demir, A., Baysal, T.** (2018). Design of Face Masks with Metal Oxide Decorated Nanofiber Layer for VOC Protection, *4th International Fiber and Polymer Research Symposium*, Bursa, Turkey, October 4-5.
- **Demir, A., Baysal, T.** (2020). Usage of Polyacrylonitrile Nanofibers Containing MgO Nanoparticles on Particulate Filtration and Toluene Adsorption, *6th International Fiber and Polymer Research Symposium*, Bursa, Turkey, January 24-25.
- **Baysal, T., Noor, N., & Demir, A.** (2020). Nanofibrous MgO Composites: Structures, Properties, and Applications. *Polymer-Plastics Technology and Materials*, 1-30. https://doi.org/10.1080/25740881.2020.1759212